DISSERTATION

# OPIOID BIOAVAILABILITY IN THE RETINA MODULATES SLEEP/WAKE BEHAVIOR

Submitted by

Casey-Tyler Berezin

Graduate Degree Program in Cell and Molecular Biology

In partial fulfillment of the requirements

For the Degree of Doctor of Philosophy

Colorado State University

Fort Collins, Colorado

Summer 2023

Doctoral Committee:

Advisor: Jozsef Vigh

Shane Hentges
Susan Bailey
Tai Montgomery

ABSTRACT

OPIOID BIOAVAILABILITY IN THE RETINA MODULATES SLEEP/WAKE BEHAVIOR

Opioids, such as the prototypical opioid morphine, primarily exert their analgesic and rewarding effects through μ-opioid receptors (MORs), and it has been shown that acute morphine treatment negatively impacts sleep/wake behavior through MORs. Continued opioid administration exacerbates sleep/wake disturbances, such that approximately 80% of chronic users report persistent sleep disturbances, including insomnia and daytime sleepiness. These opioid-induced sleep disturbances (OISD) are associated with negative outcomes such as increased drug craving, relapse and negative affect (i.e. anxiety/depression), as well as hyperalgesia in chronic pain patients. Therefore, therapeutic interventions for OISD are expected to improve the outcomes of long-term opioid use in general. However, the neuronal population(s) and cellular mechanism(s) mediating sleep/wake changes in response to chronic opioid treatment are not currently known.

Although many neuronal populations in the brain contribute to sleep/wake behavior, the photoentrainment of sleep/wake cycles to environmental light/dark cycles is uniquely regulated by intrinsically photosensitive retinal ganglion cells (ipRGCs). Importantly, light-evoked firing by ipRGCs is modulated by activation of their MORs, and endogenous MOR activation has been shown to modulate an ipRGC-driven behavior, the pupillary light reflex. Additionally, opioids (e.g. morphine) are routinely detected in the human eye to diagnose overdose-related deaths, and morphine accumulates in the mouse retina upon chronic systemic administration. Therefore, the central hypothesis addressed in the current work is that the bioavailability of opioids (i.e.

endogenous opioid peptides and/or opioid drugs) in the retina contributes to the modulation of sleep/wake behavior.

In Chapter 2, we show that endogenous opioid peptides in the retina contribute to healthy sleep/wake behavior. Using a mouse model with a cell-specific knockout of MORs expressed by ipRGCs (McKO), we show that endogenous activation of these MORs is important for maintaining activity and suppressing slow-wave sleep during the mouse's active period. Concurrent work showed that the MORs expressed by ipRGCs also contribute to morphine-driven changes in sleep/wake behavior during a chronic treatment paradigm. Thus, both endogenous opioid peptides and opioid drugs modulate sleep/wake behavior via the activation of the MORs expressed by ipRGCs.

Systemically applied opioid drugs penetrate the blood-retina barrier and accumulate in the retina. Thus, ipRGCs may be liable to opioid modulation throughout chronic opioid treatment, contributing to the development and persistence of OISD. In Chapter 3, we investigate the relationship between opioid transporter expression at the blood-retina barrier and morphine deposition in the retina. We show that low expression of the opioid extruder permeability glycoprotein (P-gp) may allow morphine to persist in the retina, compared to the brain where P-gp expression is high and morphine is more quickly cleared from the tissue. In Chapter 4, we discuss how upregulation of P-gp at the blood-retina barrier via the non-steroidal anti-inflammatory drug diclofenac may reduce opioid bioavailability in the retina, thereby alleviating OISD. This work demonstrates a previously unknown contribution of ipRGC signaling to opioid-modulated sleep/wake changes, and identifies a potential therapeutic target for OISD.

ACKNOWLEDGEMENTS

I would first like to thank Dr. Jozsef Vigh for his continued support and direction in the development of this project. In addition, the preliminary foundation of this work is thanks to several previous Vigh lab members, including Shannon Gallagher, Ryan Tooker, Allison Cleymaet and Christian Korkis. I also thank my co-authors on the publications in this work, some of whom have since moved on, including Kes Luchini, Glenda Torres-Lopez, and Sierra Curdts. I am especially grateful to Nikolas Bergum for the support and collaboration he's provided over the years. Completing a PhD is no small feat, but having a friend by your side makes that much easier.

I would also like to thank all the members of the Cell and Molecular Biology (CMB) program, and especially director Carol Wilusz, for providing a community and support system during my time here. Additionally, I am grateful for the financial support and training I received from the Quantitative CMB T32 program.

# DEDICATION

I dedicate this work to my family and friends who have supported me throughout the years, even when they couldn't explain to other people what I was doing (it's okay, it was hard for me too).

For my husband Dennis, for continually listening to me geek out and vent, pushing me to keep going, and not letting me work every night and weekend.

For my sissy, Chrissie, who has simply *always* been there and who has made me into the woman I am today.

And for my mom, who would have loved to see me take this journey.

TABLE OF CONTENTS

LIST OF TABLES

LIST OF FIGURES

# CHAPTER 1: Introduction

## 1.1 The opioid-sleep connection

The opium poppy, *Papaver somniferum* ("sleep-bringing" in Latin), was first domesticated seven thousand years ago, and by 500 B.C.E. the medicinal properties of opium were well-known (Brownstein, 1993; Hamilton and Baskett, 2000; Mahr, 2017; Nencini, 2022). Opium and its derivatives are sometimes referred to as narcotics (from Greek *narkoun* "to benumb, make unconscious" (Harper, n.d.)) and their efficacy as analgesics remains unmatched (Benyamin et al., 2008; Volkow et al., 2019). The active ingredient of opium, morphine, was first purified in the early nineteenth century and was named after Morpheus, the Greek god of dreams (Brownstein, 1993; Krishnamurti and Rao, 2016; Sertürner, 1817). While the etymological connection between opioids and sleep is clear, the effects of opioids on sleep/wake behavior and the underlying molecular mechanisms are complex and not yet fully understood.

Acute opioid treatment improves sleep quality in individuals experiencing chronic pain due to the analgesic and sedative effects of opioids (Cutrufello et al., 2020; Rosenthal et al., 2007; Webster et al., 2015). However, in healthy individuals, acute opioid treatment disturbs sleep architecture, particularly by reducing deep sleep (Dimsdale, 2022; Lewis et al., 1970; Shaw et al., 2005). Morphine's wake-inducing and sleep-reducing effects have been recapitulated in rodent and cat models (Eacret et al., 2023; Fratta et al., 1987; King et al., 1981; Locklear, 2020; Wang et al., 2013). The inhibition of sleep-promoting neurons in the ventrolateral preoptic area (VLPO), a brain region often referred to as the "sleep switch," have been implicated in these effects (Saper et al., 2001; Wang et al., 2013). Few studies have explicitly studied the effects of chronic opioids on sleep, however, recurrent opioid administration leads to exacerbated

sleep/wake disruptions, independent of treatment impetus (Coffey et al., 2016; Cutrufello et al., 2020; Eacret et al., 2023, 2020; Onen et al., 2005; Robertson et al., 2016). The vast majority of chronic opioid users (~80%) report persistent sleep disturbances such as insomnia and daytime sleepiness, and these are associated with negative outcomes including increased risk of use (Figure 1-1) (Burke et al., 2008; Hartwell et al., 2014; Huhn and Finan, 2021; Lydon-Staley et al., 2017; O'Brien et al., 2021; Stein et al., 2004; Tripathi et al., 2020; Zgierska et al., 2007). Especially concerning is the fact that chronic pain patients may experience hyperalgesia (i.e. an

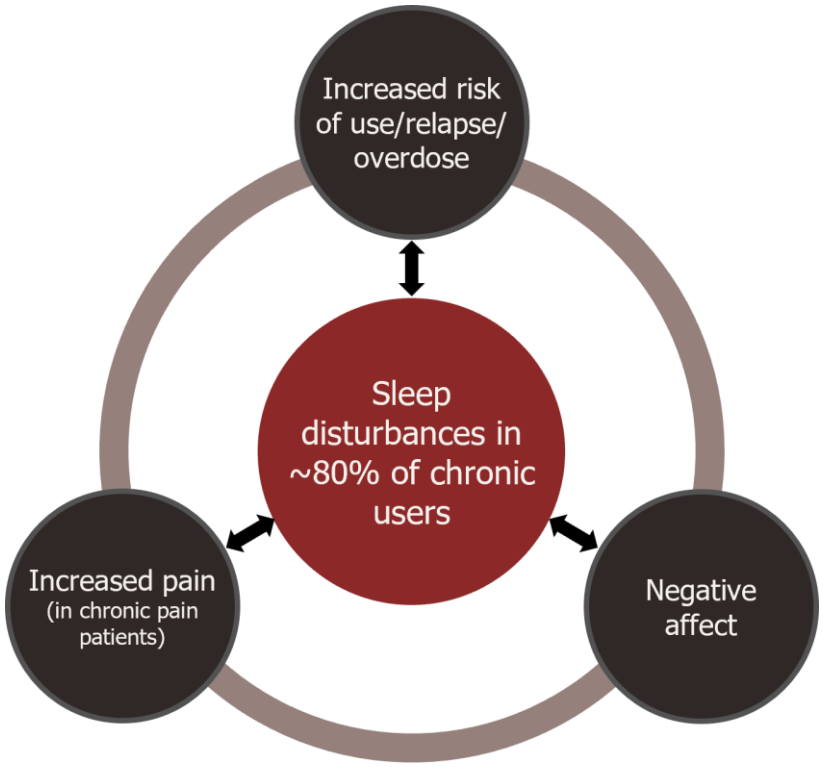


**Figure 1-1. The bidirectional relationship between opioid-induced sleep disturbances and negative outcomes.**
Sleep disturbances are reported by most chronic opioid users, including those on medication-assisted therapy (e.g. methadone). Sleep quality continues to be impaired throughout withdrawal and detoxification, and is therefore a major risk factor for relapse. Poor sleep quality, negative affect (e.g. anxiety, depression) and drug-craving interact with and reinforce one another. Sleep disturbances are especially worrisome for chronic pain patients, who can experience hyperalgesia in response to both poor sleep and continued opioid use.

increased sensitivity to feeling pain or an extreme response to pain) in response to both long-term opioid treatment and sleep disturbances (Chu et al., 2008; Roehrs et al., 2006; Roehrs and Roth, 2005; Turk et al., 2011). Furthermore, impaired sleep quality can persist even after detoxification and is a risk factor for relapse (Asaad et al., 2011; Tripathi et al., 2020). Despite opioid-induced sleep disturbances (OISD) being well-documented, the ability to develop therapeutics for OISD requires a greater mechanistic understanding of how chronic opioid treatment affects sleep (Huhn and Finan, 2021; Tripathi et al., 2020).

### 1.2 The endogenous opioid system

The effects of opioids can be difficult to characterize because they leverage the body's complex endogenous opioid system (Brownstein, 1993; Holden et al., 2005; Papini, 2018). The three classical opioid receptors (μ, δ, and κ receptors: MOR s, DORs and KORs, respectively) were discovered in the 1970s, and are inhibitory G-protein coupled receptors (GPCRs) (Pasternak and Pan, 2013; Pert et al., 1973; Simon et al., 1973; Terenius, 1973). Upon activation by a ligand, canonical $G\alpha_{i/o}$ signaling leads to the inhibition of adenylyl cyclase (and therefore, reduction of cellular cAMP) by the $G_{\alpha}$ subunit, and the opening of G protein-gated inwardly rectifying potassium (GIRK) channels and inhibition of voltage-gated calcium channels by the $G_{\beta\gamma}$ subunit (Al-Hasani and Bruchas, 2011; Gomes et al., 2020; Lešnik et al., 2021; Pineyro and Nagi, 2021; Ramirez et al., 2021). The resulting effects of opioids on physiological functions might vary based on the duration of treatment (i.e. acute versus chronic), the ligand-receptor combination, the effectors of receptor signaling and the neuronal populations involved (Gomes et al., 2020; Pineyro and Nagi, 2021). In recent years, zeta and nociception/orphanin FQ receptors, as well as receptor subtypes and splice variants have been identified (Dhaliwal and Gupta, 2022;

Pasternak and Pan, 2013). However, it has been shown that morphine and its related compounds (e.g. heroin, codeine, oxycodone) primarily exert their effects through MORs (Inturrisi, 2002; Pasternak and Pan, 2013; Schaefer et al., 2017; Williams et al., 2013). The endogenous opioid system is innately analgesic, and MOR agonists produce the most potent analgesia compared to agonists at other opioid receptors and non-opioid analgesics (Fields, 2011; Holden et al., 2005; Pathan and Williams, 2012; Trescot et al., 2008; Valentino and Volkow, 2018; Volkow et al., 2019).

There are three main families of endogenous opioid peptides, which are derived from larger precursor polypeptides: (1) endorphins ("endogenous" + "morphine"), primarily β-endorphin from proopiomelanocortin (POMC; Figure 1-2); (2) enkephalins (e.g. Met-enkephalin, Leu-enkephalin) from proenkephalin; and (3) dynorphins from prodynorphin (Cox, 1982; Goldstein et al., 1979; Hughes et al., 1975; Li et al., 1976; Loh et al., 1984). All endogenous opioid peptides share the characteristic amino acid sequence: Tyr-Gly-Gly-Phe-Leu/Met

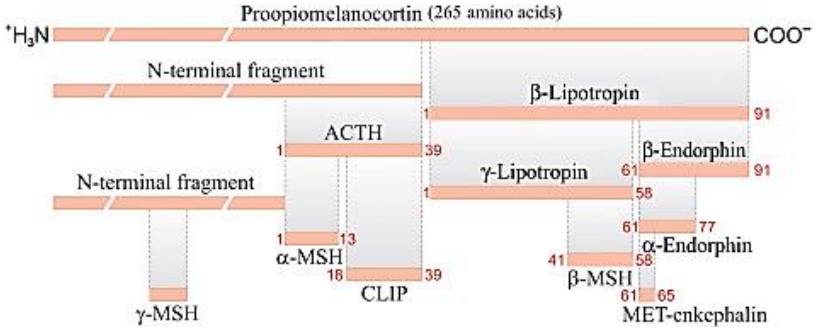


**Figure 1-2. Schematic of POMC processing into β-endorphin.**
Proopiomelanocortin (POMC) is cleaved to produce several peptides; the last 31 amino acids corresponding to β-endorphin yield the only opioidergic products. β-endorphin may be further cleaved (e.g. into α-endorphin). The first 5 amino acids are equivalent to Met-enkephalin and contain the characteristic opioid peptide sequence: Tyr-Gly-Gly-Phe-Leu/*Met*. [1]

[1] Figure reprinted from Medical Biochemistry, Blanco, A. & Blanco, G., Chapter 26 - Biochemical Bases of Endocrinology (II) Hormones and Other Chemical Intermediates, Pages 573-644, Copyright 2017, with permission from Elsevier (license #5484361186007, see Appendix B). https://doi.org/10.1016/B978-0-12-803550-4.00026-4

(Abrimian et al., 2021; Cox, 1982) (Figure 1-2). It is often said that DORs are preferentially bound by enkephalins, KORs by dynorphins, and MORs by endorphins. However, all opioid peptides will bind to any of the three classical receptors if the peptide concentration is high enough and depending on receptor availability (Corbett et al., 1993; Gomes et al., 2020; Hughes et al., 1975; Kieffer, 1995; Paterson et al., 1984; Raynor et al., 1993; Winters et al., 2017). Importantly, the actions of endogenously produced and exogenously applied peptides may differ (Winters et al., 2017). For example, Met-enkephalin has similar affinity to the MOR and DOR, yet in the amygdala, endogenous Met-enkephalin is thought to only act on DORs, while exogenous Met-enkephalin binds both receptor types (Winters et al., 2017). Furthermore, the activation of different opioid receptors by the same ligand may lead to different behavioral outcomes: exogenous activation of DORs in the amygdala by Met-enkephalin is anxiolytic while MOR activation is anxiogenic (Winters et al., 2017). Thus, when assessing the roles of endogenous opioid peptides on physiological behavior, it is important to the consider the receptor(s) they are binding to.

### 1.3 The role of endogenous opioids in sleep

There is evidence that all three families of endogenous opioid peptides influence sleep/wake behavior through their classically-associated receptors. Acute β-endorphin treatment has been shown to increase arousal and latency to sleep in rodents and cats (Fratta et al., 1987; King et al., 1981; Riou et al., 1982). β-endorphin levels are also elevated in rats exposed to sleep deprivation and in children with sleep apnea (Fratta et al., 1987; Myer et al., 1990; Przewlocka et al., 1986). Importantly, opioid receptor antagonists are effective reversal agents and treatments for these phenomena (Fratta et al., 1987; King et al., 1981; Myer et al., 1990). While the

mechanism by which β-endorphin modulates sleep remains unknown (Pilozzi et al., 2021), it is plausible that β-endorphin exerts its effects on sleep by acting on MORs. Acute infusion of the endogenous MOR agonist endomorphin 1 into the VLPO increases wakefulness in rats, while MOR-selective antagonist CTAP increases sleep (Greco et al., 2008; Saper et al., 2001). These data suggest that MOR activation, possibly by β-endorphin, contributes to the stereotypical effects of opioids on sleep/wake behavior.

Conversely, dynorphins appear to be sleep-promoting through their activation of KORs. Both application of dynorphin into the VLPO and optogenetic activation of prodynorphin-expressing neurons in the preoptic area increase non-rapid eye movement (NREM) sleep in rodents (Chung et al., 2017; Greco et al., 2008). Application of the KOR antagonist nor-binaltorphimine to the VLPO slightly increases wakefulness (Greco et al., 2008). The role of enkephalins in sleep is less clear. On one hand, Met-enkephalin administration can reduce hibernation bout duration (hibernation may be considered an extension of NREM sleep), associating the peptide with wakefulness (Beckman et al., 1992). On the other hand, delta-sleep-inducing peptide stimulates Met-enkephalin release in many brain regions, associating the peptide with sleep (Nakamura et al., 1991, 1989). Furthermore, DOR (but not MOR or KOR) agonists inhibit light-induced circadian phase advances (Tierno et al., 2002). These data could suggest that each of the three classical opioid receptors have different contributions to the homeostatic and circadian components of sleep (i.e. homeostatic sleep drive builds over the course of the day while circadian sleep/wake rhythms are entrained to external factors) (Bergum et al., 2022c; Deboer, 2018; LeGates et al., 2014).

### 1.3 Opioid action in the retina

While there are many brain regions orchestrating homeostatic sleep/wake behavior, the photoentrainment (i.e. synchronization) of circadian sleep/wake cycles to environmental light/dark cycles is uniquely regulated by retinal neurons (i.e. melanopsin-expressing intrinsically photosensitive retinal ganglion cells, or ipRGCs) (Altimus et al., 2008; Berson, 2003; Eacret et al., 2020; Güler et al., 2008; Richter et al., 2014; Scammell et al., 2017). Light perceived by the eye is the most pervasive environmental factor affecting sleep (Johnson et al., 2018; Turner et al., 2010). Furthermore, eye health has been shown to be inversely associated with sleep disturbances (Altimus et al., 2008; Kessel et al., 2011; Waller et al., 2008). In addition, there is evidence that endogenous opioid peptides and opioid drugs affect retinal signaling (Cleymaet et al., 2019; Dubocovich and Weiner, 1983). Therefore, the retina presents an interesting, and to our knowledge, previously unexplored site of action for opioids to modulate sleep/wake behavior.

The presence of endogenous opioid peptides and opioid receptors in retinal homogenates was shown in many early works (Borbe et al., 1982; Howells et al., 1980; Medzihradsky, 1976; Slaughter et al., 1985; Wamsley et al., 1981). Enkephalins are expressed by retinal amacrine cells, and enkephalins and morphine both inhibit dopamine release in the retina (Brecha, 2004; Dubocovich and Weiner, 1983; Stell et al., 1980). More recent work has confirmed the expression of β-endorphin by cholinergic amacrine cells (Gallagher et al., 2010), as well as the expression of MORs and DORs by dopaminergic amacrine cells (Gallagher et al., 2012) and MORs by ipRGCs (Cleymaet et al., 2019). Interestingly, endogenous β-endorphin in the retina has been implicated in modulating the pupillary light reflex (PLR) through MOR activation (Cleymaet et al., 2021).

PLR is a non-image forming visual function mediated by ipRGCs (Güler et al., 2008). Intravitreal application of MOR-selective antagonist CTAP enhanced PLR in dark-adapted but not in light-adapted retinas (Cleymaet et al., 2021). Therefore endogenous opioids in the retina might be more highly expressed in the dark and play an inhibitory role in PLR, possibly improving vision at night (Cleymaet et al., 2021). This would be consistent with previous reports of circadian regulation of β-endorphin in the brain, with peak expression at night (Jamali and Tramu, 1999; Kerdelhue et al., 1983; Labrecque and Vanier, 1995). Importantly, MOR activation inhibits the firing of ipRGCs, and indeed intravitreal administration of MOR-selective agonist DAMGO inhibited PLR (Cleymaet et al., 2021, 2019). This was consistent with the long-described pupillary effects of opioids (Larson, 2008; Martin, 1967; Murray et al., 1983; Pickworth and Sharpe, 1985). However, PLR was unaffected by DAMGO in mice lacking MORs expressed by ipRGCs (Cleymaet et al., 2021). Together these data suggest that endogenous opioid peptides in the retina modulate PLR by activating the MORs expressed by ipRGCs (Cleymaet et al., 2021, 2019).

Neuromodulatory processes affecting ipRGC activity (i.e. MOR activation) are expected to alter other ipRGC-driven behaviors, such as photoentrainment. In response to light, ipRGCs fire action potentials (Berson, 2003) and release neurotransmitters (glutamate and pituitary adenylate cyclase-activating peptide) through the retinohypothalamic tract onto neurons in the central circadian pacemaker, the suprachiasmatic nucleus of the hypothalamus (SCN) (Hastings et al., 2018). As such, light-evoked firing by ipRGCs increases the firing rate of SCN neurons and promotes sleep in the nocturnal mouse and wakefulness in humans (Altimus et al., 2008; Hastings et al., 2018; Lupi et al., 2008). ipRGCs also modulate sleep/wake behavior in response to acute light/dark exposure via their monosynaptic projections to areas such as the VLPO and

other preoptic areas (Altimus et al., 2008; Hattar et al., 2006; LeGates et al., 2014; Lupi et al., 2008; Zhang et al., 2021). However, no studies have assessed the role of ipRGCs in the modulation of sleep by opioids, nor whether chronic morphine treatment alters circadian sleep/wake cycles via modulation of ipRGCs and/or their projection areas (e.g. SCN, VLPO).

### 1.4 Opioid transport at blood-retina barrier

Beyond the ability of intravitreally injected MOR agonists to modulate ipRGC-driven behaviors (Cleymaet et al., 2021), evidence suggests systemically applied opioid drugs can penetrate the blood-retina barrier (BRB). Morphine and other opioids are routinely detected in human vitreous humor samples to diagnose overdose-related deaths (Fernández et al., 2013; Wyman and Bultman, 2004). In addition, our recent work showed that after an intraperitoneal injection of morphine, the drug is detected in the mouse retina as quickly as 30 minutes later (Bergum et al., 2022a). The drug persists at detectable levels for at least twelve hours, and critically, continues to accumulate to higher levels with repeated morphine administration (Bergum et al., 2022a). Importantly, MOR-expressing ipRGCs are situated in the ganglion cell layer in contact with the vitreous humor, making them liable to opioid modulation throughout a chronic treatment paradigm. This is consistent with opioids modulating PLR via ipRGCs, as described above (Cleymaet et al., 2021; Larson, 2008; Martin, 1967; Murray et al., 1983; Pickworth and Sharpe, 1985). However, our understanding of opioid pharmacokinetics and transport at the BRB is limited.

Movement across the blood-brain barrier (BBB) and/or BRB is regulated by specialized endothelial cells that line blood vessels, as well as the tight junction proteins (e.g. occludin, claudins) between them (Benyamin et al., 2008; Bergum et al., 2022a; Morcos et al., 2001;

Obermeier et al., 2013; Schaefer et al., 2017; Yang et al., 2018). Thus, many large and hydrophobic substrates are actively transported across blood-CNS barriers (Liu and Liu, 2019; Yang et al., 2018). The mechanisms of opioid influx across blood-CNS barriers are still unknown: it is possible they are small enough to passively cross these barriers and/or their influx is facilitated by transporters expressed on the basolateral face of endothelial cells (Liu and Liu, 2019; Yang et al., 2018).

The mechanisms of opioid efflux from CNS tissues back into systemic circulation are much better understood, especially at the BBB. Opioid efflux is primarily mediated by ATP-binding cassette (ABC) transporter proteins (Liu and Liu, 2019; Yang et al., 2018). The ABC superfamily of transmembrane proteins, composed of nearly 50 genes in humans, collectively transports a wide range of molecules (e.g. ions, sugars, peptides) (Dean and Dean, 2002). Of these, *ABCB1* (*Abcb1a*/*Abcb1b* in mice), commonly known as permeability glycoprotein (P-gp), is often considered the most important opioid transporter at the BBB (Dean and Dean, 2002; Gharavi et al., 2015; Liu and Liu, 2019; Yang et al., 2018). It is also the best-studied in terms of morphine transport (Chaves et al., 2017; Dagenais et al., 2001; Inturrisi, 2002; Loscher and Potschka, 2005; Schaefer et al., 2017; Seleman et al., 2014; Xie et al., 1999). P-gp transports morphine and β-endorphin, as well as the morphine metabolites M3G and M6G; the synthetic opioid fentanyl, methadone (used in medication-assisted treatment for opioid use disorder); and MOR-selective agonist DAMGO; but not all classes of opioids (e.g. Leu- and Met-enkephalin, codeine and oxycodone) (Yang et al., 2018). P-gp expression has been shown to be negatively correlated with the efficacy of morphine-induced analgesia, as it limits the penetration of the drug into the brain through its efflux activity (Hamabe et al., 2007; Sanchez-Covarrubias et al., 2014).

Compared to the BBB, we know relatively little about the transport of opioids across the BRB (Chapy et al., 2016; Liu and Liu, 2019; Yang et al., 2018). Several studies have found reduced P-gp function at the BRB compared to the BBB in both rodents (Chapy et al., 2016; Fujii et al., 2014) and humans (Bauer et al., 2017), however these studies have only assessed the non-opioid P-gp substrates quinidine and verapamil. Importantly, ABC transporter expression and function is substrate-, species- and tissue-dependent (Bebawy and Chetty, 2009; Dalla et al., 2022; Robison et al., 2019; Tanaka et al., 2005). Despite evidence that P-gp transports opioids across the BBB and is functional at the BRB, the contributions of ABC transporters at the BRB to opioid pharmacokinetics in the retina are relatively unknown (Bergum et al., 2022a). Since morphine persistence in the eye could modulate ipRGC activity and ipRGC-driven behaviors throughout chronic opioid treatment, it is critical to characterize the mechanisms of morphine transport at the BRB.

The central hypothesis of the current work is that the bioavailability of opioids (i.e. endogenous opioid peptides and/or opioid drugs) in the retina contributes to the modulation of sleep/wake behavior. In Chapter 2, we characterize the role of endogenous opioid signaling through the MORs expressed by ipRGCs in sleep/wake behavior. Concurrent work that assessed the contribution of MORs expressed by ipRGCs to morphine-induced sleep/wake changes (Bergum et al., 2022b) is discussed in Chapter 4. In Chapter 3, we interrogate ABC transporters expressed at the BRB that may underlie morphine persistence in the retina. These data support a potential therapeutic intervention for opioid-induced sleep disturbances via the modulation of opioid transporter (i.e. P-gp) expression, which is discussed in Chapter 4.

# CHAPTER 2: Endogenous opioid signaling in the retina modulates sleep/wake activity in mice[2]

## 2.1 Summary

Circadian sleep/wake rhythms are synchronized to environmental light/dark cycles in a process known as photoentrainment. We have previously shown that activation of β-endorphin-preferring μ-opioid receptors (MORs) inhibits the light-evoked firing of intrinsically photosensitive retinal ganglion cells (ipRGCs), the sole conduits of photoentrainment. Although we have shown that β-endorphin is expressed in the adult mouse retina, the conditions under which β-endorphin is expressed are unknown. Moreover, it is unclear whether endogenous activation of the MORs expressed by ipRGCs modulates the photoentrainment of sleep/wake cycles. To elucidate this, we first measured the mRNA expression of β-endorphin's precursor, proopiomelanocortin (POMC), at various times of day by quantitative reverse-transcription PCR. POMC mRNA appears to have cyclic expression in the mouse retina. We then studied β-endorphin expression with immunohistochemistry and found that retinal β-endorphin is more highly expressed in the dark/at night. Finally, we used telemetry to measure activity, EEG and EMG in freely moving animals to compare sleep/wake cycles in wild-type and transgenic mice in which only ipRGCs lack functional MORs. Results from these experiments suggest that the MORs expressed by ipRGCs contribute to the induction and maintenance of activity in the dark phase in nocturnal mice, via the promotion of wakefulness and inhibition of slow-wave sleep. Together, these data suggest that endogenous β-endorphin activates MORs expressed by ipRGCs to modulate sleep/wake activity via the photoentrainment pathway.

[2] Berezin et al. (2022). Endogenous opioid signaling in the retina modulates sleep/wake activity in mice. *Neurobiol. Sleep Circ. Rhyt.*, 13, 100078. https://doi.org/10.1016/j.nbscr.2022.100078. Reproduced with minor modifications for clarity pursuant to the open access CC-BY-NC-ND license and Elsevier's Author Rights (Appendix C).

## 2.2 Introduction

Sleep is an essential behavior across the animal kingdom, but the regulation of sleep states is complex and therefore not fully understood (Richter et al., 2014; Scammell et al., 2017). Across multiple brain regions, there are several neurotransmitter systems and neuropeptides, such as galanin (Richter et al., 2014) and endogenous opioids (Fratta et al., 1987; Myer et al., 1990), that play a role in the central regulation of sleep processes (Richter et al., 2014; Scammell et al., 2017). In addition, sleep is regulated by numerous physiological and environmental factors. Light is the most pervasive environmental factor influencing sleep cycles: circadian sleep/wake rhythms are synchronized to environmental light/dark cycles (i.e. photoentrainment) (LeGates et al., 2014). A classic experiment showed that the photoreceptors driving photoentrainment are in the eye, but they are neither rods nor cones (Freedman et al., 1999), consistent with the fact that non-light perceptive individuals can remain entrained to the 24-hour day (Czeisler et al., 1995).

Indeed, a series of studies proved that melanopsin-expressing intrinsically photosensitive retinal ganglion cells (ipRGCs) are the sole conduit of photoentrainment (Berson, 2003; Güler et al., 2008). In addition to transmitting light information to the suprachiasmatic nucleus (SCN) (Fernandez et al., 2016), ipRGCs send monosynaptic projections to sleep-promoting centers, such as the preoptic area (Beier et al., 2021; Hattar et al., 2006), to mediate the acute effects of light on sleep (Altimus et al., 2008; Lupi et al., 2008; Zhang et al., 2021). Neuromodulatory processes inhibiting ipRGCs are expected to alter light-evoked behaviors mediated by ipRGCs, such as photoentrainment and/or pupillary light reflex (PLR) (Güler et al., 2008). Our recent work has shown that ipRGCs express μ-opioid receptors (MORs) and that the MOR-selective agonist [D-Ala$^2$, MePhe$^4$, Gly-ol$^5$]-enkephalin (DAMGO) inhibits light-evoked firing by ipRGCs

(Cleymaet et al., 2019). Intraocular injection of DAMGO eliminated PLR triggered by light intensities activating rods and cones, and slowed PLR evoked by bright light sufficient to activate the melanopsin in ipRGCs (Cleymaet et al., 2021). Interestingly, PLR was not inhibited by DAMGO in mice which lacked MORs globally (MKO) or specifically from ipRGCs (McKO), suggesting MORs expressed by ipRGCs are important for mediating the effect of opioids on PLR (Cleymaet et al., 2021). Furthermore, the MOR-selective antagonist D-Phe-Cys-Tyr-D-Trp-Arg-Thr-Pen-Thr-$NH_2$ (CTAP) enhanced rod/cone-driven PLR in dark-adapted retinas, suggesting that endogenous activation of MORs expressed by ipRGCs in the dark inhibits PLR (Cleymaet et al., 2021).

Opioid receptors in the retina have been shown by numerous studies (Borbe et al., 1982; Cleymaet et al., 2019; Gallagher et al., 2012; Medzihradsky, 1976; Slaughter et al., 1985; Wamsley et al., 1981), and of the endogenous opioid peptides, enkephalins have been detected in amacrine cells of guinea pig (Altschuler et al., 1982) and β-endorphin in a subset of cholinergic amacrine cells of mice (Gallagher et al., 2010). Endogenous opioid peptides are cleaved from larger precursor proteins (Russo, 2017), for example, proopiomelanocortin (POMC) can give rise to β-endorphin as well as non-opioidergic products, such as adrenocorticotropic hormone (ACTH) and α-melanocyte stimulating hormone (α-MSH) (Burbach, 2010; Cawley et al., 2016). However, in the inner retina only β-endorphin, not ACTH nor α-MSH (Gallagher et al., 2010), was detected, consistent with the notion that POMC processing is both cell- and tissue-specific (Bicknell, 2008).

Taken together, there is strong evidence for expression of the endogenous opioid β-endorphin in the adult mammalian retina (Gallagher et al., 2010) and for the activation of β-endorphin-preferring MORs in modulating ipRGC function (Cleymaet et al., 2021). However, it

is not known under what conditions retinal β-endorphin is expressed, nor have the neuromodulatory effects of endogenous β-endorphin in the mammalian retina been studied. Accordingly, the aim of the current investigation was two-fold: (1) determine if light exposure and/or circadian timing influences β-endorphin expression in the adult mouse retina, and (2) examine if endogenous β-endorphin signaling in the retina contributes to the photoentrainment of sleep/wake behavior in the nocturnal mouse via MORs expressed by ipRGCs.

## 2.3 Materials and Methods

### *2.3A Animals*

Wild-type (WT) C57BL/6J mice were purchased from Jackson Laboratories, Bar Harbor, ME (strain #000664). Mice with Cre recombinase expressed upstream of the melanopsin (*Opn4*) promoter [Tg(*Opn4*-cre)SA9Gsat/Mmucd, #036544-UCD; *Opn4*-cre] were purchased from the Mutant Mouse Resource and Research Center (MMRRC) at the University of California at Davis. These *Opn4*-cre mice were backcrossed into a 100% C57BL/6J background prior to purchase and maintained as hemizygotes (*Opn4*-cre +/-). McKO mice, in which only ipRGCs lack functional MORs, were generated as described previously (Cleymaet et al., 2021; Weibel et al., 2013). In brief, *Oprm1*$^{fl/fl}$ breeders (Jackson Labs strain #030074) were generously provided by Dr. Brigitte Kieffer (Douglas Research Center, McGill University). *Oprm1*$^{fl/fl}$ mice have exons 2 and 3 of the MOR (*Oprm1*) gene flanked by a loxP site and were maintained on a 50% C57BL/6J-50% 129Sv background for 5 generations before receipt (Weibel et al., 2013). To establish a 100% C57BL/6J background, *Oprm1*$^{fl/fl}$ mice were backcrossed to WT C57BL/6J mice for ≥10 generations. Finally, *Oprm1*$^{fl/fl}$ and *Opn4*-cre mice were crossed to obtain McKO mice with the floxed *Oprm1* gene on both alleles and *Opn4*-cre on one allele. Mice lacking

functional MORs globally (B6.129S2-*Oprm1*$^{tm1Kff}$/J; MKO) were purchased from Jackson Labs (strain #007559). MKO mice were backcrossed to C57BL/6J mice for at least 12 generations prior to purchase. Adult male and female animals (8-23 weeks) were kept on a 12-hour light:12-hour dark cycle with lights on at 6:00 AM (Zeitgeber time ZT 0), fed standard chow and water ad libitum. Animals were handled in compliance with the Colorado State University Institutional Animal Care and Use Committee and all procedures met the guidelines outlined by the National Research Council's Guide for the Care and Use of Laboratory Animals.

*2.3B Reverse Transcription Quantitative PCR (qRT-PCR)*

**RNA Preparation**

Adult male and female mice were anesthetized with Fluriso (isoflurane, VetOne) and euthanized by cervical dislocation or decapitation. Under RNase-free conditions, retinas were microdissected in 0.1 M phosphate buffered saline (PBS; pH 7.4) then placed in RNAlater solution (Sigma-Aldrich) at 4°C until all samples were collected. Total RNA was extracted using the RNeasy Mini Kit (Qiagen) according to manufacturer's instructions. Briefly, RNAlater solution was washed off by placing the tissue into 0.1 M PBS, then the tissue lysed in Buffer RLT with DTT (GoldBio) by disruption with a micropipette followed by homogenization of the solution by passing it through a 20-gauge needle 5 times. Hypothalami were dissected from the mouse brain and immediately homogenized in Buffer RLT with DTT (GoldBio) by passing it through 20-gauge and 27-gauge needles 5 times each. The lysate was centrifuged, and the supernatant combined with 70% ethanol before being put on the column. After RNA was eluted from the column, the concentration and quality ($A_{260}/A_{280}$) of each sample was assessed using a Nanodrop (ThermoFisher NanoDrop2000 or ThermoFisher NanoDrop Lite). Genomic DNA

(gDNA) was digested using DNase I, RNase-free (ThermoFisher) according to manufacturer's instructions. RNA concentration was again measured using a Nanodrop, and RNA integrity and successful DNase treatment was assessed on a 1% agarose gel. All samples displayed strong 28S and 18S rRNA bands, no gDNA contamination, and no degradation.

**Reverse Transcription**

Reverse transcription of RNA was performed using the GoScript™ Reverse Transcription System (ProMega) according to manufacturer's instructions. 200 ng RNA was used in each reaction and a no-reverse transcription (NRT) control was performed alongside each sample. cDNA was stored at -20°C until used for qRT-PCR amplification.

**qRT-PCR Primer Design**

Primers and probes were designed using Integrated DNA Technologies' PrimerQuest™ Tool. For each target, primers were designed to span an exon-exon junction, have melting temperatures between 60°C and 65°C, have GC content between 45-65%, and be no more than 30 nucleotides long. Probes were designed to have melting temperatures at least 5°C higher than the primers, have GC content between 45-75%, and be no more than 30 nucleotides. Amplicons were required to be shorter than 150 nucleotides. All other parameters were left to the default. The multiplexed primers (500 nM) and probe (250 nM) were resuspended in IDTE buffer (10 mM Tris, 0.1 mM EDTA in $H_2O$) upon receipt then stored at -20°C.

For each primer set, a temperature gradient was used to determine the optimal annealing temperature. Reaction parameters were first determined in singleplex reactions before multiplexing. PCR products from each primer set were run on a 2% agarose gel to assess the

specificity of the primers. For all genes, one clear band was seen with no gDNA contamination or additional products.

In the mouse retina, *β-actin* is a commonly used reference gene (Sawant et al., 2017) and *Tbp* has been shown to be an appropriate reference gene (Adachi et al., 2015). Both genes were stably expressed in all samples. For the *Oprm1* (MOR) experiments, both *Tbp* and *β-actin* were used as reference genes. For the *POMC* experiments, only *Tbp* was used as a reference gene because the cycling requirements for *β-actin* were not compatible with the requirements for *POMC*. Primer and probe sequences can be found in Table 2-1.

**qRT-PCR Protocol**

Reactions were set up using GoTaq® Probe qPCR Master Mix (ProMega) according to manufacturer's instructions, however because our primers and probes arrived multiplexed, only 1

**Table 2-1. Primer and probe sequences for qRT-PCR experiments.**

| **Target** | **Forward Primer (5'-3')** | **Reverse Primer (5'-3')** | **Probe Sequence (5'-3')** | **Notes** |
|---|---|---|---|---|
| Proopiomelanocortin (*Pomc*), NM_001278581.1, transcript variant 1 | GATGCAAGC CAGCAGGT | GATTCTGCT ACAGTCGCT CAG | /6-FAM/ATAGATGT G/ZEN/ TGGAGCTGGTG CCTG/IABkFQ/ | This is the longest transcript of 5 transcripts that produce the same protein and only differ in their 5' UTR. |
| Opioid receptor, mu 1 (*Oprm1*), NM_001304955.1, transcript variant MOR-1U | ACGTGAGGG TGCAATCTA TG | GCAACTGGA TCCTCTCTTC TG | /6-FAM/CTGCCCGT A/ZEN/ ATGTTCATGGC AACC/IABkFQ/ | This is the longest transcript. |
| β-actin (*Actb*), NM_007393.5 | GTCATCCAT GGCGAACTG G | ACTGTCGAG TCGCGTCC | /HEX/CGTTGCCG G/ZEN/ TCCACACCCGC CA/IABkFQ/ | This is the only transcript. |
| TATA box binding protein (*Tbp*), NM_013684.3 | CCATGAAAT AGTGATGCT GGGC | GGGTATCTG CTGGCGGTT T | /HEX/TGCGGTCG C/ZEN/ GTCATTTTCTCC GCAGT/IABkFQ/ | This is the only transcript. |

μL was used and an additional 2 μL of nuclease-free water was added in the total 20 μL reaction mix.

The cycling conditions for *POMC* were as follows: 2 min, 95°C, GoTaq® DNA polymerase activation, then 35 cycles of denaturation (95°C, 15 s) and annealing/extension (63.2°C, 30 s). The cycling conditions for *Oprm1* were as follows: 2 min, 95°C, GoTaq® DNA polymerase activation, then 35 cycles of denaturation (95°C, 15 s) and annealing/extension (57.2°C, 30 s).

Each plate contained a standard curve, run in triplicate, which included three 10-fold dilutions. Every experimental sample was run in triplicate using 2 μL of cDNA. A NRT control and no-template control ($H_2O$ instead of cDNA or RNA; NTC) was included in each run. No amplification was seen in any NRT or NTC controls. Assay plates were prepared in-lab then run on a CFX96 Touch Real-Time PCR Detection System (BioRad).

**Data Analysis**

The CFX Manager™ Software, version 3.1 (BioRad) was used to set the threshold for each reaction (highest $R^2$ just above the background) and to assess the efficiency of the reaction based on the standard curve (90-110%). It was also used to normalize data between plates when samples needed to be re-run or run on multiple plates. In these cases, at least one identical sample was run on each plate and used as an inter-run calibrator. The quantification cycle (Cq) values for each experiment were downloaded as an Excel spreadsheet and the ΔΔCt method was used for analysis (Hellemans et al., 2007; Livak and Schmittgen, 2001). For each gene, the Cq values for all samples in the control group were averaged and used as the reference to calculate relative gene expression (RGE) in each sample. Where multiple reference genes were used, the

geometric mean of those genes' relative quantities was used to calculate RGE (Vandesompele et al., 2002).

*2.3C Immunohistochemistry*

Both adult male and female mice were adapted to the light condition (i.e. light or dark) for at least 2 hours before anesthetization with Fluriso (isoflurane, VetOne) and sacrificed by cervical dislocation. For daytime β-endorphin measurements, mice were sacrificed between ZT 4 and ZT 8. For nighttime β-endorphin measurements, mice were sacrificed between ZT 19 and ZT 20, as indicated by previously reported β-endorphin peak levels in the brain (Jamali and Tramu, 1999; Kerdelhue et al., 1983; Labrecque and Vanier, 1995). In dark-adapted conditions, mice were sacrificed and retinas microdissected under infrared illumination with the aid of OWL Night Vision Scopes (BE Meyers) mounted on Olympus SZ51 stereoscopes to maintain the retina in a fully dark-adapted state. Mice were enucleated and the eyes placed in 0.1 M PBS, then a small incision was made at the ora serrata and the whole eye fixed in freshly prepared 4% paraformaldehyde (PFA) in PBS for 20 min at room temperature (RT). Retinas were then dissected out in PBS and placed in the same fixative solution for an additional 5 min. Retinas were washed 3 × 20 min in 0.1 M PBS at RT, then incubated in a blocking solution (5% serum and 0.5% Triton X-100 in PBS) for 3 hours on a shaker table at RT. Retinas were incubated in primary antibodies diluted in the blocking solution for at least 30 hours on a shaker table at RT (goat anti-choline acetyltransferase 1:200, Millipore; rabbit anti-β-endorphin 1:5000, NHPP-NIDDK). Retinas were then washed (3 × 20 min) in PBS and incubated, either at RT for 4 hours or overnight at 4°C, in the appropriate secondary antibodies. After a final 3 × 20 min wash in

PBS, retinas were mounted on Superfrost Plus microscope slides (Fisher Scientific) in Vectashield Plus Antifade Mounting Medium (Vector Laboratories, Burlingame, CA).

*2.3D RNAscope in situ hybridization*

Adult male and female mice were anesthetized with Fluriso (isoflurane, VetOne) and euthanized by cervical dislocation. Under RNase-free conditions, eyecups were dissected in 0.1 M PBS, fixed in cold 4% PFA for 25 minutes, and immersed in 30% sucrose at 4°C for several days prior to being embedded in Optimal Cutting Temperature (O.C.T.) Compound (Tissue-Tek). The tissue was sectioned at 20 µm on a ThermoFisher CryoStar NX50 cryostat, directly applied to SuperFrost Plus slides (Fisher Scientific), and stored at -20°C until use. The RNAscope Multiplex Fluorescent Assay v2 was performed according to the manufacturer's protocol for fixed-frozen tissue (Advanced Cell Diagnostics, Newark, CA). In brief, after washing off the OCT with PBS, slides were baked at 60°C in the HybEZ Oven (ACDbio) for 30 minutes. Slides were post-fixed in 4% PFA for 15 minutes, then dehydrated in a series of ethanol gradients at room temperature for 5 minutes each (50%, 70%, 100% x2). During pretreatment, slides were boiled in the supplied Target Retrieval reagents for 15 minutes. The probes used were specific to sequences in the *Oprm1* (*Mus musculus* opioid receptor mu 1 #544731) and *Opn4* (*Mus musculus* opsin 4 [melanopsin] #438061-C2) genes. Probes were labelled with Opal dyes 520 and 570 (Akoya Biosciences), respectively. Opal dyes were used at a 1:1500 dilution initially then adjusted according to signal intensity (i.e. increased to 1:1000 for *Oprm1*).

*2.3E Confocal Laser Microscopy*

All images were obtained on a Zeiss LSM 900 confocal microscope (Carl Zeiss, Oberkochen, Germany). For all acquisitions, sequential scans at the different wavelengths were performed. For immunohistochemical experiments performed in whole-mount retinas, tiling was used to capture 1 $mm^2$ images including the center and periphery regions of the retina. Where high-quality images of this size could not be taken in the remaining periphery regions, additional images were at least 300 $\mu m^2$. All images were taken at 0.5 or 1 μm increments through the ganglion cell layer (GCL) and inner nuclear layer (INL) with a 20x air objective. Somas immunopositive for ChAT and β-endorphin in the same optical section were counted manually and totaled using the Cell Counter plugin (De Vos, University of Sheffield) in Fiji (Schindelin et al., 2012). For RNAscope *in situ* hybridization experiments, Z-stack images were taken at 0.5 to 1 μm increments through the full thickness of the sections with a 40x oil-immersion objective. Quantitative analysis was performed on projections of all Z-stacks using Fiji (Schindelin et al., 2012).

*2.3F Surgery & Telemetry Recordings*

Adult male WT and McKO mice were surgically implanted with mini-telemetry transmitters (HD-X02, DSI) as previously described (Locklear, 2020; Zhang et al., 2021). In brief, mice were deeply anesthetized with isoflurane (5%) and fitted with a nose cone for continuous isoflurane delivery (1-5%). Core body temperature and respiratory rate were monitored throughout surgery. Transmitters were subcutaneously inserted in the dorsal abdomen, electromyogram (EMG) leads were inserted into the cheek muscles, and electroencephalogram (EEG) leads were placed into holes drilled into the skull (1.0 mm posterior to bregma, 1.0 mm

left of midline; 2.0 mm posterior to bregma, 1.0 mm right of midline). A screw was drilled into the skull (2.5 mm posterior to bregma, 1.0 mm left of midline), and dental acrylic was used to adhere the leads to the skull and the screw. After the incisions were sutured, mice received an injection of the non-steroidal anti-inflammatory drug (NSAID) OstiLox (3 mg/kg meloxicam, VetOne) and their status was recorded every 5 minutes for the first 30 minutes post-surgery. Mice continued to be monitored for 3 days in separate cages under a standard 12-hour light:12-hour dark cycle with lights on at 7:00 AM (ZT 0). After recovery, each cage was placed on a receiver (DSI), which relayed the telemetry signals to a computer for recording.

**Activity Measurements**

The implanted transmitters recorded the x-y movement of WT and McKO mice in their cages for at least 4 days continuously. Activity, measured in arbitrary units, was recorded each minute. Mice were considered inactive when no x-y movement was recorded during that minute. Data analysis was performed using the *Rethomics* set of R packages, a framework for high-throughput behavioral analysis (Geissmann et al., 2019).

**Sleep/Wake Measurements**

The implanted transmitters recorded activity, EEG and EMG data from WT and McKO mice for at least 3 days continuously. Artifacts in recording were minimized in Neuroscore software (DSI) using Nan Substitution of the previously recorded value. Wake, slow-wave sleep (SWS), or paradoxical (REM) sleep were scored automatically by the software in 10-second epochs. In brief, wake is characterized by low-amplitude EEG and high-amplitude EMG/activity,

SWS by high-amplitude EEG and low-amplitude EMG/activity, and REM sleep by low-amplitude EEG and low-amplitude EMG/activity (Borniger et al., 2013; McDowell et al., 2014).

*2.3G Statistical Analysis*

Statistical tests were performed in either R (version 4.1.2) or SigmaPlot (version 11.2). For all tests, $p<0.05$ was considered significant. The qRT-PCR data was analyzed by t-test (McKO validation in retina) or ANOVA (POMC measurements, McKO validation in retina/hypothalamus), immunohistochemical data analyzed by multivariate ANOVA, and RNAscope data analyzed by t-test. The behavioral data were analyzed by ANOVA in most cases, except for the whole-day sleep/wake recordings which were analyzed by the non-parametric Wilcoxon rank-sum test due to non-normality and non-homogenous variance of the data. ANOVAs were followed by Tukey-adjusted post-hoc pairwise comparisons. Where multiple measurements were made from the same mouse (e.g. qRT-PCR in the retina and hypothalamus; behavioral experiments) a linear mixed effects model was fit to the data.

**2.4 Results**

*2.4A POMC mRNA expression in the retina appears to have cyclic variation across the day*

Some evidence suggests that *POMC* mRNA is more highly expressed at night in the rodent hypothalamus, particularly in the arcuate nucleus (Agapito et al., 2014; Chen et al., 2004; Orozco-Solís et al., 2011; Steiner et al., 1994). POMC expression is known to be region- and tissue-specific (Bicknell, 2008), and to our knowledge, no studies have assessed changes in *POMC* mRNA throughout the day in the mammalian retina. Thus, we used quantitative reverse-transcription PCR (qRT-PCR) to quantify *POMC* mRNA in the retina and hypothalamus of male

WT mice sacrificed at the midpoint of the light phase [Zeitgeber time (ZT) 6, n=5] or the dark phase (ZT 18, n=5). At ZT 18, mice were sacrificed and the retinas dissected under infrared illumination to maintain the animals in a dark-adapted state. The expression of *POMC* in each sample, relative to the reference gene *Tbp*, was calculated using the retina samples at ZT 6 as the control group. Relative gene expression values were log-transformed to satisfy the assumptions of ANOVA. We found that there was a significant interaction of light condition and tissue type ($F_{1,8}$=11.17, $p$=0.0102, ANOVA). In the retina, there was significantly less *POMC* mRNA at ZT 6 compared to ZT 18 (t(15.7)= -3.025, $p$=0.0082; Figure 2-1a). At ZT 6, *POMC* expression in the hypothalamus was about 60-fold higher than in the retina (4-fold on the log scale, t(8)=18.609, $p$<0.0001; Figure 2-1b, Figure 2-2). At ZT 18, *POMC* expression in the hypothalamus was about 40-fold higher than in the retina (3-fold on the log scale, t(8)=13.883, $p$<0.0001; Figure 2-1b, Figure 2-2). Interestingly, we did not find that *POMC* mRNA in the hypothalamus was different between ZT 6 and 18 (t(15.7)=1.362, $p$=0.1924; Figure 2-1b).

We wanted to elicit further information on potential cyclic variations in *POMC* mRNA expression in the mouse retina, so we sacrificed male WT mice every 8 hours [ZT 2 (n=6), ZT 10 (n=6), and ZT 18 (n=5)] (Figure 2-1c). Sample collections at ZT 18 were again performed under infrared illumination in accordance with the light-dark cycle. In this experiment, we found that the time-of-day was not a significant predictor of retinal *POMC* mRNA expression ($F_{2,14}$=0.047, $p$=0.95, ANOVA). Thus, there were no significant differences in the average relative expression of *POMC* between samples obtained at ZT 2 (1.01 ± 0.43), ZT 10 (1.06 ± 0.38), nor at ZT 18 (1.09 ± 0.52) (Figure 2-1c). This data suggests that *POMC* mRNA in the retina could have an

ultradian (i.e. less than 24-hour cycle) rhythm, possibly consisting of 8-hour cycles of expression with peaks at ZT 2, 10 and 18 (Figure 2-1d).

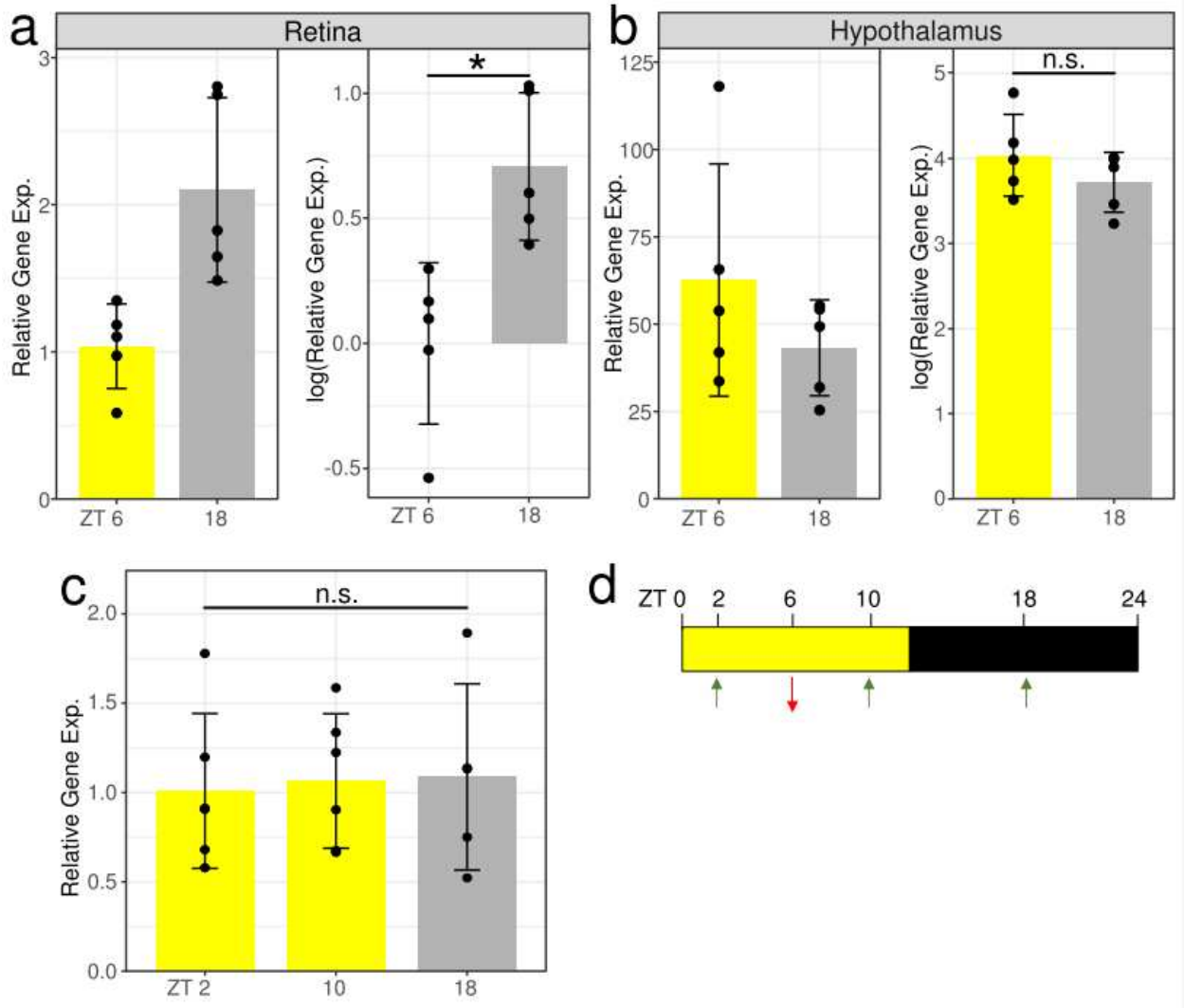


**Figure 2-1. *POMC* mRNA in the retina appears to have cyclic variation across the day.** (**a, b**) Male WT mice were sacrificed in the middle of the light phase (Zeitgeber Time ZT 6, n=5) or dark phase (ZT 18, n=5). *POMC* mRNA in the retina and hypothalamus (relative to the reference gene *Tbp)* was measured by quantitative reverse-transcription PCR (qRT-PCR) with ZT 6 retinas as the control group. Relative gene expression values (left) were log transformed (right) to satisfy the assumptions of ANOVA. (**a**) *POMC* mRNA is significantly higher in the retinas of mice sacrificed at ZT 18 than ZT 6 (* $p$=0.0082). (**b**) There was not a significant difference in hypothalamic *POMC* mRNA between ZT 6 and 18 ($p$=0.1924). (**c**) *POMC* mRNA was quantified in WT retinas collected every 8 hours (ZT 2 n=6, ZT 10 n=6, ZT 18 n=5). The time of sacrifice was not a significant predictor of *POMC* expression (p=0.95, ANOVA), and there were no significant differences in relative *POMC* expression in any of the three groups. All bars represent mean ± s.d. Yellow bars indicate light adaptation, while grey bars indicate dark adaptation. (**d**) Summary of results, where arrows indicate the relative expression of *POMC* mRNA at each timepoint.

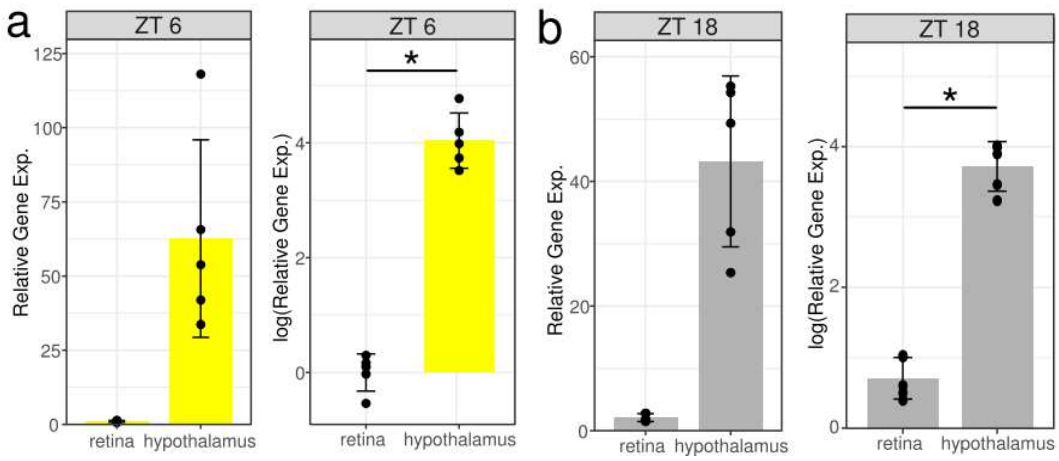


**Figure 2-2. *POMC* mRNA expression in the mouse retina is significantly lower than in the hypothalamus.**
(**a**) At ZT 6 (noon), relative *POMC* mRNA expression, quantified by qRT-PCR, is about 60-fold higher in the hypothalamus compared to the retina (* $p<0.0001$). (**b**) At ZT 18 (midnight), *POMC* expression in the hypothalamus is about 40-fold higher than in the retina (* $p<0.0001$). (**a, b**) Relative gene expression values (left) were log-transformed (right) to satisfy the assumptions of ANOVA. Bars represent mean ± s.d. Yellow bars indicate light adaptation, while grey bars indicate dark adaptation.

*2.4B β-endorphin protein expression is regulated by circadian and light-driven mechanisms*

In our original study of POMC and β-endorphin expression in the retina (Gallagher et al., 2010), we found that more cells expressed POMC-DsRed signal than β-endorphin. This could be explained by the POMC-DsRed signal being maintained even when β-endorphin is broken down and undetectable by immunohistochemistry, or by β-endorphin expression being rhythmic as it is in other rodent brain regions (Jamali and Tramu, 1999; Kerdelhue et al., 1983; Labrecque and Vanier, 1995). In this study, we tested the hypothesis that β-endorphin expression is dependent on light condition and/or circadian time-of-day using immunohistochemical experiments. In the mouse retina, β-endorphin is expressed by a subset of cholinergic amacrine cells (Gallagher et al., 2010), which can be reliably labeled by their expression of choline acetyltransferase (ChAT), the rate-limiting enzyme for acetylcholine synthesis. ChAT+ cholinergic amacrine cells can be

found in the inner nuclear layer (INL) and ganglion cell layer (GCL) of the rodent retina (Voigt, 1986), with greater cell numbers in the INL (Whitney et al., 2008).

To assess whether β-endorphin expression in the retina is under circadian and/or light-driven regulation, we quantified the colocalization of β-endorphin immunolabeling with that of ChAT+ somas in four conditions: light-adapted during the subjective day, dark-adapted during the subjective day, dark-adapted during the subjective night, and light-adapted during the subjective night (n=3 mouse retinas/group; Figure 2-3a, c). Representative images of β-endorphin and ChAT immunolabeling are shown in Figure 2-4. We first confirmed that the average numbers of ChAT-immunopositive cells per $mm^2$ across the center and periphery regions of the INL and GCL (980 ± 206 and 842 ± 219, respectively) were comparable to previously published cholinergic amacrine cell densities in C57BL/6J mice (Gallagher et al., 2010; Whitney et al., 2008; Zhang et al., 2005) and not significantly different between groups (Tables 2-2, 2-3). Furthermore, the number of β-endorphin-immunopositive ChAT+ cells per $mm^2$ in the INL and GCL of retinas that were light-adapted during the subjective day (67 ± 11 and 41 ± 13, respectively) were comparable to our original study on β-endorphin expression (Gallagher et al., 2010). The average percentage of ChAT+ cells that expressed β-endorphin appeared to be lowest in mice that were light-adapted during the subjective day (ZT 4-8) in both the INL (7% versus 18-24%) and GCL (5% versus 7-12%). The average number of β-endorphin-immunopositive cells per $mm^2$ was higher in the INL (170 ± 101) than in the GCL (72 ± 35). We have included a representative Video[3] showing each optical section through the GCL, inner plexiform layer (IPL) and INL to demonstrate the quality of the whole-mount preparation and ChAT/β-endorphin labeling in each layer. The expression of β-endorphin in each group was

[3] The video can be viewed in the digital version of Berezin et al. (2022) https://doi.org/10.1016/j.nbscr.2022.100078

compared using a multivariate ANOVA (MANOVA) with the number of β-endorphin+ ChAT+ cells per $mm^2$ of retina in the INL and GCL as two dependent variables, and time-of-day and light condition as independent variables. In this multivariate analysis, light condition and time-

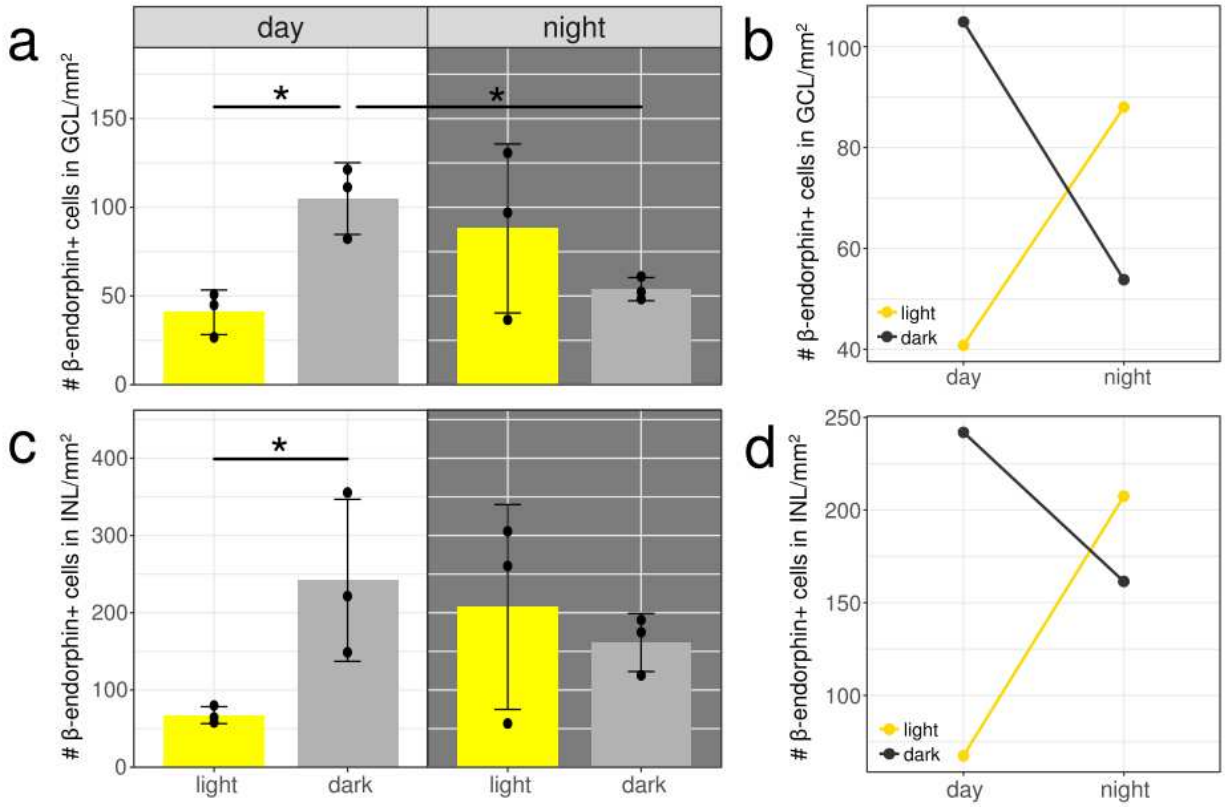


**Figure 2-3. β-endorphin expression in the mouse retina depends on both light condition and circadian time-of-day.**
(**a, c**) Points represent the number of β-endorphin-immunopositive ChAT+ cells per square millimeter of the (**a**) ganglion cell layer (GCL) and (**c**) inner nuclear layer (INL) of each mouse retina (n=3 per group). There were no significant differences in the number of ChAT+ cells in the INL or GCL across all the groups (980 ± 206 and 842 ± 219, respectively). β-endorphin expression is most significantly increased when mice are dark-adapted for 2 hours during the subjective day, but expression levels are generally higher in any samples that are dark-adapted and/or obtained in the subjective night. Bars represent mean ± s.d. * = $p<0.05$ (**b, d**) The interaction of light and time influences β-endorphin expression in both the GCL ($p=0.013$, **b**) and INL ($p=0.059$, **d**). Dark-adaptation is associated with more β-endorphin+ cells in the INL and GCL during the subjective day, but light-adaptation is associated with more β-endorphin+ cells in the subjective night.

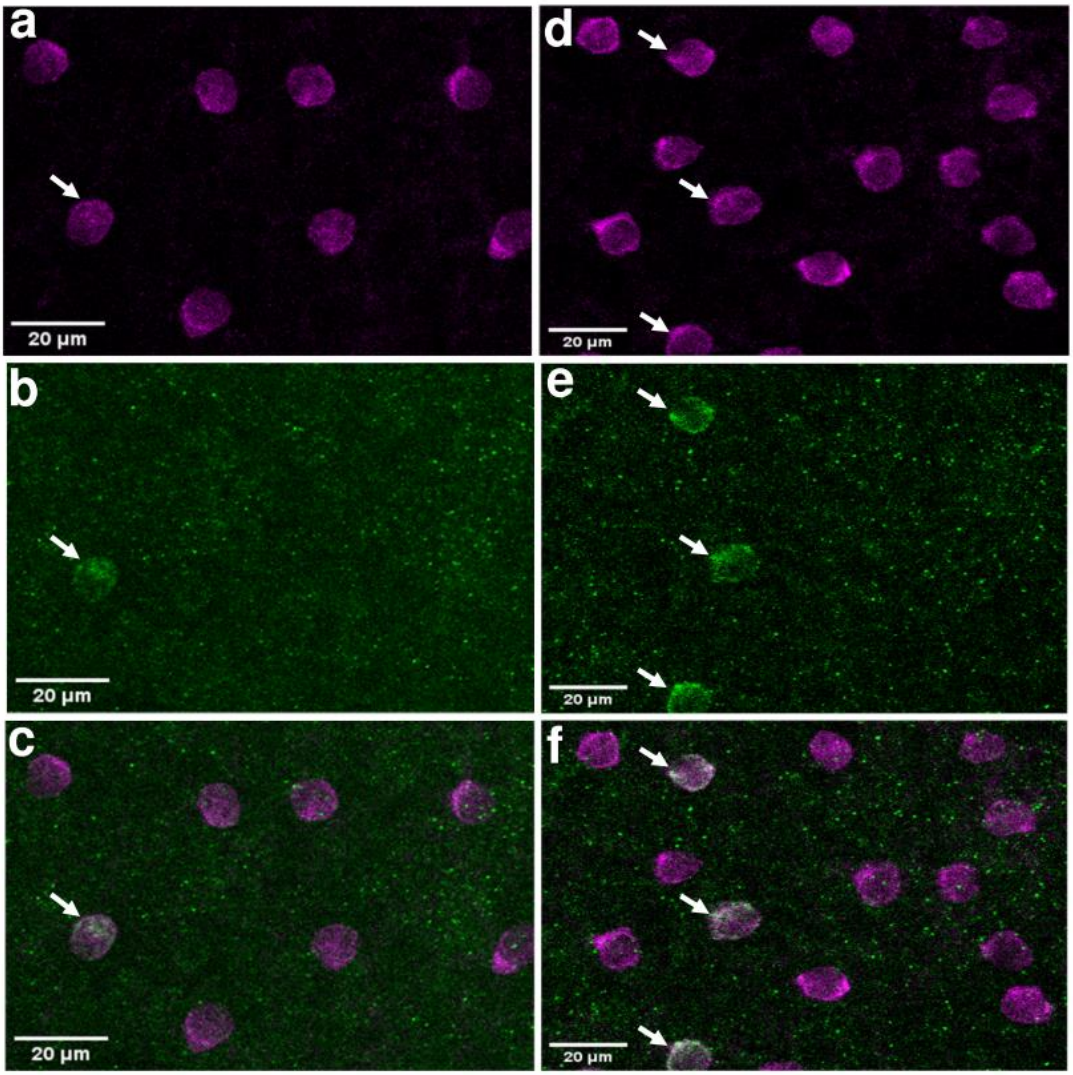


**Figure 2-4. Representative immunolabeling of choline acetyltransferase (ChAT) and β-endorphin in light- and dark-adapted retinas.**
Each image is a maximum projection of all z-stacks containing the cells in the imaged region. (**a**) ChAT expression in the inner nuclear layer (INL) of a light-adapted retina obtained in the daytime. (**b**) β-endorphin expression in the same retina as (**a**). (**c**) Merged composite of (**a**) and (**b**). (**d**) ChAT expression in the inner nuclear layer (INL) of a dark-adapted retina obtained in the daytime. (e) β-endorphin expression in the same retina as (**d**). (**f**) Merged composite of (**d**) and (**e**). Colocalization of magenta and green results in white; arrows indicate β-endorphin+/ChAT+ cells.

of-day were not significant predictors individually ($F_{2,7}$=0.75, $p$=0.51 and $F_{2,7}$=0.83, $p$=0.48, respectively), but the interaction of light condition and time-of-day was a significant predictor of the number of β-endorphin+ ChAT+ cells per mm$^2$ of retina ($F_{2,7}$=4.85, $p$=0.048). Thus, the number of β-endorphin+ ChAT+ cells per mm$^2$ is generally elevated in retinas that are dark-

adapted and/or obtained during the subjective night (Figure 2-3, Tables 2-2, 2-3). We followed up our MANOVA analysis with individual univariate analyses for the INL and GCL. In the GCL, the interaction of light condition and time-of-day ($F_{1,8}$=10.05, $p$=0.013) was again a significant predictor, while light condition ($F_{1,8}$=0.93, $p$=0.36) and time-of-day ($F_{1,8}$=0.02, $p$=0.9) were not. The interaction plot for β-endorphin expression in the GCL shows that while dark-adaptation is associated with more β-endorphin+ ChAT+ cells during the subjective day, light-adaptation is associated with more β-endorphin+ ChAT+ cells during the subjective night (Figure 2-3b). Tukey-adjusted post-hoc comparisons revealed a significant increase in the average number of β-endorphin+ ChAT+ cells per mm2 in the GCL (Table 2-2) in dark-adapted (105 ± 20) versus light-adapted retinas during the subjective day (41 ± 13; t(8)= -2.92, $p$=0.0192) (Figure 2-3a). Furthermore, β-endorphin expression was higher in dark-adapted retinas during the subjective day than during the subjective night (54 ± 6; t(8)=2.33, $p$=0.0482) (Figure 2-3a). Lastly, the difference in the number of β-endorphin+ cells between light-adapted retinas during

**Table 2-2. Summary of ChAT and β-endorphin immunolabeling in the GCL.**

| Light Condition | Time of Day | n | Total ChAT+ cells | Total β-endorphin+ ChAT+ cells | Average ChAT+ cells/mm$^2$ | Average β-endorphin+ ChAT+ cells/mm$^2$ |
|---|---|---|---|---|---|---|
| light | day | 3 | 8795 | 413 | 779 ± 92 | 41 ± 13 |
| light | night | 3 | 12345 | 1191 | 909 ± 453 | 88 ± 48 |
| dark | day | 3 | 13001 | 1504 | 901 ± 121 | 105 ± 20 |
| dark | night | 3 | 11936 | 830 | 781 ± 109 | 54 ± 6 |

**Table 2-3. Summary of ChAT and β-endorphin immunolabeling in the INL.**

| Light Condition | Time of Day | n | Total ChAT+ cells | Total β-endorphin+ ChAT+ cells | Average ChAT+ cells/mm$^2$ | Average β-endorphin+ ChAT+ cells/mm$^2$ |
|---|---|---|---|---|---|---|
| light | day | 3 | 10834 | 767 | 954 ± 123 | 67 ± 11 |
| light | night | 3 | 14180 | 2782 | 1029 ± 438 | 207 ± 133 |
| dark | day | 3 | 14630 | 3416 | 1008 ± 61 | 242 ± 105 |
| dark | night | 3 | 14103 | 2573 | 929 ± 116 | 161 ± 38 |

the subjective night (88 ± 48) and the subjective day was slightly increased (t(8)= -2.15, $p$=0.06) (Figure 2-3a).

Interestingly, in the INL, neither light condition ($F_{1,8}$=1.64, $p$=0.24, ANOVA), time-of-day ($F_{1,8}$=0.35, $p$=0.57), nor the interaction of light condition and time-of-day ($F_{1,8}$=4.84, $p$=0.059) were statistically significant predictors of β-endorphin expression. However, we found that dark-adaptation is associated with increased β-endorphin expression during the subjective day in INL just as it is in the GCL (Figure 2-3d). Moreover, light-adaptation during the subjective night, compared to dark-adaptation, is not as strongly associated with an increase in the number of β-endorphin+ ChAT+ cells in the INL as it is in the GCL, thus the expression of β-endorphin in the INL is relatively similar in both light conditions in the subjective night (Figure 2-3d). Tukey-adjusted post-hoc comparisons revealed a significant increase in β-endorphin expression in dark-adapted (242 ± 105) versus light-adapted retinas during the subjective day (67 ± 11; t(8)=2.46, $p$=0.0392) (Table 2-3, Figure 2-3c). Furthermore, there was a slight increase in the expression in light-adapted retinas during the subjective night (207 ± 133) compared to subjective day (t(8)= -1.98, $p$=0.0835) (Figure 2-3c).

In both the INL and GCL, the light-adapted samples obtained during the subjective day had the lowest average expression of β-endorphin. Changes to the light condition (i.e. dark-adaptation) and/or time-of-day (i.e. sacrificing mice at night) led to increases in the average number of ChAT+ cells that express β-endorphin (Figure 2-3). Notably, dark-adaptation during the subjective day resulted in the largest increase in β-endorphin expression. The expression of β-endorphin in samples obtained in the subjective night, regardless of light condition, tended to be higher than samples light-adapted during the subjective day, despite this difference not being statistically significant. The fact that the expression in dark-adapted samples obtained during the

subjective night is not higher than in the subjective day is consistent with the circadian effect not being statistically significant. Overall, increased β-endorphin expression appears to be associated with acute dark adaptation during the subjective day, or sacrifice during the circadian night phase, periods when nocturnal mice should be active and awake.

### *2.4C Validation of the McKO mouse line*[4]

To test whether endogenous β-endorphin signaling via MORs expressed by ipRGCs influences the photoentrainment of circadian activity in nocturnal mice, we generated a mouse line wherein only ipRGCs lack functional MORs due to the Cre-dependent deletion of exons 2 and 3 (McKO) (Cleymaet et al., 2021; Weibel et al., 2013). In order to validate this McKO mouse line, we used both qRT-PCR and RNAscope *in situ* hybridization. In our qRT-PCR experiments, we quantified *Oprm1* (MOR) mRNA expression in male and female WT (n=6) and McKO (n=5) mice using primers that targeted the deleted region. *MOR* expression relative to the reference genes *Tbp* and *β-actin* was calculated using the average Cq values in the WT group as the control. Retinas from McKO animals had significantly lower *MOR* mRNA expression (0.33 ± 0.2) than retinas from WT mice (1.02 ± 0.2) ($t(8.604)=5.88$, $p<0.001$, T-test; Figure 2-5a). This is consistent with the observation that, in the mouse retina, although MOR expression is not extensive, several cell types are labeled with the anti-MOR antibody, including Brn-3a positive putative ganglion cells, a few GAD67-expressing putative amacrine cells, and dopaminergic amacrine cells (Gallagher et al., 2012). Nonetheless, the present data indicates that MORs expressed by ipRGCs represent a major fraction of retinal MOR expression. Importantly, mice lacking functional MORs globally (MKO) were also generated by the deletion of exons 2 and 3

[4] Additional information regarding the validation of the McKO mouse line can be found in Appendix A.

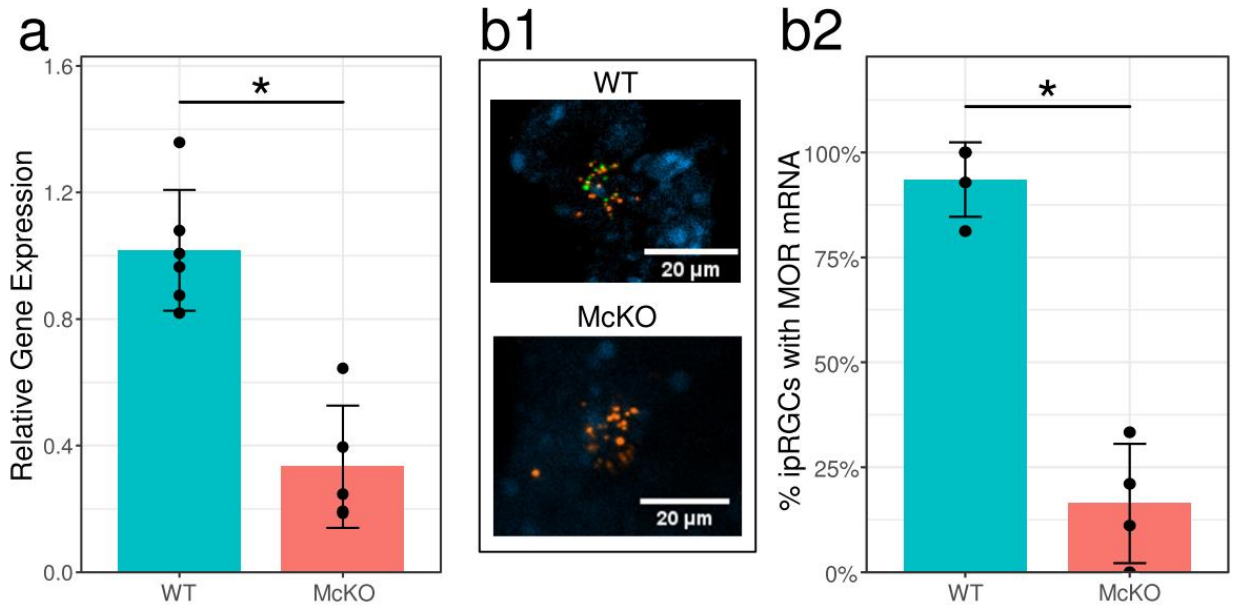


**Figure 2-5. Retinal µ-opioid receptor (MOR) mRNA expression is decreased in McKO mice compared to WT mice.**
McKO mice lack functional MORs only on intrinsically photosensitive retinal ganglion cells (ipRGCs) but retain functional MOR expression in other retinal cells. (**a**) MOR mRNA was measured in total retina extracts from WT (n=6) and McKO (n=5) mice by quantitative reverse transcription PCR (qRT-PCR). Expression was significantly lower in McKO mice (* $p$<0.001). (**b1**) Representative images of RNAscope *in situ* hybridization used to fluorescently label melanopsin (*Opn4*) mRNA expressed by ipRGCs and MOR (*Oprm1*) mRNA. Images are average intensity projections of all z-stacks including these cells. *Opn4* mRNA was labeled with Opal 570 (orange), *Oprm1* mRNA with Opal 520 (green), and cell nuclei with DAPI (blue). (**b2**) Quantification of RNAscope *in situ* hybridization. Fewer ipRGCs express MOR mRNA in McKO mice (n=4) compared to WT mice (n=4) (* $p$<0.001). Bars represent mean ± s.d.

(Matthes et al., 1996), therefore they served as a negative control. Indeed, when we used the same *Oprm1* primers in these MKO mice (n=5), we confirmed that there was no measurable amplification of *MOR* mRNA (data not shown). Furthermore, we quantified *MOR* mRNA in the hypothalamus and retina of WT and McKO mice and found no decrease in MOR expression in the hypothalamus of McKO mice (Figure 2-6). Interestingly, MOR expression was approximately 15-fold higher in the hypothalamus than the retina ($t(7)= -44.412$, $p$<0.0001; Figure 2-6).

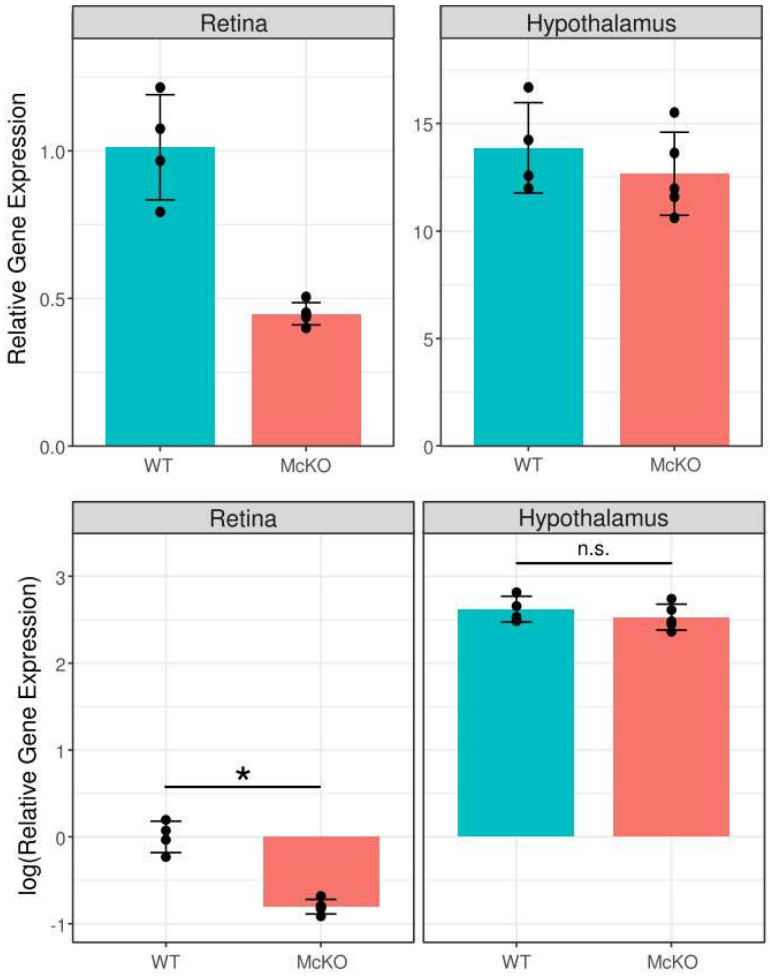


**Figure 2-6. MOR mRNA is not decreased in the hypothalamus of McKO mice.**
MOR mRNA from the hypothalamus and retina of WT and McKO mice was quantified by qRT-PCR. Relative gene expression values (top) were log-transformed (bottom) to satisfy the assumptions of ANOVA. MOR mRNA is significantly decreased in the retina (* = $p$<0.0001), but not hypothalamus, of McKO mice. Note that MOR expression is about 15-fold higher in the hypothalamus than retina ($p$<0.0001). Bars represent mean ± s.d.

Using RNAscope *in situ* hybridization, we visualized melanopsin (*Opn4*) and MOR (*Oprm1*) mRNA (Figure 2-5b1) in male and female WT (n=4) and McKO (n=4) mice with probes that targeted exons 2 and 3 of *Oprm1*, the region deleted in the McKO mouse line and the same region targeted by our qRT-PCR primers. We found a statistically significant decrease in the percentage of *Opn4*+ cells (ipRGCs) that expressed *MOR* mRNA in McKO mice (16% ± 14%) compared to WT mice (94% ± 9%) (t(5.024)= -9.22, $p$=0.00025, T-test; Figure 2-5b2). In

WT mice, the percentage of *Opn4*+ cells which expressed *MOR* mRNA ranged from 81.25% to 100%, while the percentage of *Opn4*+ cells which expressed *MOR* mRNA in McKO mice ranged from 0% to 33.3% (Figure 2-5b2). Our observation that not all *Opn4*+ cells in WT mice express *MOR* mRNA is in line with our previous work on MOR immunoreactivity in ipRGCs. We showed MOR expression in M1-M3 ipRGC subtypes (Cleymaet et al., 2019), but whether M4-M6 subtypes express MORs is unknown (Quattrochi et al., 2019; Schmidt et al., 2011). Furthermore, an incomplete decrease in *MOR* mRNA has previously been shown in the exon 2 and 3-deletion model (Severino et al., 2020; Weibel et al., 2013), and while *MOR* mRNA transcripts lacking exons 2 and 3 may still be transcribed, the coding sequence for the protein is disrupted and the receptor is therefore non-functional (Matthes et al., 1996).

*2.4D Endogenous activation of MORs expressed by ipRGCs modulates activity in the dark*

In order to determine the contribution of MORs expressed by ipRGCs on the photoentrainment of activity cycles, the x-y movement of male WT (n=9) and McKO (n=7) mice was measured by surgically implanted mini-telemetry transmitters (DSI). Each minute, movement (activity) was measured in arbitrary units (a.u.), and the activity measurements from each mouse were then averaged over at least 4 consecutive days (Figure 2-7). Mice were considered inactive if no x-y movement was recorded for the entire minute. Bouts of inactivity (i.e. no x-y movement) lasting longer than 40 seconds are an excellent approximation of sleep, as they show high agreement with estimates of sleep obtained by EEG and EMG recordings (Fisher et al., 2012; Pack et al., 2007). Using longer bouts of inactivity (e.g. 1 minute as here) may underestimate sleep amounts (Pack et al., 2007).

The activity data was analyzed using a linear mixed model with activity or inactivity as the response variable, and genotype and phase as predictor variables grouped by the mouse ID. As expected for nocturnal animals, WT mice displayed more activity in the dark phase (0.18 ± 0.04) than in the light phase (0.06 ± 0.02; t(14)= -7.837, $p$<0.0001, Tukey-adjusted comparisons) (Figures 2-7a, b). Conversely, they spent more time inactive in the light phase (64% ± 6%) than

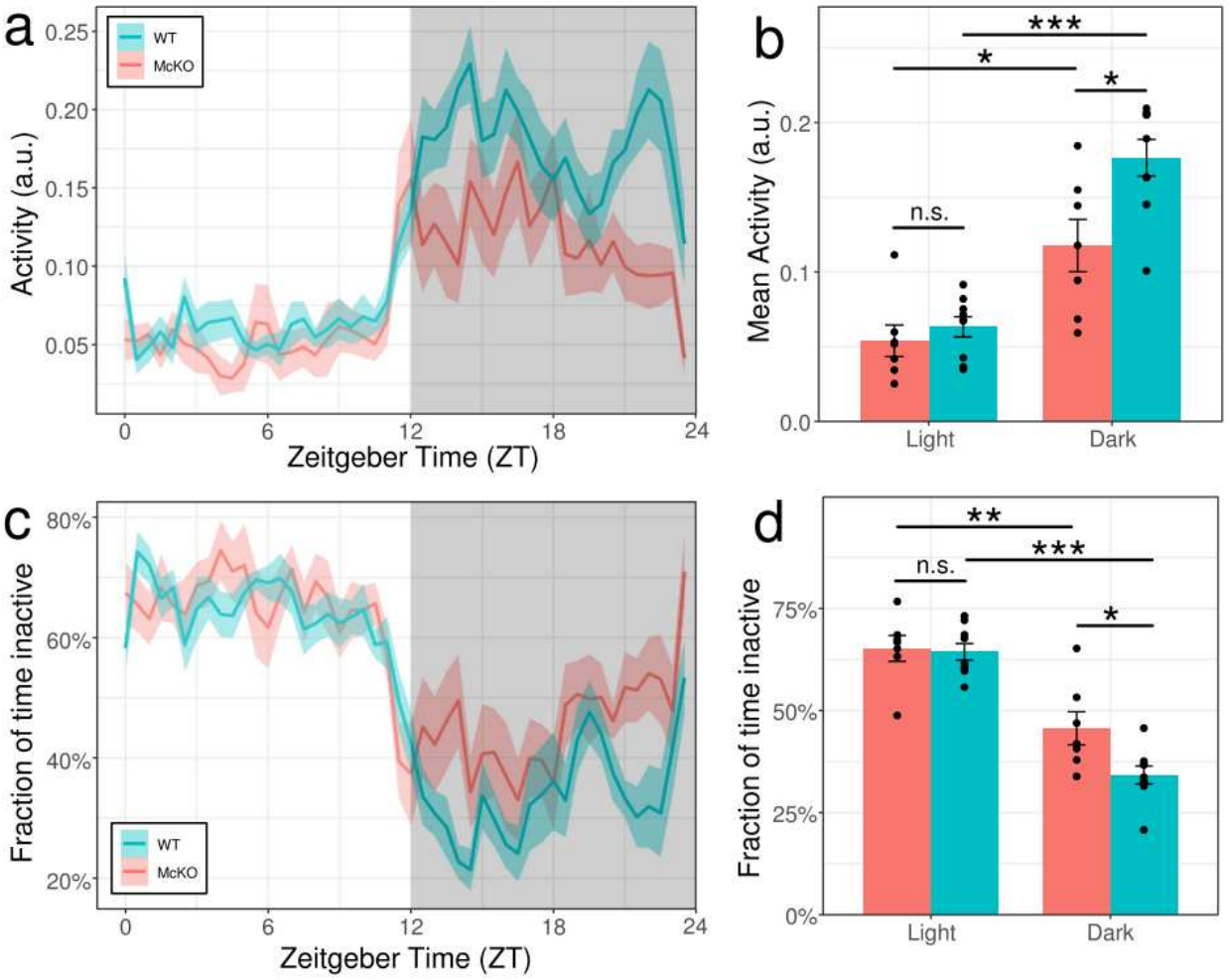


**Figure 2-7. McKO mice are less active in the dark phase than WT mice but retain nocturnal circadian behavior.**
(**a**) Average activity (x-y movement) of all WT (n=9) and McKO (n=7) mice over 24 hours, averaged from recordings across at least 4 days. (**b**) Quantification of the average activity of each individual mouse in the light and dark phases. (**c**) Average fraction of time all WT and McKO mice spent inactive (i.e. no x-y movement for 1 minute) over 24 hours, averaged from recordings across at least 4 days. (**d**) Quantification of the average fraction of time each individual mouse spent inactive in the light and dark phases. Bars represent mean ± s.e. * = $p$<0.01, ** = $p$<0.001, *** = $p$<0.0001

in the dark phase (34% ± 7%; t(14)=8.081, $p$<0.0001) (Figures 2-7c, d). We found that McKO mice retained nocturnal circadian behavior, with higher activity in the dark phase (0.12 ± 0.05) compared to the light phase (0. 05 ± 0.03; t(14)= -3.892, $p$=0.0016) (Figure 2-7a, b). Accordingly, they spent more time inactive in the light phase (65% ± 8%) than in the dark phase (46% ± 11%; t(14)=4.618, $p$=0.0004) (Figure 2-7c, d). Furthermore, the overall pattern of activity/inactivity was similar in both WT and McKO mice, as the onset of activity occurred approximately 30 minutes before the dark phase began in both groups (Figures 2-7a, c).

Despite the preservation of nocturnal circadian behavior, McKO mice were significantly less active (0.12 ± 0.05) than WT mice (0.18 ± 0.04) in the dark phase (t(27.2)= -3.459, $p$=0.0018; Figure 2-7b). Accordingly, McKO mice displayed higher levels of inactivity (46% ± 11%) than WT mice (34% ± 7%) in the dark phase (t(28)= 2.871, $p$=0.0077). Interestingly, in the light phase, there were no significant differences in activity (t(27.2)= -0.55, $p$=0.5868) nor inactivity (t(28)=0.222, $p$=0.8347; Figure 2-7d), suggesting MORs expressed by ipRGCs might play a more important role in modulating nocturnal activity in the dark.

*2.4E Endogenous activation of MORs expressed by ipRGCs modulates healthy sleep/wake*

Although inactivity lasting longer than 40 seconds can approximate sleep (Fisher et al., 2012; Pack et al., 2007), we wanted to perform a more detailed analysis of sleep architecture to determine the contribution of MORs expressed by ipRGCs on the photoentrainment of sleep/wake activity. Male WT (n=10) and McKO (n=9) mice were implanted with telemetry transmitters (DSI) that recorded EEG and EMG as well as x-y movement activity for at least 3 consecutive days. These data were used to classify behavior into 10-second periods of wake, slow-wave sleep (SWS) or paradoxical (REM) sleep. The amount of time in each stage was

totaled and averaged across all recorded days. The amount of artifact was less than 1% of the recorded time for all mice.

The sleep data was analyzed using a linear mixed model with the amount of wake, SWS, or REM sleep as the response variable, and genotype and phase as predictor variables grouped by the mouse ID. As in our activity analysis, our sleep/wake analysis showed that McKO mice retain nocturnal circadian sleep/wake behavior. McKO mice display more wakefulness in the dark phase (54.6% ± 7%) compared to the light phase (22.4% ± 3.5%; t(435)=15.043, $p$<.0001, Tukey-adjusted comparisons), just as WT mice do (56% ± 4.1% and 26.8% ± 3.6%; t(435)=14.387, $p$<.0001) (Figure 2-8a). Furthermore, McKO mice display more SWS during the light phase (70.4% ± 5.8%) than the dark phase (41.4% ± 7%; t(435)= -14.571, $p$<0.0001), as do WT mice (65.5% ± 7% and 39.2% ± 5.6%; t(435)= -13.93, $p$<0.0001). The same pattern is found in REM sleep, wherein levels in McKO mice are higher in the light phase (7.2% ± 3.5%) compared to the dark phase (3.8% ± 1.8%; t(435)= -9.535, $p$<0.0001), just as they are in the WT mice (7.4% ± 4% and 4.4% ± 2%; t(435)= -9.375, $p$<0.0001).

Across the 24-hour day, we found no significant differences between McKO and WT mice in the median amount of wake (37.2% and 40.1%, respectively; Z=0.38, $p$=0.2427), REM sleep (5.9% and 4.3%, respectively; Z=0.24, $p$=0.4598), nor SWS (57.9% and 53.4%, respectively; Z=0.47, $p$=0.1447) using the non-parametric Wilcoxon rank-sum test. However, when analyzing the average amount of wakefulness in each phase by ANOVA, we found that McKO mice spent less time awake (22.4% ± 3.5%) than WT mice (26.8% ± 3.6%) in the light phase (t(56.7)= -2.038, $p$=0.0463, Tukey-adjusted comparisons), but not in the dark phase (54.6% ± 7% and 56% ± 4.1%, respectively; t(56.7)=-0.67, $p$=0.51; Figure 2-8a). Accordingly, there was a slight increase in the amount of SWS in the light phase in McKO (70.4% ± 5.8%)

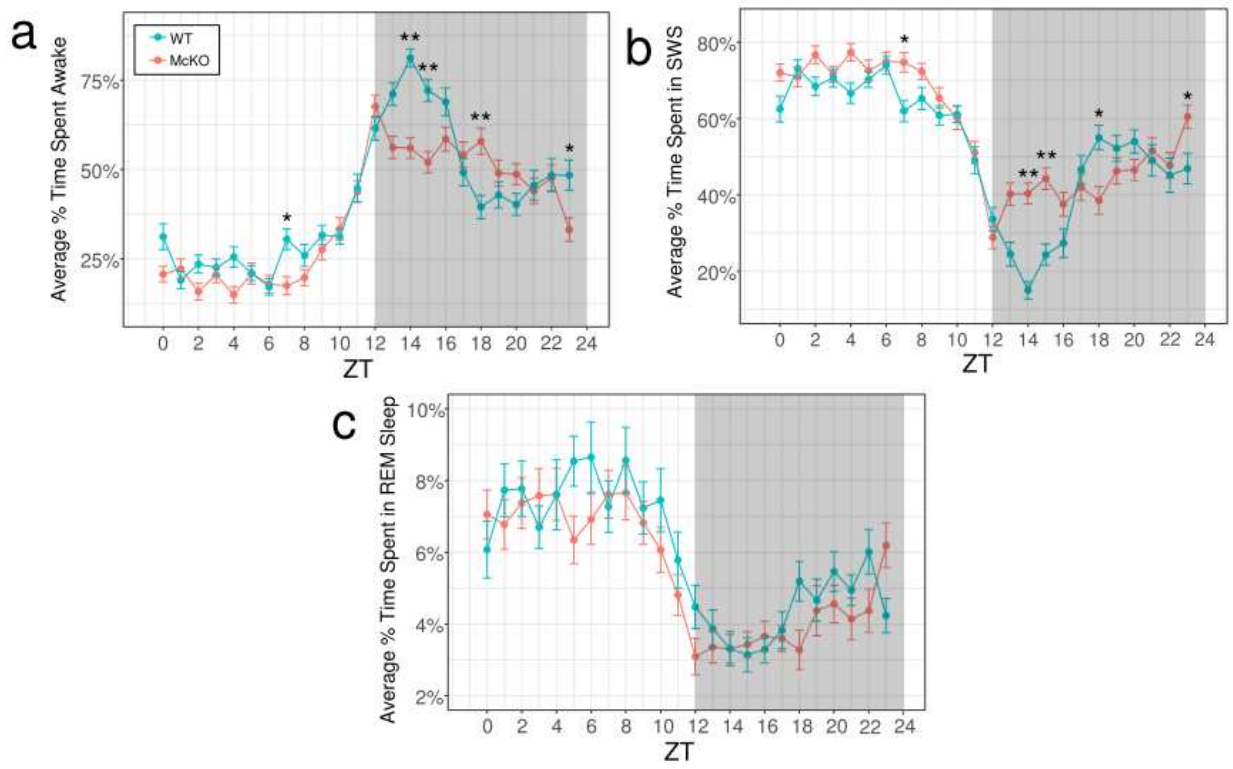


**Figure 2-8. McKO mice have reduced wakefulness and increased slow-wave sleep (SWS) compared to WT mice.**
Sleep/wake architecture based on activity, EEG and EMG recordings from WT (n=10) and McKO mice (n=9) averaged over at least 3 consecutive days. Average percent of time mice spent (**a**) awake, in (**b**) SWS, and (**c**) REM sleep. Grey box indicates the dark phase. Error bars represent mean ± s.e. * = $p<0.05$, ** = $p<0.01$

compared to WT mice (65.5% ± 7%; t(29.1)=1.733, $p$=0.0937), but not in the dark phase (42.4% ± 7% and 39.2% ± 5.6%, respectively; t(29.1)=0.774, $p$=0.4451; Figure 2-8b). Despite no significant differences across the entire dark phase, we found differences in wakefulness and SWS at the level of individual ZTs (Figures 2-8a, 2-8b). Most strikingly, in the dark phase, WT mice experienced a peak in wakefulness of about 81% (ZT 14), while the peak of wakefulness in McKO mice only reached 68% (ZT 12; Figure 2-8a). Furthermore, the lowest amount of SWS in one ZT hour was much lower in WT mice (15% at ZT 14) than in McKO mice (29% at ZT 12; Figure 2-8b). Interestingly, we did not detect any differences in REM sleep between genotypes in either phase or at any ZT (Figure 2-8c).

A detailed analysis of the number and average length of sleep/wake bouts per day in each phase revealed no significant differences between McKO and WT mice (Figure 2-9). Together, these data suggest that McKO mice retain relatively normal nocturnal sleep/wake architecture but do exhibit lower levels of wakefulness compared to WT mice in the light phase and at several time points in the dark phase, which may be related to increased levels of SWS, but not REM sleep.

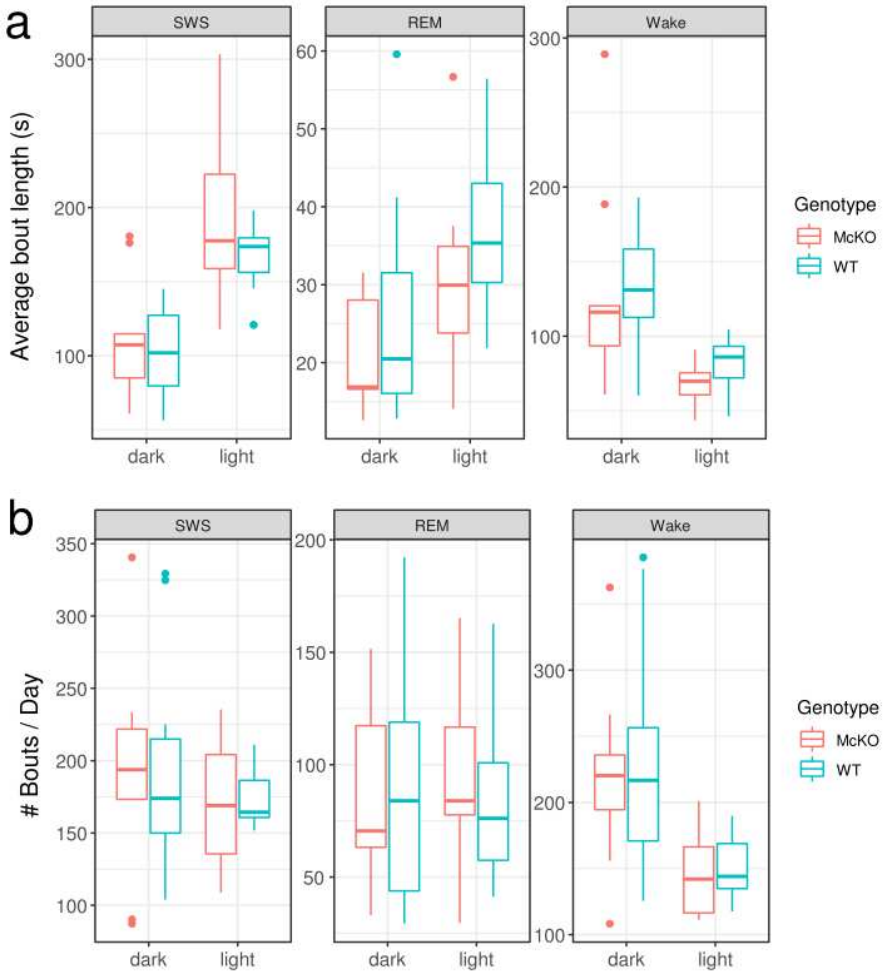


**Figure 2-9. No significant differences exist between McKO and WT mice in terms of (a) average bout length and (b) number of bouts of slow-wave sleep (SWS), paradoxical/rapid eye movement (REM) sleep, and wakefulness.**
Values based on at least 3 consecutive days of activity, electroencephalographic (EEG) and electromyographic (EMG) recordings of WT (n=10) and McKO mice (n=9). There was a slight increase in the average bout length of SWS in the light phase in McKO mice compared to WT mice ($p$=0.07).

## 2.5 Discussion

### *2.5A Regulation of POMC and β-endorphin Expression in the Mouse Retina*

Studies have suggested that *POMC* mRNA is more highly expressed in the rodent brain at night, with most work focusing on the arcuate nucleus (Agapito et al., 2014; Chen et al., 2004; Steiner et al., 1994). Other studies, especially those which measured POMC in the whole rodent hypothalamus, including ours, have failed to uncover such cyclic variation (Lu et al., 2002; Stütz et al., 2007; Xu et al., 1999). This may be consistent with the notion that POMC expression is region-specific (Bicknell, 2008), and thus cyclic variation in particular hypothalamic regions could be masked when using the whole tissue. Furthermore, our data suggests that *POMC* mRNA in the mouse retina might have an ultradian rhythm that peaks in expression every 8 hours. Ultradian gene expression, especially with periods of ~8 h, may be more common than previously thought, but documenting ultradian rhythms is complicated by the need for frequent sampling and the fact that genes can have both circadian and ultradian expression patterns (Ono et al., 2015; van der Veen and Gerkema, 2017).

While cyclic variation in *POMC* mRNA may be sufficient to drive circadian β-endorphin expression, post-transcriptional regulation is also thought to be critical to the production of circadian proteins and several mechanisms have been proposed, particularly the activity of RNA-binding proteins and microRNAs (Chiang et al., 2014; Kojima et al., 2011; Reddy et al., 2006). The mechanisms underlying rhythmic POMC processing and light-driven β-endorphin expression in the retina may also involve changes in the expression and/or activity of the enzymes that cleave POMC into β-endorphin, including prohormone convertase 1/3 (PC1/3), PC2, and Yapsin A (Cawley et al., 2016). Expression of PC1/3 and PC2 in the human retina has been demonstrated (Fuller et al., 2009), but we are not aware of any reports confirming Yapsin A

expression in the retina. Future studies will examine the circadian expression of these enzymes in the mammalian retina.

*2.5B Role of β-endorphin in sleep*

The findings presented in this study implicate retinal β-endorphin in modulating sleep/wake behavior via activation of MORs expressed by ipRGCs in the dark. Most β-endorphin+ cells in the retina are ChAT+ (~80%) and since the identities of the other β-endorphin-expressing in the mouse retina have not been elucidated (Gallagher et al., 2010), they were not quantified here. Future studies should characterize all β-endorphin-expressing cell types in the mouse retina and determine whether circadian timing and/or light condition also affects β-endorphin expression in these populations. Furthermore, while we cannot exclude that retinal β-endorphin also exerts neuromodulatory effects on other MOR-expressing cells in the retina, the behavioral data from our McKO mouse line implicates the activation of MORs expressed by ipRGCs in contributing to the modulation of sleep/wake cycles in mice. We propose this may occur via altered signaling in the photoentrainment pathway (i.e. ipRGCs projecting to the SCN and sleep/wake centers such as the preoptic area).

Increased retinal β-endorphin expression during the active (i.e. dark) phase of nocturnal mice appears to coincide with the existing body of literature regarding β-endorphin's role in sleep/wake behavior (Pilozzi et al., 2021). Early studies showed intraventricular injection of β-endorphin led to increased arousal in cats (King et al., 1981) and rats (Riou et al., 1982). In rats, sleep deprivation is associated with increased plasma β-endorphin levels (Przewlocka et al., 1986), and administration of β-endorphin increases the latency to sleep while MOR-selective antagonist naloxone reduces sleep latency (Fratta et al., 1987). In humans, β-endorphin levels are

elevated in the cerebral spinal fluid of children with sleep apnea, and the opioid receptor antagonist naltrexone is an effective treatment (Myer et al., 1990).

Despite evidence that β-endorphin acting on MORs is associated with changes in sleep/wake activity in model organisms as well as humans, how endogenous β-endorphin may modulate sleep/wake behavior is not currently well understood. The data presented in this study implicate β-endorphin in modulating natural sleep/wake processes via the activation of MORs expressed by ipRGCs. We propose that increased β-endorphin expression in the dark may inhibit the spontaneous firing activity of ipRGCs (Zhao et al., 2014) through increased endogenous activation of MORs (Cleymaet et al., 2019) in order to promote wakefulness in the nocturnal mouse.

*2.5C Activity vs. Sleep/Wake Measurements*

Our activity and sleep/wake analyses provided similar, though not identical, results. In general, we found that McKO mice exhibited less activity/wakefulness and more inactivity/SWS compared to WT mice. In our activity analysis, we found that McKO mice were less active than WT mice in the dark phase. Although we did not detect any differences in average wakefulness across the dark phase in our sleep/wake analysis, we found a significant decrease in the peak in wakefulness at the beginning of the dark phase in McKO mice compared to WT mice, which is consistent with our activity data.

Scoring activity based on x-y movement is limited due to its inability to measure movements such as scratching, grooming, and sniffing, where the mouse is awake but not moving around the cage. Additionally, while bouts of inactivity longer than 40s are a good approximation of sleep in mice, bouts of 60 seconds as used here may underestimate sleep

(Fisher et al., 2012; Pack et al., 2007). Conversely, scoring wakefulness not only based on activity but also EEG and EMG recordings provides a nuanced and precise determination of sleep/wake state (e.g. SWS or REM) as well as precise calculations of bout length. Thus, while our activity analysis only uncovered a difference between McKO and WT mice in the dark phase, our sleep/wake analysis uncovered differences in both the light and dark phases. Importantly, this analysis revealed that changes in McKO sleep/wake behavior may stem from changes in SWS, but not REM sleep. It is worth noting that our sleep analysis, like our activity analysis, is limited in its ability to quantify stationary behavior. Thus, while increased SWS contributes to the decreased activity in McKO mice, changes to stationary or anxiety behavior may also play a role.

*2.5D Proposed mechanism of MORs expressed by ipRGCs modulating sleep/wake behavior*

Light-evoked ipRGC firing activity (Berson, 2003) is known to induce sleep in nocturnal mice, while exposure to darkness induces wakefulness in an ipRGC-dependent manner (Altimus et al., 2008). It has been theorized that ipRGCs continuously signal the presence of light to the brain in the absence of a repression of signaling (Altimus et al., 2008; Schmidt et al., 2011). This could be supported by evidence that ipRGCs exhibit spontaneous activity in the dark (Zhao et al., 2014) and their membrane potential in the dark is near their spike threshold (i.e. the small depolarization caused by the adsorption of a single photon can increase their spiking rate several-fold) (Do et al., 2009). Thus, endogenous activation of the MORs expressed by ipRGCs in the dark, when mice should be awake, may serve to inhibit spontaneous ipRGC firing. In doing so, it might prevent ipRGC spiking activity which would otherwise be interpreted by the brain as a signal for light and therefore prevent the induction and maintenance of sleep.

The firing activity of ipRGCs is directly communicated to the suprachiasmatic nucleus (SCN), the master regulator of circadian rhythms, via the retinohypothalamic tract (RHT). Light stimulates neurotransmitter release through the RHT to the SCN and increases the firing rate of SCN neurons in both nocturnal and diurnal organisms, although the behavioral responses to SCN activation (i.e. sleep or wake) differ (Hastings et al., 2018). Photoentrainment, the alignment of circadian sleep/wake cycles to environmental light/dark cycles, requires ipRGC innervation to the SCN (Güler et al., 2008). Circadian rhythms in the SCN are thought to be maintained by cells in the eye - presumably ipRGCs due to their direct projections to the SCN (Fernandez et al., 2016) - even in the absence of light (Lee et al., 2003). This supports our assertion that, in the dark, inhibition of ipRGC firing via activation of their MORs could contribute to circadian rhythms of sleep/wake activity.

Furthermore, modulation of ipRGC activity by β-endorphin activating MORs expressed by ipRGCs may also influence sleep/wake activity through projections to the preoptic area (POA), including the ventrolateral preoptic nucleus (VLPO). Although the ipRGC-SCN circuit is necessary for circadian regulation of sleep/wake, it is not sufficient to induce sleep in response to acute light (Rupp et al., 2019). Recent work showed that ipRGCs, specifically the M1 subtype that comprises most of the input to the SCN (Baver et al., 2008), innervate the POA to a greater extent than previously thought (Zhang et al., 2021). Chemogenetic activation of this ipRGC-POA circuit led to an increase in acute light-induced non-rapid eye movement (NREM) sleep, but interestingly, did not affect REM sleep (Zhang et al., 2021). Conversely, inhibition of the ipRGC-POA circuit inhibits NREM, not but REM, sleep (Zhang et al., 2021). Accordingly, the light-responsive POA neurons necessary for light-induced NREM sleep project to brain regions known to be involved in wakefulness, such as the lateral hypothalamus, but not to regions that

promote or suppress REM sleep, such as the pedunculopontine nucleus or locus coeruleus, respectively (Scammell et al., 2017; Zhang et al., 2021).

Moreover, the VLPO receives input from both ipRGCs and the SCN (LeGates et al., 2014), and VLPO neurons are sometimes referred to as a sleep switch, wherein activation of sleep-promoting VLPO neurons (Sherin et al., 1996) leads to sleep while inhibition of VLPO neurons by wake-active orexin neurons leads to wakefulness (Fuller et al., 2006; Saper et al., 2001). Then, it is tempting to speculate that McKO mice lacking MORs expressed by ipRGCs have less inhibition of ipRGC activity (and therefore less inhibition of VLPO neurons), which may explain the decreased wakefulness we see in these mice. Together, this body of literature suggests that inhibition of ipRGC activity in the dark, by β-endorphin activating MORs expressed by ipRGCs, may be important for inhibiting SCN neurons and sleep-promoting VLPO to lead to wakefulness. Since ipRGCs project to brain regions involved in the regulation of both circadian (e.g. SCN) and acute light-induced (e.g. VLPO) sleep to coordinate photoentrainment, the alterations to sleep/wake behavior in McKO mice might be underscored by changes in multiple ipRGC projection areas.

*2.5E The effect of opioid drugs on sleep/wake*

Both acute and chronic opioid use produce sleep disturbances, which are associated with negative outcomes like depression and increased risk of relapse and dependence (Huhn and Finan, 2021; Tripathi et al., 2020). Sleep disturbances have recently emerged as an important, yet understudied, therapeutic target for improving outcomes for individuals on long-term opioid therapy and medications for opioid use disorder (e.g. methadone) (Huhn and Finan, 2021). Although opioids like morphine have been used for millennia (Brownstein, 1993), the

mechanism by which sleep disturbances occur is not well understood (Tripathi et al., 2020). It is possible that a single opioid dose may have distinct effects from chronic dosing, as is the case with pupillary light reflex (Grace et al., 2010). Acute morphine treatment is thought to promote wakefulness in rats by inhibiting the sleep-promoting neurons of the VLPO (Wang et al., 2013). This mechanism, however, may not explain the persistent and progressive sleep disturbances associated with long-term opioid use.

Long-term opioid users sleep and wake at inappropriate times of day (i.e. insomnia and daytime sleepiness) (Zgierska et al., 2007), which suggests alterations to photoentrainment. Photoentrainment is exclusively mediated by ipRGCs (Güler et al., 2008), which reside in the ganglion cell layer of the retina in contact with the vitreous humor. It is known that opioid metabolites deposit in the vitreous humor of the human eye post-mortem (Fernández et al., 2013; Wyman and Bultman, 2004), and that most opioid drugs exert their effects through MORs (Raynor et al., 1993). As such, the ability of β-endorphin to modulate the photoentrainment of sleep/wake rhythms by activating the MORs expressed by ipRGCs might be disrupted by the deposition of opioid metabolites in the vitreous humor. Moreover, morphine administration in mice abolishes the circadian rhythm of β-endorphin release into the plasma that occurs in response to pain (Rasmussen and Farr, 2003). Therefore, morphine might be able to abolish the rhythmicity of retinal β-endorphin release, thus altering the natural rhythm of sleep/wake cycle modulation by ipRGCs. It is tempting to speculate that if the novel endogenous opioid pathway discussed here is present in human retinas, then one or another of these mechanisms could contribute to opioid-induced sleep disturbances.

## 2.6 Conclusions

The major conclusions of this study are as follows: in the mouse retina, (1) mRNA expression of β-endorphin's precursor *POMC* appears to have a cyclic rhythm, (2) β-endorphin expression is regulated by light-driven and circadian mechanisms such that expression increases in the dark and/or in the subjective night when mice are active, and (3) endogenous opioid signaling through μ-opioid receptors on ipRGCs, perhaps driven by β-endorphin, plays a modulatory role in establishing healthy sleep/wake cycles. This final point was determined using mice with a cell-specific knockout of functional MORs expressed by ipRGCs (McKO). A detailed analysis of sleep architecture showed that McKO mice were awake for less time in both the light and dark phases, and this was associated with an increase in the amount of slow-wave sleep but not paradoxical/rapid eye movement (REM) sleep.

# CHAPTER 3: Morphine pharmacokinetics and opioid transporter expression at the blood-retina barrier of male and female mice[5]

## 3.1 Summary

Opioids are effective analgesics for treating moderate to severe pain, however, their use must be weighed against their dangerous side effects. Investigations into opioid pharmacokinetics provide crucial information regarding both on- and off-target drug effects. Our recent work showed that morphine deposits and accumulates in the mouse retina at higher concentrations than in the brain upon chronic systemic exposure. We also found reduced retinal expression of P-glycoprotein (P-gp), a major opioid extruder at the blood-brain barrier (BBB). Here, we systematically interrogated the expression of three putative opioid transporters at the blood-retina barrier (BRB): P-gp, breast cancer resistance protein (Bcrp) and multidrug resistance protein 2 (Mrp2). Using immunohistochemistry, we found robust expression of P-gp and Bcrp, but not Mrp2, at the inner BRB of the mouse retina. Previous studies have suggested that P-gp expression may be regulated by sex hormones. However, upon acute morphine treatment we found no sex differences in morphine deposition levels in the retina or brain, nor on transporter expression in the retinas of males and females with a high or low estrogen:progesterone ratio. Importantly, we found that P-gp, but not Bcrp, expression significantly correlated with morphine concentration in the retina, suggesting P-gp is the predominant opioid transporter at the BRB. In addition, fluorescence extravasation studies revealed that chronic morphine treatment did not alter the permeability of either the BBB or

[5] Berezin et al. (2023). Morphine pharmacokinetics and opioid transporter expression at the blood-retina barrier of male and female mice. *Frontiers in Pharmacology, Drug Metabolism and Transport, 14.* doi: 10.3389/fphar.2023.1206104. Reproduced with minor modifications for clarity pursuant to the open access CC-BY-NC-ND license (Appendix C).

BRB. Together, these data suggest that reduced P-gp expression mediates retinal morphine accumulation upon systemic delivery, and in turn, potential effects on circadian photoentrainment.

## 3.2 Introduction

Opioid drugs have been used as effective analgesics for acute and chronic pain for thousands of years (Benyamin et al., 2008; Brownstein, 1993; Williams et al., 2013). However, their use can trigger adverse effects including addiction, sleep/wake disturbances and overdose-related death (Benyamin et al., 2008; Huhn and Finan, 2021; Tripathi et al., 2020). To safely use opioid drugs for pain management, it is crucial to elucidate the pharmacokinetics of opioid drugs in their target tissues (Nafziger and Barkin, 2018).

Opioids exert both their desired (i.e. analgesic) and undesired on-target effects through μ-opioid receptors expressed in the central nervous system (CNS) (Benyamin et al., 2008; Pasternak and Pan, 2013; Schaefer et al., 2017; Bergum et al., 2022c). The movement of opioids from the systemic circulation into their CNS targets is restricted by the blood-brain barrier (BBB) and blood-retina barrier (BRB) (Yang et al., 2018; Liu and Liu, 2019). The integrity of these barriers and the transporters contributing to the movement of opioids across them are therefore critical determinants of opioid pharmacokinetics. ATP-binding cassette (ABC) transporters, expressed by the specialized endothelial cells that constitute blood-CNS barriers, are involved in the efflux of a wide range of metabolites, peptides, and drugs, and are key mediators of opioid drug transport (Yang et al., 2018; Liu and Liu, 2019). Importantly, the efficacy of opioid extrusion by different ABC transporters depends on the specific opioid substrates (Miller, 2015; Yang et al., 2018). Permeability glycoprotein (P-gp) is the best-studied

ABC transporter with respect to the prototypical opioid, morphine, and has been considered the most critical for opioid transport in the brain(Xie et al., 1999; Dagenais et al., 2001; Inturrisi, 2002; Loscher and Potschka, 2005; Seleman et al., 2014; Chaves et al., 2017; Schaefer et al., 2017). Nonetheless, others such as breast cancer resistance protein (Bcrp) and multidrug resistance proteins (e.g. Mrp2, Mrp4) may also contribute (Gharavi et al., 2015; Chapy et al., 2016; Yang et al., 2018). Indeed, morphine has been shown to be a substrate for P-gp and Mrps at the BBB, and may also alter the transport activity of P-gp, Mrps, and Bcrp at this barrier (Yang et al., 2018). Furthermore, P-gp and Mrps appear to be involved in the transport of the endogenous opioid peptide, β-endorphin (King et al., 2001; Su, 2002; Su and Pasternak, 2013; Yang et al., 2018).

We recently observed that morphine deposits and accumulates in the mouse retina at higher concentrations than the brain following systemic administration (Bergum et al., 2022a). Using quantitative reverse transcription PCR (qRT-PCR) we also found that P-gp mRNA expression is significantly lower in the retina than the brain (Bergum et al., 2022a). These findings are consistent with reports of reduced P-gp function at the BRB compared to the BBB in both rodents (Fujii et al., 2014; Chapy et al., 2016; Liu and Liu, 2019) and humans (Bauer et al., 2017). Despite evidence that P-gp transports opioids across the BBB and is functional at the BRB, the contributions of ABC transporters at the BRB to opioid pharmacokinetics in the retina are relatively unknown (Bergum et al., 2022a).

Furthermore, basic and preclinical research studies have only recently begun to examine the role of sex (i.e. biological sex, estrus/menstrual cycle, and sex hormones) on drug pharmacokinetics and pharmacodynamics. These studies are essential as women experience chronic pain with greater frequency and duration compared to men (Bartley and Fillingim,

2013). In rodents, males are more responsive to opioid-induced analgesia compared to female mice (Candido et al., 1992; Gabel et al., 2021). While this effect has been primarily attributed to sex-dependent differences in opioid receptor expression (Loyd et al., 2008; Guajardo et al., 2017), the role of sex/sex hormones on opioid metabolism and pharmacokinetics warrants further research (Gabel et al., 2021). Several studies have suggested that ABC transporter (i.e. P-gp and Bcrp) expression is higher in females than males, particularly in the liver (Piquette-Miller et al., 1998; Tanaka et al., 2005; Suzuki et al., 2006; Shchul'kin et al., 2017). However, efforts to determine how sex differences in transporter expression affect the behavioral outcomes of opioids are complicated by tissue-, substrate- and species-dependent expression and function (Tanaka et al., 2005; Bebawy and Chetty, 2009; Robison et al., 2019; Dalla et al., 2022).

Here, we aimed to characterize which putative opioid transporters (P-gp, Bcrp, and Mrp2) expressed at the inner BRB (iBRB) of male and female mice, and to elucidate their contributions to morphine pharmacokinetics in the mouse retina. We quantified transporter expression and morphine deposition in the retina and brain by qRT-PCR and liquid chromatography-tandem mass spectrometry (LC-MS/MS), respectively, 1 hour after systemic morphine administration. Although the expression of P-gp and Bcrp was higher in female brains than male brains, we found no differences in transporter expression or morphine deposition in the retina between male mice, females with a high estrogen/progesterone ratio (High E/P; proestrus and estrus) and females with a low estrogen/progesterone ratio (Low E/P; metestrus and diestrus). Our results suggest that P-gp and Bcrp, but not Mrp2, are positioned to play a significant role in the transport of morphine at the BRB. In addition, we show that P-gp, but not Bcrp, expression significantly correlates with morphine content in the retina. Furthermore, we found that chronic morphine exposure does not affect BBB or BRB permeability. Thus, the

findings presented here highlight P-gp as a significant regulator of morphine pharmacokinetics, not only at the BBB, but at the BRB of both male and female mice.

## 3.3 Materials and Methods

### *3.3A Animals*

Adult male and female mice (8-26 weeks) were kept on a 12-hour light:12-hour dark cycle with lights on at 7:00 AM (Zeitgeber time ZT 0), fed standard chow and water ad libitum. All animal protocols were approved by the Colorado State University Institutional Animal Care and Use Committee in accordance with the NIH Guide for the Care and Use of Laboratory Animals.

Mice with Cre recombinase expressed upstream of the melanopsin (*Opn4*) promoter [Tg(*Opn4*-cre)SA9Gsat/Mmucd, #036544-UCD; *Opn4*-cre] were purchased from the Mutant Mouse Resource and Research Center (MMRRC) at the University of California at Davis. *Opn4*-cre mice were backcrossed into a 100% C57BL/6J background prior to purchase and maintained as hemizygotes (*Opn4*-cre +/−).

McKO mice, in which only ipRGCs lack functional MORs, were generated as described previously (Weibel et al., 2013; Cleymaet et al., 2021; Berezin et al., 2022; Bergum et al., 2022b). *Oprm1*$^{fl/fl}$ breeders (Jackson Labs strain #030074) were generously provided by Dr. Brigitte Kieffer (Douglas Research Center, McGill University). *Oprm1*$^{fl/fl}$ mice have exons 2 and 3 of the μ-opioid receptor (*Oprm1*) gene flanked by loxP sites and were maintained on a 50% C57BL/6J-50% 129Sv background for 5 generations before receipt (Weibel et al., 2013). *Oprm1*$^{fl/fl}$ and *Opn4*-cre mice were crossed to produce 50% *Oprm1*$^{fl/fl}$ mice and 50% McKO mice with the floxed *Oprm1* gene on both alleles and *Opn4*-cre on one allele. This Mu$^{fl}$/McKO line was maintained on a background containing at least 75% C57BL/6J and 25% 129Sv. Male and

female McKO mice, and their littermate controls, were used for the mass spectrometry and qRT-PCR experiments in the context of morphine treatment. Mice of this mixed background have been used in previously published studies on retinal morphine pharmacokinetics, and the pharmacokinetics of morphine in the retina and the brain were not found to be significantly different between McKO mice and their wild-type (C57BL/6J) counterparts (Bergum et al., 2022b, 2022b).

Mice carrying a bacterial artificial chromosome (BAC) in which the melanopsin (*Opn4*) promoter drives expression of enhanced green fluorescent protein (EGFP) [Tg(Opn4-EGFP)ND100Gsat/Mmucd] were obtained from the Gene Expression Nervous System Atlas (GENSAT) project. These mice are hereafter referred to as *Opn4*::EGFP mice and were maintained on a C57BL/6J background. Untreated male and female *Opn4*::EGFP and *Opn4*-cre mice, and their littermate controls, were used for immunohistochemical and quantitative reverse transcription PCR (qRT-PCR) experiments, as both strains are on the commonly used C57BL/6J background.

*Opn4*-cre mice were crossed to Ai14 (Jackson Labs strain #007914) mice to express tdTomato following *Opn4*-driven Cre-dependent recombination (*Opn4*-cre-tdTomato). *Opn4*-cre-tdTomato mice were on a 100% C57BL/6J background. Male *Opn4*-cre-tdTomato mice, and their littermate controls, were used in the fluorescence extravasation studies. Positive *Opn4*-cre-tdTomato expression in the ganglion cell layer was used to guide the imaging of distinct retinal vasculature layers and did not affect FITC extravasation.

**Estrous staging and grouping**

Vaginal lavage was performed on group-housed female mice each morning for at least one estrus cycle (5+ d). The stage of estrus was determined by cytological evaluation as previously described (McLean et al., 2012). We aimed to group female mice into two groups based on their hormone profiles: females in proestrus and estrus, in which the ratio of estrogen to progesterone is relatively high (High E/P); and females in metestrus and diestrus, in which the estrogen to progesterone ratio is lower (Low E/P). As mice were regularly cycling, the day of sacrifice was determined by the predicted stage(s) needed to secure a large enough sample size in the Low E/P and High E/P groups. Based on our previous qRT-PCR experiments measuring P-gp expression, our target sample size was 5 to achieve 0.95 power to detect a 1.5-fold change with a standard deviation of 0.5.

**Morphine treatment**

Mice were weighed to ensure proper dosing. For acute treatment, mice were injected with a single i.p. dose of 20 mg/kg morphine (Morphine sulfate salt pentahydrate, Sigma-Aldrich Saint Louis, MO, USA; Product Number: M8777, dissolved in sterile saline) at light onset (ZT 0) as previously described (Bergum et al., 2022a). The chronic morphine treatment paradigm consisted of 5 days of twice daily 20 mg/kg morphine (administered at ZT 0 and ZT 12), followed by a final 20 mg/kg i.p. injection at ZT 0 on day 6 of the treatment paradigm (Bergum et al., 2022a).

*3.3B Morphine analysis by Liquid Chromatography tandem-Mass Spectrometry*

**Tissue sample collection: retina, brain, and plasma**

Mice were deeply anesthetized with isoflurane, decapitated, and trunk blood was collected into EDTA-coated tubes (BD Vacutainer K2 EDTA 7.2 mg tube 4.0 mL). Then, the cortex was removed, weighed, and placed in tubes containing 100 µL 0.1 M PBS. Whole retinas were then microdissected from the eyes of each animal and placed in tubes containing 100 µL 0.1 M PBS. Blood was centrifuged and the plasma, brain and retina were stored at –20°C.

**Retina batch preparation**

We prepared retina samples from analysis as previously described (Bergum et al., 2022a). In short, to prepare retina samples for analysis, 10 µL of 10 µg/mL D6-morphine internal standard solution (Morphine-D6 solution, Cerilliant, Round Rock, TX, USA) was added to whole-retina samples and matrix-matched standards. Subsequently, 200 µL ice-cold acetonitrile was added to the retina samples/standards and the samples/standards were sonicated at maximum power (40 kHz) for 30 min using a Branson Bransonic® 5800 Ultrasonic bath (Emerson Electric Co. Saint Louis, MO, USA). Retina samples were then spun down at 14,000 rpm for 5 min, and 100 µL supernatant was added to sample vials containing 200 µL 0.1% formic acid in water and then transferred to autosampler vials fitted with 400 µL glass inserts. The limit of detection was 20 ng/mL morphine.

**Brain batch preparation**

We prepared brain samples from analysis as previously described (Bergum et al., 2022a). To prepare brain samples for analysis, 10 µL of 1 µg/mL D6-morphine internal standard solution

was added to brain samples and matrix-matched standards. Next, brain samples/standards were then homogenized for 10 s using a BeadBug™ 3 Position Bead Microtube homogenizer (Benchmark Scientific, Inc. Sayreville, NJ, USA) in 400 µL ice-cold acetonitrile. Samples were then centrifuged 14,000 rpm for 5 min and supernatant was added to Phenomenex Strata-X-Drug B solid phase columns. Columns were washed with 2 mL 0.1% formic acid in water and 2 mL methanol. Columns were then dried for 10 min prior to elution. Two successive aliquots of a solution containing 50% acetonitrile, 42% methanol, and 8% 7N ammonium in methanol were used to elute samples from the columns. Eluents were collected into a clean glass test tube and dried under nitrogen at 40°C. Dried eluents were reconstituted with 200 µL 95:5% water:acetonitrile and transferred to autosampler vials fitted with 400 µL glass inserts. The limit of detection was 0.2 ng/mL morphine.

**Plasma batch preparation**

We prepared plasma samples from analysis as previously described (Bergum et al., 2022a). To prepare serum samples for analysis, 10 µL of 1 µg/mL D6-morphine internal standard solution was added to serum samples and matrix-matched standards. Serum samples/standards were prepared for solid phase extraction by adding 20 µL zinc sulfate (5% weight/volume), followed by the addition of 300 µL ice-cold acetonitrile to each tube. Samples were then centrifuged 14,000 rpm for 5 min and supernatant was added to Phenomenex Strata-X-Drug B solid phase columns. Columns were washed with 2 mL 0.1% formic acid in water and 2 mL methanol. Columns were then dried for 10 min prior to elution. Two successive aliquots of a solution containing 50% acetonitrile, 42% methanol, and 8% 7N ammonium in methanol were used to elute samples from the columns. Eluents were collected into a clean glass test tube and

dried under nitrogen at 40°C. Dried eluents were reconstituted with 200 µL 95:5% water: acetonitrile and transferred to autosampler vials fitted with 400 µL glass inserts. The limit of detection was 0.5 ng/mL morphine.

**Data Acquisition and Analysis**

Samples were analyzed with an Agilent 1290 UHPLC coupled to an Agilent 6460 triple quadrupole mass spectrometer equipped with an Agilent Jet Stream electrospray ionization. Morphine was chromagraphically separated on a Restek Raptor biphenyl column (3.0 × 50 mm, 2.7 µm) held at 40°C. A sample volume of 10 µL was injected into a mobile phase mixture of 95% water with 0.1% formic acid (A) and acetonitrile with 0.1% formic acid (B). The flow rate of 0.4 mL/min was kept consistent throughout the run time. The mobile phase composition was held at 3% B for 1.5 min, increased to 40% B at 3 min, and finished at 100% B at 4 min. The ionization source conditions used were as follows: positive polarity and nebulizer 40 psi; gas flow of 10 L/min at 320°C; sheath gas flow of 12 L/min at 380°C; capillary voltage of 3750 V; and nozzle voltage of 500 V. The ion transitions monitored were 286.2- > 152 and 128 m/z for morphine and 292.2- > 152 and 128 m/z for D6-morphine. Analytes were confirmed by retention time and the product ion ratio correlation between the sample peaks and corresponding standards (± 20%). The data collection and processing were performed by using Agilent (Santa Clara, CA, USA) Mass Hunter Quantitative software (v.B.08.01). Quantitation was performed with linear regression using seven-point calibration curves from 0.5 ng/mL to 500 ng/mL (for brain and serum) or six-point calibration curves from 5 ng/mL to 1 µg/mL (for retina). These calibration curves were made from matrix (brain, serum, or retina tissue derived from untreated animals)

spiked with morphine standards (Morphine solution, Sigma-Aldrich Saint Louis, MO, USA; Product Number: M-005).

*3.3C Immunohistochemistry*

Procedures were as previously described (Berezin et al., 2022). Mice were anesthetized with Fluriso (isoflurane, VetOne) and sacrificed by cervical dislocation. After enucleation, the eyes were dissected in 0.1 M phosphate buffered saline (PBS; pH 7.4) and fixed in freshly prepared 4% paraformaldehyde (PFA) in PBS. For cryosectioning, eyecups were immersed in 30% sucrose at 4°C for several days prior to being embedded in Optimal Cutting Temperature (O.C.T.) Compound (Tissue-Tek). The tissue was sectioned at 20 μm on a ThermoFisher CryoStar NX50 cryostat, directly mounted on SuperFrost Plus slides (Fisher Scientific), and stored at −20°C until use. For whole-mount preparations, immunohistochemistry was performed immediately following fixation. Both tissue types were subject to antigen retrieval. As previously described (Gallagher et al., 2012), the tissue was incubated in boiling 10 mM sodium citrate in PBS for 15 min followed by incubation in 5% sodium borohydride in PBS for 45 min. The tissue was then incubated in a blocking solution (5% serum and 0.5% Triton X-100 in PBS) for 3 hours on a shaker table at RT. Retinas were incubated in primary antibodies diluted in the blocking solution for 24-36 hours on a shaker table at RT (rabbit anti-P-glycoprotein 1:200, Abcam [EPR10364-57] #ab170904; rat anti-Bcrp 1:50, Enzo [BXP-53] #ALX-801-036; rabbit anti-Mrp2 1:100, Bioss #bs-1092R; mouse anti-occludin 1:250, Invitrogen [OC-3F10] #33-1500). Sections were then washed in PBS and incubated, either at RT for 2 hours or overnight at 4°C, in the appropriate secondary antibodies. After the final washes in PBS, retinas were stained with

DAPI (Advanced Cell Diagnostics, Newark, CA) and mounted in Vectashield Plus Antifade Mounting Medium (Vector Laboratories, Burlingame, CA).

*3.3D Image Analysis*

All images were obtained on a Zeiss LSM 900 confocal microscope (Carl Zeiss, Oberkochen, Germany). For all acquisitions, sequential scans at the different wavelengths were performed. For immunohistochemical experiments performed in whole-mount retinas, four to five ~320 $\mu m^2$ areas of the peripheral retina were imaged. Z-stack images were taken at 1 μm increments, starting with the ganglion cell layer through the apparent end of the retinal vasculature (≥20 μm) with a 20x air objective. For immunohistochemical experiments performed on cryosectioned retinas, five to six Z-stack images were taken per mouse at 1 μm increments throughout the thickness of sections (~20 μm) with a 20x air objective (image size ~320 $\mu m^2$) or 40x oil-immersion objective (image size ~160 $\mu m^2$). Images were denoised using the Despeckle and Remove Outlier (6 pixel radius, threshold=3) functions in Fiji (Schindelin et al., 2012). Colocalization of P-glycoprotein and occludin was determined using Manders' coefficients (Manders et al., 1993) as well as Costes' automatic threshold and randomization procedures (Costes et al., 2004) using the Coloc2 plugin in Fiji (Schindelin et al., 2012). True colocalization was found when Costes' P-value was greater than 95% (Costes et al., 2004).

*3.3E Quantitative Reverse Transcription PCR (qRT-PCR)*

Procedures were performed as previously described (Berezin et al., 2022), with minor modifications described below.

**cDNA Preparation**

Mice received morphine or saline as described in Chapter 3.3A. One hour after the (last) injection (ZT 1), the mice were anesthetized with isoflurane and sacrificed by decapitation. Hypothalamic tissue was dissected from the brain and immediately processed, while retinas were microdissected in 0.1 M phosphate buffered saline (PBS; pH 7.4) and placed in RNAlater solution (Sigma-Aldrich R0901) at 4°C until all samples were obtained. Total RNA was extracted from both tissues using the Extracta Plus RNA Kit (Quantabio, Beverly, MA), which contains a genomic DNA removal column, according to the manufacturer's instructions. Briefly, the tissues were lysed in Buffer EPRL supplemented with DTT (GoldBio, St. Louis, MO, USA). Hypothalamic tissue was homogenized by passing it through a 20 g needle 5 times, followed by a 27 g needle 5 times, then frozen at -80°C until all samples were obtained. Retinal tissue was disrupted with a micropestle and homogenized by passing it through a 20 g needle 5 times. The lysates were centrifuged, and the supernatants combined with 70% ethanol before being put on the column. After RNA was eluted from the column, the concentration and quality (A260/A280) of each sample was assessed using a Nanodrop (ThermoFisher NanoDrop Lite, Waltham, MA, USA). RNA integrity was assessed on a 1% agarose gel. All samples displayed strong 28S and 18S rRNA bands, no gDNA contamination, and no degradation. From each sample, 200 ng RNA was reverse-transcribed into cDNA using qScript cDNA SuperMix (Quantabio, Beverly, MA) according to the manufacturer's instructions. The cDNA was then stored at -20°C until it was used for qPCR amplification.

## Primer Design

Primer sequences against rat *Abcb1a* (P-gp) were previously adapted for use in mouse (Bergum et al., 2022a; Yousif et al., 2008). Primers against *Abcg2* (Bcrp) were adapted from previously published primers used in rat (Yousif et al., 2012). Primers against *Abcc2* (Mrp2) were obtained from previously published sequences (Liu et al., 2018). The probe sequences for P-gp, Bcrp and Mrp2, as well as primer and probe sequences for the reference genes β-actin and Tbp, were designed using Integrated DNA Technologies' PrimerQuest™ Tool. β-actin is a commonly used reference gene that has been used successfully in mouse retina (Sawant et al., 2017), and Tbp has been shown to be an appropriate reference gene for adult mouse retina (Adachi et al., 2015). The primer and probe sequences can be found in Table 3-1.

For primer design using the Integrated DNA Technologies' PrimerQuest™ Tool, primers were designed to span an exon–exon junction, have melting temperatures of between 60°C and 65°C, have a GC content of between 45–65%, and be no more than 30 nucleotides long. Probes were designed to have melting temperatures at least 5°C higher than the primers, have a GC content of between 45–75%, and be no more than 30 nucleotides long. Amplicons were required

**Table 3-1. Primer and probe sequences used for qRT-PCR.**

| Target | Forward Primer Sequence (5'-3') | Reverse Primer Sequence (5'-3') | Probe Sequence (5'-3') |
|---|---|---|---|
| P-gp (*Abcb1a*), NM_011076.3 | CAGCCAGCATTCTCCGTAATA | CCCAAGGATCAGAAACAACA | /56-FAM/CAGCGGCAG/ZEN/AACAGCAACTTGTTT/3IABkFQ/ |
| Bcrp (*Abcg2*), NM_001381927.1 | CAGCAGGTTACCACTGTGAG | CATCACAGCAGAAGAATCTCCA | /56-FAM/CCCTACAAC/ZEN/AACCCTGCGGATTT/3IABkFQ/ |
| Mrp2 (*Abcc2*), NM_013806.2 | GGATAATGAGGCGCCGTGGGT | CCGGCCGATACCGCACTTGA | /56-FAM/CCGACAAGA/ZEN/AGCCTCCGGCAGATT/3IABkFQ/ |
| β-actin (*Actb*), NM_007393.5 | GTCATCCATGGCGAACTGG | ACTGTCGAGTCGCGTCC | /5HEX/CGTTGCCGG/ZEN/TCCACACCCGCCA/3IABkFQ/ |
| TATA box binding protein (*Tbp*), NM_013684.3 | CCATGAAATAGTGATGCTGGGC | GGGTATCTGCTGGCGGTTT | /5HEX/TGCGGTCGC/ZEN/GTCATTTTCTCCGCAGT/3IABkFQ/ |

to be shorter than 150 nucleotides. All other parameters were left as defaults.

Upon receipt, the multiplexed primers (500 nM) and probe (250 nM) were resuspended in an IDTE buffer (10 mM Tris, 0.1 mM EDTA in H2O) upon receipt, then stored at -20°C. PCR products from each primer set were run on a 2% agarose gel to assess the specificity of the primers. For all genes, one clear band was seen with no gDNA contamination or additional products. The reaction parameters were first determined in singleplex reactions before multiplexing. For each primer set, a temperature gradient was used to determine the optimal annealing temperature.

**qRT-PCR Protocol and Analysis**

Reactions were set up using GoTaq® Probe qPCR Master Mix (ProMega) according to the manufacturer's instructions; however, because our primers and probes arrived multiplexed, only 1 µL total was used, and an additional 2 µL of nuclease-free water was added to the total 20 µL reaction mix. The cycling conditions were as follows: 2 min, 95°C, GoTaq® DNA polymerase activation, and then 35 cycles of denaturation (95°C, 15 s) and annealing/extension (63°C, 30 s).

Each plate contained a standard curve run in triplicate, which included three 10-fold dilutions. Every experimental sample was run in triplicate using 2 µL of cDNA. Both reference genes were stably expressed in all samples. In each run, a "no reverse-transcription" control (RNA that was not reverse-transcribed) and no-template control ($H_2O$ instead of cDNA or RNA) was included in each run. No amplification was seen in any negative controls. Assay plates were run on a CFX96 Touch Real-Time PCR Detection System (BioRad, Hercules, CA, USA).

The CFX Manager™ Software Version 3.1 (BioRad, Hercules, CA, USA) was used to set the threshold for each reaction (the highest $R^2$ just above the background) and to assess the efficiency of the reaction based on the standard curve (90-110%). It was also used to normalize the data between plates when samples needed to be re-run or run on multiple plates. In these cases, at least one identical sample was run on each plate and used as an inter-run calibrator. The Cq values for each experiment were downloaded as an Excel spreadsheet and the ΔΔCt method was used for analysis (Hellemans et al., 2007; Livak and Schmittgen, 2001). For each gene, the Cq values for all samples in the control group were averaged and used as the reference to calculate the relative gene expression (RGE) in each sample. Because multiple reference genes were used, the geometric mean of those genes' relative quantities was used to calculate the RGE (Vandesompele et al., 2002).

*3.3F Fluorescence Extravasation Assays*

Male mice received i.p. injections of chronic morphine or vehicle (saline) as described in Section 4.2.1. One hour following the last injection, mice were deeply anesthetized with Fluriso (isoflurane, VetOne) and kept anesthetized by continuous isoflurane delivery via a nose-cone. Mice were transcardially perfused with 10 ml of FITC (fluorescein isothiocyanate, 1 mg/ml, ThermoScientific #46424) or FITC-Dextran (fluorescein isothiocyanate dextran 10 kDa, 0.5 mg/ml Fisher Scientific #F0918100MG) dissolved in PBS (0.1 mg/ml) at a rate of 4 ml/min using a syringe pump (New Era Pump Systems NE-300). Mice were then perfused with 15 ml of 4% PFA in PBS. The eyes were enucleated and post-fixed in 4% PFA at RT for 25 min (20 min puncture-fix, retinas dissected, 5 min fixation). Retinas were washed in PBS and then mounted in Vectashield Plus Antifade Mounting Medium (Vector Laboratories, Burlingame, CA). Whole

brains were removed and post-fixed in 4% PFA at 4°C for at least 24 h and then cut into 100 μm coronal sections on a Leica vibratome (VT1200S).

To evaluate the permeability of the blood-brain barrier, we assessed the densely vascularized paraventricular nucleus of the hypothalamus (PVN). Z-stacks of PVN vasculature (≥20 μm) were taken in 1 μm increments on either side of the third ventricle. To evaluate the permeability of the blood-retina barrier, we obtained one to two representative Z-stack images of the central arterioles and venules and one to two representative Z-stack images of the capillary vasculature of the peripheral retina (all in 1 μm increments). Retinal capillaries were imaged from the superficial plexus in the ganglion cell layer through the apparent end of the retinal vasculature (≥20 μm). All images were ~320 $\mu m^2$ and obtained with a 20x air objective on a Zeiss LSM 900 confocal microscope (Carl Zeiss, Oberkochen, Germany).

Images were denoised using rolling ball background subtraction (25 pixels) followed by the Despeckle and Remove Outlier (3 pixel radius, threshold=10) functions in Fiji (Schindelin et al., 2012). Maximum intensity Z-stack projections were created from each image (retinal capillary images were split into two stacks: one from the superficial plexus to the intermediate plexus, and the second from the intermediate plexus to the deep plexus terminating in the outer plexiform layer). Each maximum projection image is composed of 5-10 single optical sections taken at 1 μm increments, and thus represents approximately 5-10 μm of tissue vasculature. Images were thresholded using the Li method in Fiji and converted to binary masks. A composite image of each mask and the denoised image were visually inspected to ensure accurate representation of the imaged vasculature. Barrier leakage was quantified as previously described (Frahm and Tobet, 2015). The mask containing vessel "objects" was redirected to the denoised image and the average intensity within each vessel was measured. Each vessel "object" was

expanded by 2 μm and the region outside each vessel was saved; the average intensity in each outside region was measured. Leakage index was defined as the average intensity outside the vessel divided by the average intensity inside the vessel. The final reported leakage index is the average across all vessels in all images of the PVN or retina of each mouse.

In order to determine whether FITC type should be included as a factor in our statistical model, we compared two mixed models of the data by ANOVA: (1) with tissue and treatment as dependent variables, and (2) with tissue, treatment, and FITC type as dependent variables. Both models had leakage index as the independent variable and had samples identified by mouse ID number. We found that the more complex model (2) was not significantly better than model (1) without FITC type ($p$=0.223): the simpler model (1) had a lower Akaike Information Criterion (AIC; -65.8 compared to -62.1) and Bayes Information Criterion (BIC; -57.1 compared to-46.8).

*3.3G Statistical Analysis*

All data processing, visualizations and statistical tests were performed using R (v4.2.1; R Core Team, 2022) in RStudio (v2022.7.2.576; RStudio Team, 2022). Data visualizations were made using the *ggplot2* package in R (Wickham, 2016). For all tests, $p$<0.05 was considered significant. T-tests and ANOVAs with post-hoc Tukey adjustments were used when data were normally distributed and (if applicable) had homogeneous variance across groups. Whether the data was transformed (e.g. $\log_2$ or ln) to satisfy these assumptions is noted in the text. Linear mixed-effects models were fit using the *lme4* package in R (Bates et al., 2015), and pairwise comparisons were calculated using the *emmeans* package in R (Lenth, 2022).

## 3.4 Results

*3.4A P-gp and Bcrp, but not Mrp2, may transport morphine at the BRB*

We characterized the expression of three ABC transporters in the retina: P-gp (*Mdr1a*/*Abcb1a*), Bcrp (*Abcg2*), and Mrp2 (*Abcc2*). We previously reported that P-gp mRNA is expressed in the retinas of mice that received chronic morphine (20 mg/kg for 6 d, twice daily) or vehicle (saline) intraperitoneal (i.p.) injections (Bergum et al., 2022a). Using the RNA extracted from those same saline-treated retinas (n=5), we performed qRT-PCR to measure Bcrp and Mrp2 expression relative to the reference genes *β-actin* and *Tbp* (Figure 3-1). We confirmed that Bcrp (relative gene expression [RGE]: 1.01 ± 0.12) and Mrp2 (1.02 ± 0.2) mRNA are detectable in the whole mouse retina at similar levels ($t(4) = -0.11$, $p=0.92$; Figure 3-1).

We then performed immunohistochemistry (IHC) with fluorescence confocal microscopy to evaluate P-gp, Bcrp and Mrp2 expression at the iBRB of male and female mice (Figure 3-2). The iBRB was labeled using an antibody against occludin, a marker for the tight junctions of the endothelial cells which make up the iBRB (Morcos et al., 2001). The iBRB extends from the inner capillary bed in the ganglion cell layer (GCL), through the inner plexiform layer (IPL) and inner nuclear layer (INL), to the outer capillary bed in the outer plexiform layer (OPL) (Figure 3-2). The literature suggests that both endogenous opioid peptides and their receptors are predominantly expressed in the inner retina (Wamsley et al., 1981; Altschuler et al., 1982; Gallagher et al., 2010; Cleymaet et al., 2019; Berezin et al., 2022). Previous work has also suggested that P-gp and Bcrp are not expressed at the outer BRB (Chapy et al., 2016). Therefore, the outer BRB, which is established by the retinal pigment epithelium, was not analyzed in this study.

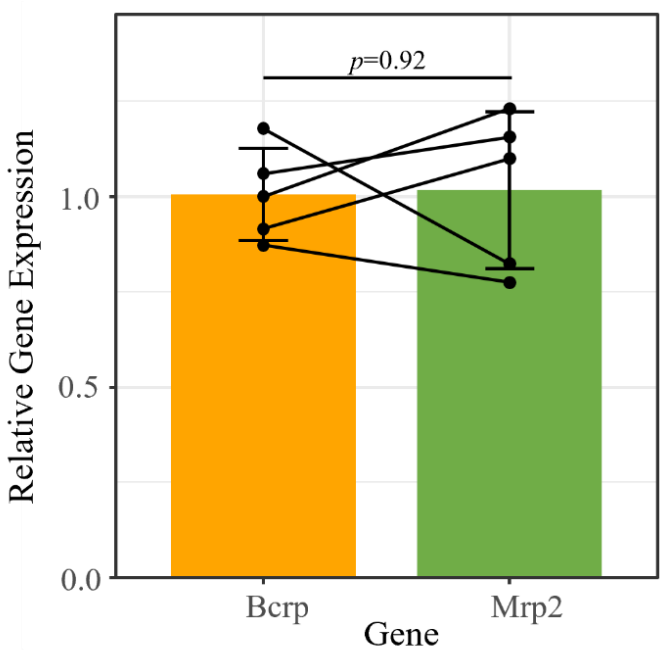


**Figure 3-1. Bcrp and Mrp2 have similar mRNA expression levels in the mouse retina.** *Bcrp* and *Mrp2* mRNA expression quantified by qRT-PCR, relative to the reference genes *Tbp* and *β-actin*. Lines connect samples from the same animal. Data presented as mean ± SD. Paired t-test, t(4)= -0.11, $p$=0.92.

Immunolabeling of occludin and P-gp was performed in both retinal cryosections (n=4, Figure 3-2 A-D) and whole-mount preparations (n=6, Figure 3-3 A-C) from male and female mice. In cryosections, we found extensive P-gp staining exclusively in the iBRB (Figure 3-2 A-D). However, in the whole-mount retinas, we commonly observed regions of the occludin-positive vasculature with strong and some with weaker P-gp co-labeling (Figure 3-3 A-C). Across all the images obtained from both preparations (4-6/mouse, n=51), the average Pearson's correlation coefficient ($r$) was 0.32 ± 0.16 (mean ± s.d.). Using Costes' automatic threshold and randomization procedures, we found this to represent true colocalization in all cases (P=100%) (Costes et al., 2004). Colocalization parameters ($r$, Mander's coefficients $M_1$ and $M_2$) were then averaged across all images obtained from a single mouse. Consistent with the observed staining patterns, the average $r$ was significantly lower in whole-mount retinas (0.24 ± 0.12) than

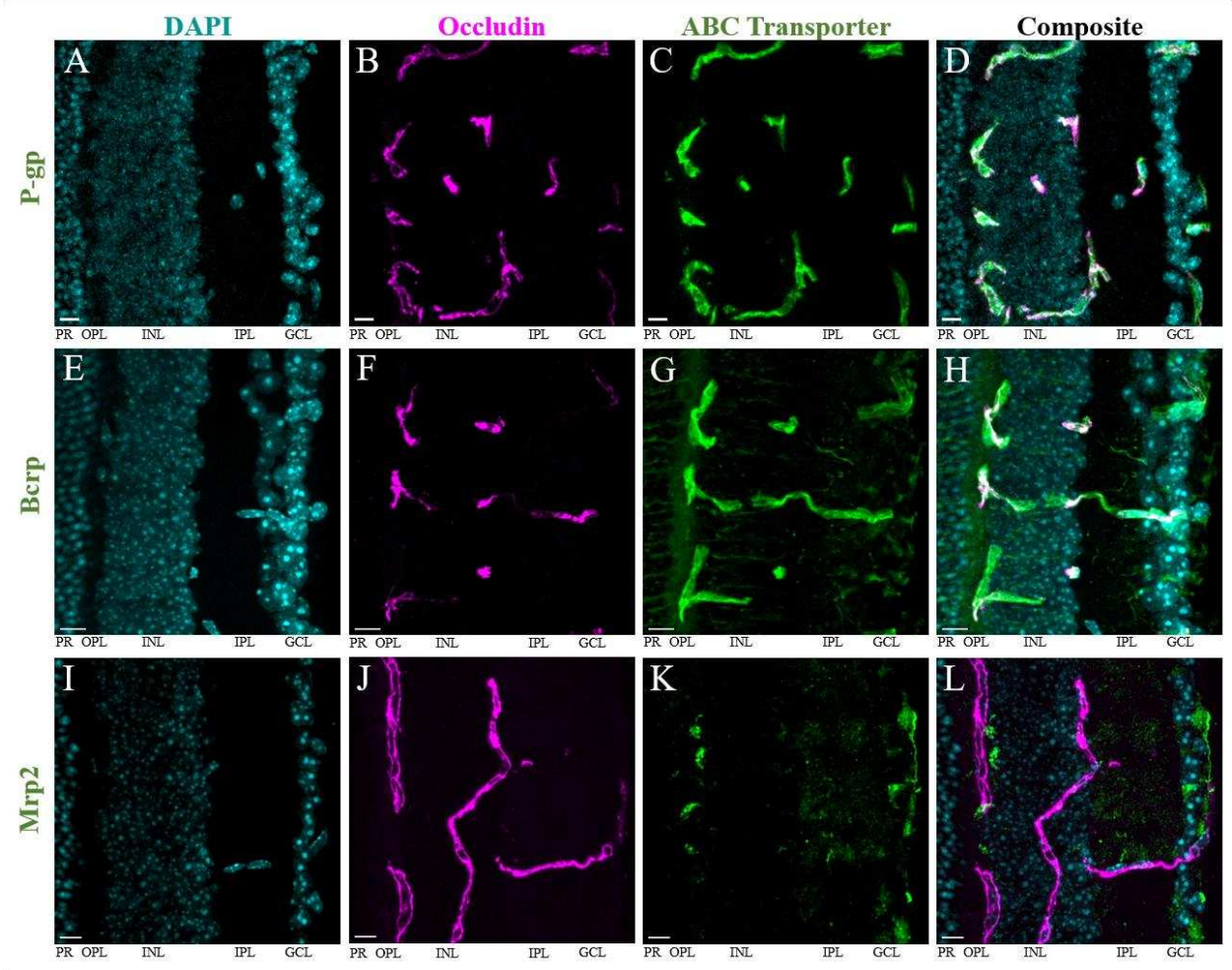


**Figure 3-2. P-gp and Bcrp, but not Mrp2, are primarily expressed at the iBRB.** Immunohistochemistry in retinal cryosections reveals robust expression of (**A-D**) P-gp and (**E-H**) Bcrp, but not Mrp2 (**I-L**), at the inner blood-retina barrier (iBRB). DAPI (blue) labels nuclei within the retina (**A, E, I**), occludin (magenta, pseudocolored) labels tight junctions between endothelial cells that make up the iBRB (**B, F, J**). All images are maximum projections of all Z-stack images containing the tissue. The average Pearson's correlation coefficient (*r*) of colocalization of the transporter with occludin was (**A-D**) 0.42 ± 0.16 for P-gp; (**E-H**) 0.46 ± 0.1 for Bcrp; and (**I-L**) 0.10 ± 0.07 in regions of positive colocalization of Mrp2 and occludin, and -0.006 ± 0.03 in regions of negative colocalization of Mrp2 and occludin. Scale bars = 10 μm. GCL = ganglion cell layer, IPL = inner plexiform layer, INL = inner nuclear layer, OPL = outer plexiform layer, PR = photoreceptor layer

cryosections (0.42 ± 0.16) ($p$=0.04, t-test, t(6.4)=2.57; Figure 3-3 D). There was no significant difference in the Mander's colocalization coefficient $M_1$ (indicating the extent of occludin-labeled area overlapping with P-gp) (Manders et al., 1993) between whole-mounts (0.20 ± 0.29) compared to the cryosections (0.41 ± 0.31) ($p$=0.1, t-test, t(7.4)=1.9; Figure 3-3 E). Similarly,

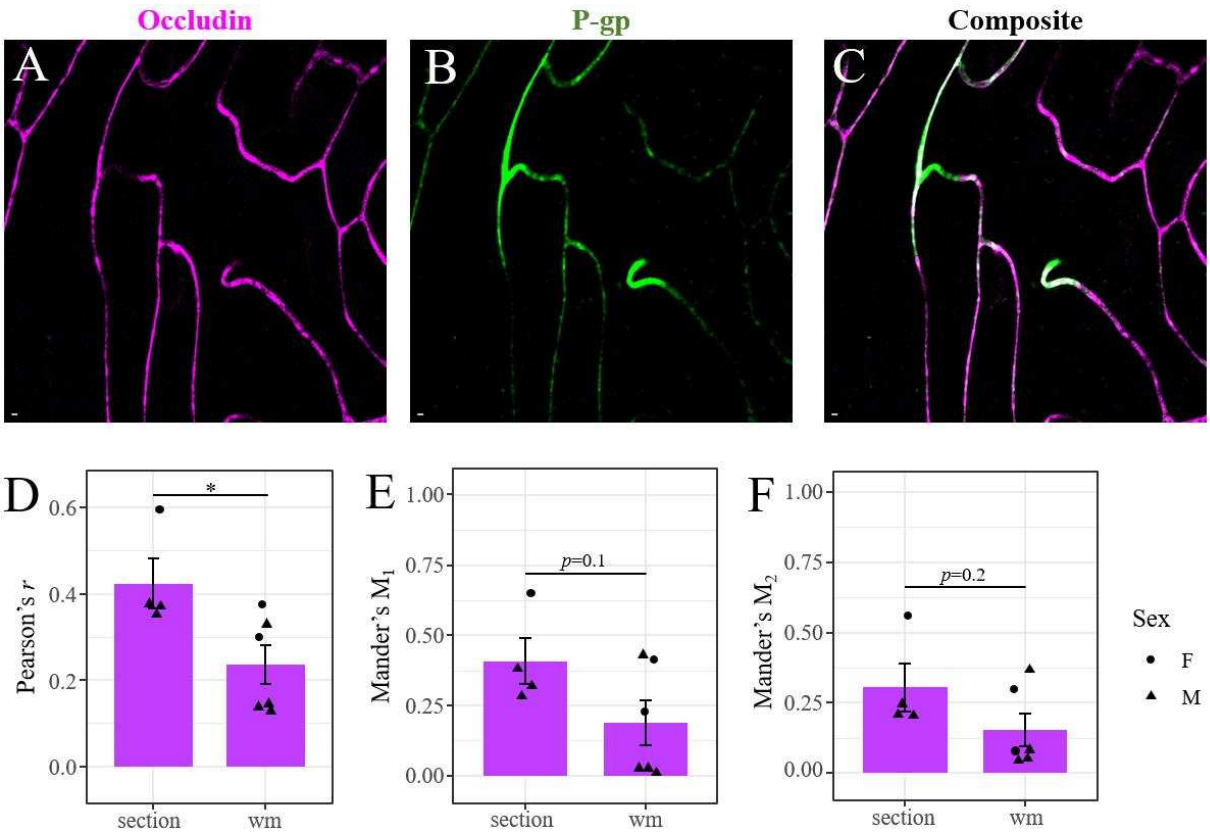


**Figure 3-3. P-gp expression is restricted to the iBRB in a whole mount retina.**
(**A-C**) Immunohistochemistry in male (triangles) and female (circles) whole-mount retinas reveals P-gp (**B**, green) labeling is restricted to the occludin-labeled iBRB (**A**, magenta [pseudocolored]), however the robustness of P-gp immunolabeling varies throughout the vasculature. P-gp positively colocalized with occludin in all images (Costes' methods, P=100%; n=27 [4-5/mouse, 6 mice]). Image is a single optical section, scale bar = 5 µm. (**D-F**) Pearson's correlation coefficient (*r*) and Mander's $M_1$ and $M_2$ coefficients (indicating the extent of occludin-labeled area overlapping with P-gp, and vice versa); each point represents the average across all images obtained from a single mouse. Data presented as mean ± SEM. * $p<0.05$

there was no significant difference in the $M_2$ coefficient (indicating the extent to which P-gp overlaps with occludin) between whole-mount (0.16 ± 0.21) and cryosection preparations (0.30 ± 0.31) ($p$=0.196, t-test, t(5.6)=1.5; Figure 3-3 F). These results are consistent with the qualitative differences in P-gp immunostaining described above, and support the idea that while the level of P-gp expression may vary throughout the vasculature, P-gp expression in the mouse retina is confined to blood vessels. Importantly, we found no significant qualitative or quantitative (*r*, $M_1$,

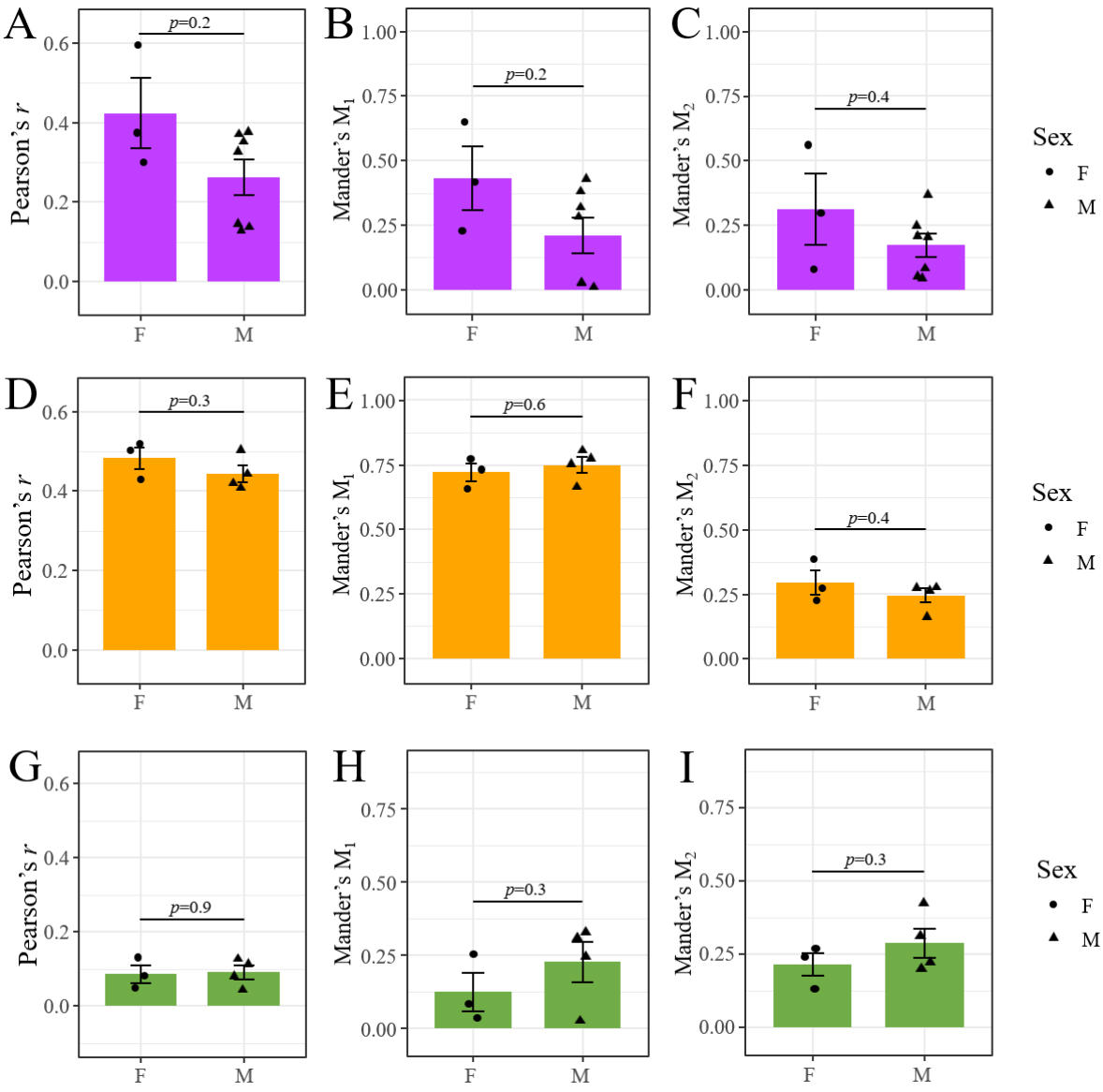


**Figure 3-4. Immunolabeling for P-gp, Bcrp and Mrp2 are not quantitatively different between male and female mice.**
Colocalization parameters for P-gp (**A-C**, purple), Bcrp (**D-F**, orange), and Mrp2 (**G-I**, green) in male (triangles) and female (circles) mice; each point represents the average across all images obtained from a single mouse. We found no statistically significant differences between males and females in (**A, D, G**) Pearson's correlation coefficient (*r*), (**B, E, H**) Mander's $M_1$ coefficient (indicating the extent of occludin-labeled area overlapping with the transporter) or (**C, F, I**) Mander's $M_2$ coefficient (indicating the extent of transporter-labeled area overlapping with occludin). Data presented as mean ± SEM. T-tests, $p<0.05$ is significant.

or $M_2$) differences between male and female mice (n=7 and 3, respectively) ($p>0.05$, t-test; Figure 3-4 A-C).

Bcrp immunolabeling in retinal cryosections from male and female mice (n=7) also revealed robust expression of Bcrp in occludin-labeled iBRB blood vessels (Figure 3-2 E- H). ). However, Bcrp labelling was not restricted to iBRB, but found in other structures in the inner retina and photoreceptor layer as well. Outside blood vessels, the anti-Bcrp antibody appeared to label neuronal projections, as well as a diffuse pattern in the OPL and GCL (Figure 3-2 E-H). Across all images (6/mouse, n=42), the average *r* was 0.46 ± 0.1. We found true colocalization in all images (P=100%) (Costes et al., 2004). Colocalization parameters (*r*, Mander's coefficients $M_1$ and $M_2$) were then averaged across all images obtained from a single mouse. Consistent with diffuse Bcrp staining in the inner retina, the average $M_1$ coefficient (indicating the extent of occludin-labeled area overlapping with Bcrp) was high (0.74 ± 0.13) compared to our results for P-gp. Conversely, the average $M_2$ coefficient (indicating the extent to which Bcrp overlaps with occludin) was more similar to the results for P-gp at 0.27 ± 0.09. As with P-gp, we found no significant qualitative or quantitative (*r*, $M_1$, or $M_2$) differences between male and female mice (n=4 and 3, respectively) ($p$>0.05, t-test; Figure 3-4 D-F). Despite the presence of Bcrp in some retinal cells outside the iBRB, its robust expression throughout the vasculature suggests it could be a significant transporter at the mouse iBRB.

Mrp2 immunostaining in retinal cryosections (n=8) from male and female mice did not result in robust colocalization with occludin-labeled blood vessels (Figure 3-2 I-L). Rather, it primarily labeled structures at the proximal INL, OPL and GCL, in addition to diffuse labeling of the IPL (Figure 3-2 I-L). There were some imaged regions where Mrp2 appeared to overlap with occludin-labeled blood vessels, which we isolated for colocalization analysis (13-22/mouse, n=145) (Figure 3-5 A-H). We found true colocalization (P>95%) in about a third of the 145 regions analyzed (Costes et al., 2004). Colocalization parameters (*r*, Mander's coefficients $M_1$

and $M_2$) were then averaged across all negatively or positively colocalizing regions obtained from a single mouse. After accounting for paired samples (i.e. one mouse has both positive and negative regions), the average *r* in regions with negative colocalization (n=90, -0.006 ± 0.03, Figure 3-5 E-H) was significantly lower than in images with positive colocalization (n=55, 0.10 ± 0.07, Figure 3-5 A-D) ($p$=0.0012, paired t-test, t(7)=-5.25; Figure 3-5 I). Accordingly, the $M_1$ coefficient (indicating the amount of occludin overlapping Mrp2) was significantly lower in

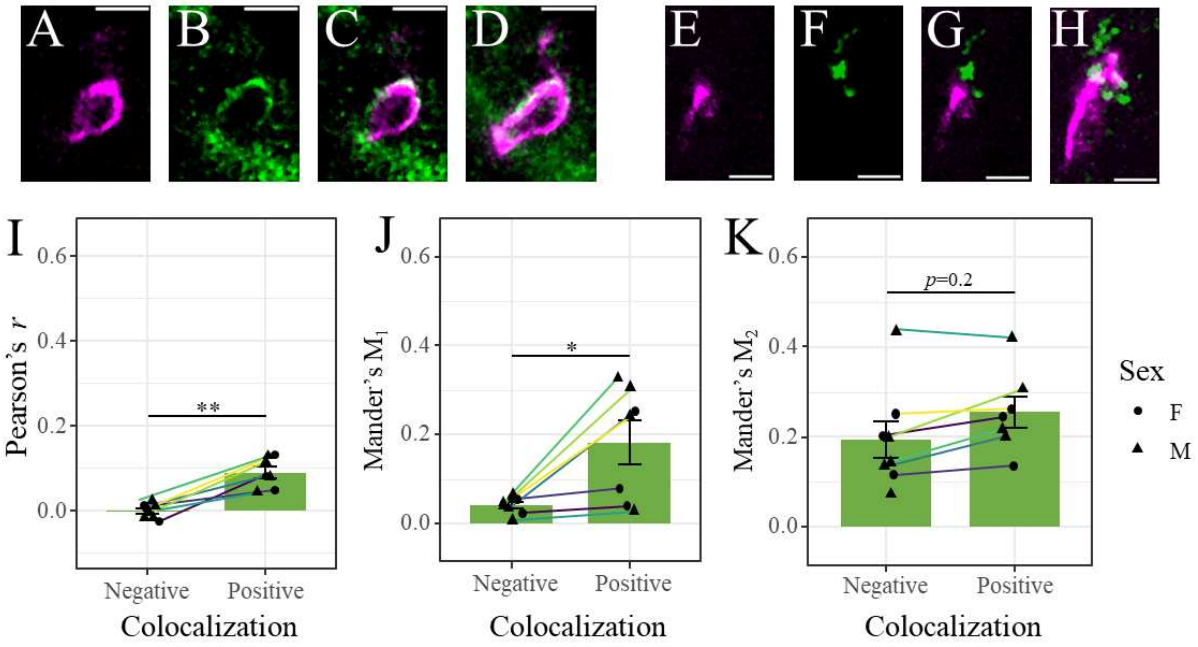


**Figure 3-5. Mrp2 expression in the retina is not exclusive to the iBRB.**
(**A-D**) Representative image of positive colocalization (P>95%, Costes' methods) of occludin (magenta [pseudocolored]), **A**) and Mrp2 (green, **B**) in a single optical section. Merged signals in (**C**) a single optical section and (**D**) in a maximum projection image through the thickness of the section. Image reveals Mrp2 expression overlapping an occludin-labeled retinal blood vessel. (**E-H**) Representative image of negative colocalization of occludin and Mrp2 immunolabeling (P<95%, Costes' methods), presented as in (**A-D**). Image shows that Mrp2 immunolabeling is often near, but not overlapping, occludin-labeled retinal blood vessels. Scale bars = 5 µm. (**I-K**) Colocalization parameters for instances of positive and negative colocalization in male (triangles) and female (circles) mice. Each point represents the average value across all positively/negatively colocalizing regions obtained from a single mouse; lines connect values from the same mouse (n=55 positive and 90 negative regions across 8 mice, 13-22 regions/mouse). (**I**) Pearson's correlation coefficient (*r*) and (**J**) Mander's $M_1$ coefficient (indicating the extent of occludin-labeled area overlapping with Mrp2) were significantly higher in positively colocalizing regions. We found no difference in (**K**) Mander's $M_2$ coefficient (indicating the extent of Mrp2-labeled area overlapping with occludin). Data presented as mean ± SEM. Paired t-tests * $p$<0.05 ** $p$<0.01

regions with no colocalization (0.04 ± 0.07) than in positive regions (0.23 ± 0.16) ($p$=0.04, paired t-test, t(7)=-2.52; Figure 3-5 J). The $M_2$ coefficient (indicating the amount of Mrp2 overlapping occludin) was also not significantly different between images without colocalization (0.187 ± 0.166) than with colocalization (0.24 ± 0.14) ($p$=0.18, paired t-test, t(7)=-1.5; Figure 3-5 K), likely due to diffuse Mrp2 staining. As with P-gp and Bcrp, we found no significant qualitative or quantitative ($r$, $M_1$, or $M_2$) differences in positively colocalizing regions between male and female mice (n=5 and 3, respectively) ($p$>0.05, t-test; Figure 3-4 G-I). Despite Mrp2's occasional presence at the iBRB, its expression primarily by other cell types suggests that its principal function in the retina is not the extrusion of substrates from vascular endothelial cells. Thus, we chose to focus only on P-gp and Bcrp in our subsequent analyses.

*3.4B Morphine deposits similarly in the brain and retina of male and female mice*

We previously investigated the pharmacokinetics of morphine in the plasma, brain and retina of male mice in the 11 h after systemic morphine administration (20 mg/kg, i.p.) (Bergum et al., 2022a). Morphine content peaked in the plasma, brain and retina 1 h following injection (Bergum et al., 2022a). Here, we investigated whether morphine deposition at this time point differs between the sexes and/or between females in different estrous stages. Male mice (n=9), as well as Low E/P (estrogen:progesterone) females (n=8) and High E/P females (n=20) received a single injection of morphine (20 mg/kg, i.p.) and were sacrificed 1 h later. The mean weight in the male group was 26.9 ± 1.82 g, 21.4 ± 1.17 g in the High E/P female group, and 20.8 ± 0.81 g in the Low E/P female group. Raw morphine content (ng/ml) in the plasma, brain and retina was quantified by LC-MS/MS. The raw concentrations detected in the male mice in this study were comparable to our previously published data (Bergum et al., 2022a), with an average

concentration in the brain of 47.7 ± 19.3 ng/ml (mean ± SD), 96.6 ± 12.7 ng/ml in the retina, and 346 ± 63.2 ng/ml in the plasma detected here. The data were $\log_e$ (ln) transformed to satisfy the assumptions of ANOVA. We found that tissue type, but not sex/estrus group (F=0.68, $p$=0.51), was a significant predictor of morphine content (F=378, $p$<2e-16). Raw morphine content was significantly higher in the plasma than retina in all groups: males (t(68)=8.8, $p$<0.0001), Low E/P females (t(68)=8.2, $p$<0.0001) and High E/P females (t(68)=13.5. $p$<0.0001) (Figure 3-6). Furthermore, raw morphine content was significantly higher in the retina than in the brain in all

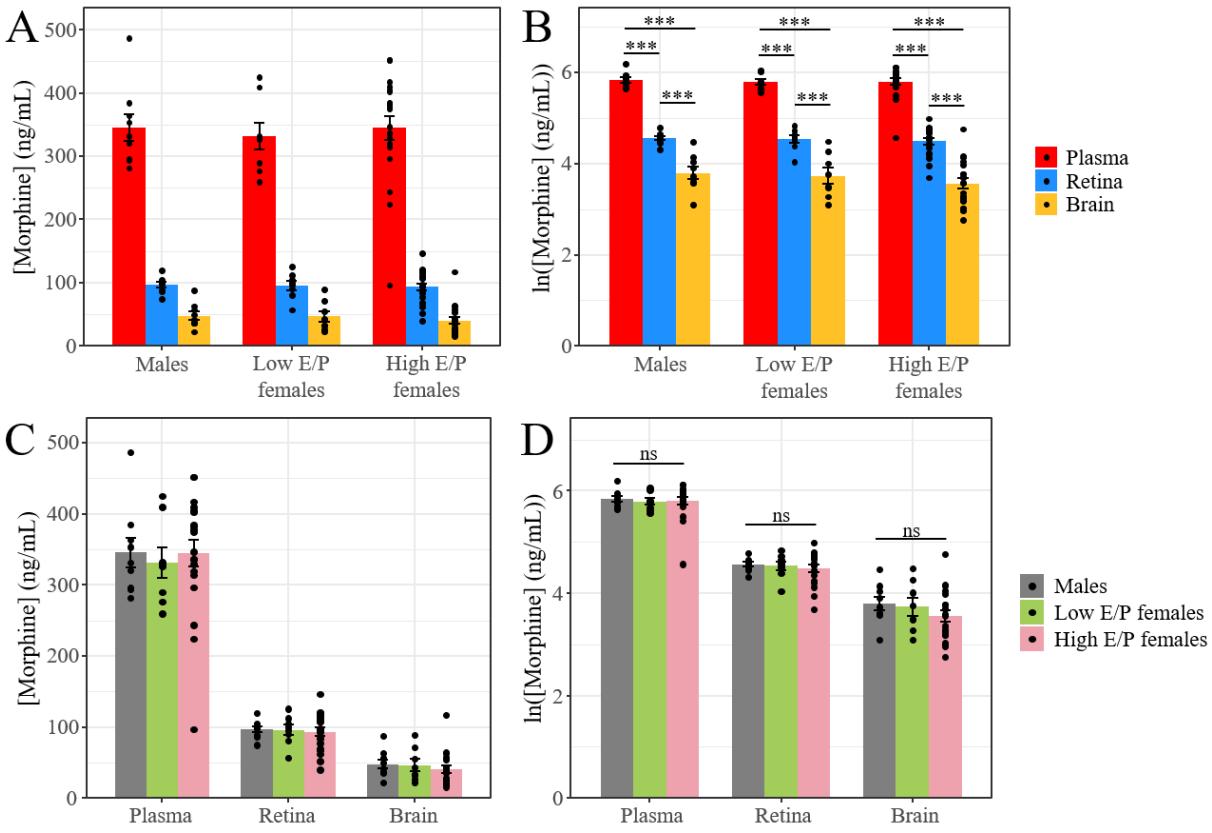


**Figure 3-6. Morphine concentrations in the plasma, retina and brain are unaffected by differences in sex/sex hormones.**
(**A**) Plasma, retina and brain morphine concentrations and (**B**) natural logarithmic (ln) transformed morphine concentrations collected from mice sacrificed 1 h following a 20 mg/kg i.p. morphine injection at light onset (ZT 0). (**C** & **D**) No significant differences exist in morphine deposition in any tissue between male and female mice. Data presented as mean ± SEM. Two-way ANOVA with Tukey post-hoc adjustments was performed on the ln scale. ns=not significant ($p$>0.05), *** = $p$<0.0001

groups: males (t(68)=5.3, $p$<0.0001), Low E/P females (t(68)=5.2, $p$<0.0001) and High E/P females (t(68)=9.6, $p$<0.0001) (Figure 3-6). We found no significant sex or estrous stage differences ($p$>0.05) in morphine deposition in the plasma, retina, or brain (Figure 3-6).

To account for differences in the tissue weight of each harvested brain/retina sample, we normalized morphine content in the retina and brain to the tissue weight (average of 4.76 ± 0.74 mg and 17.4 ± 8.77 mg, respectively). The data were again ln transformed for statistical analysis.

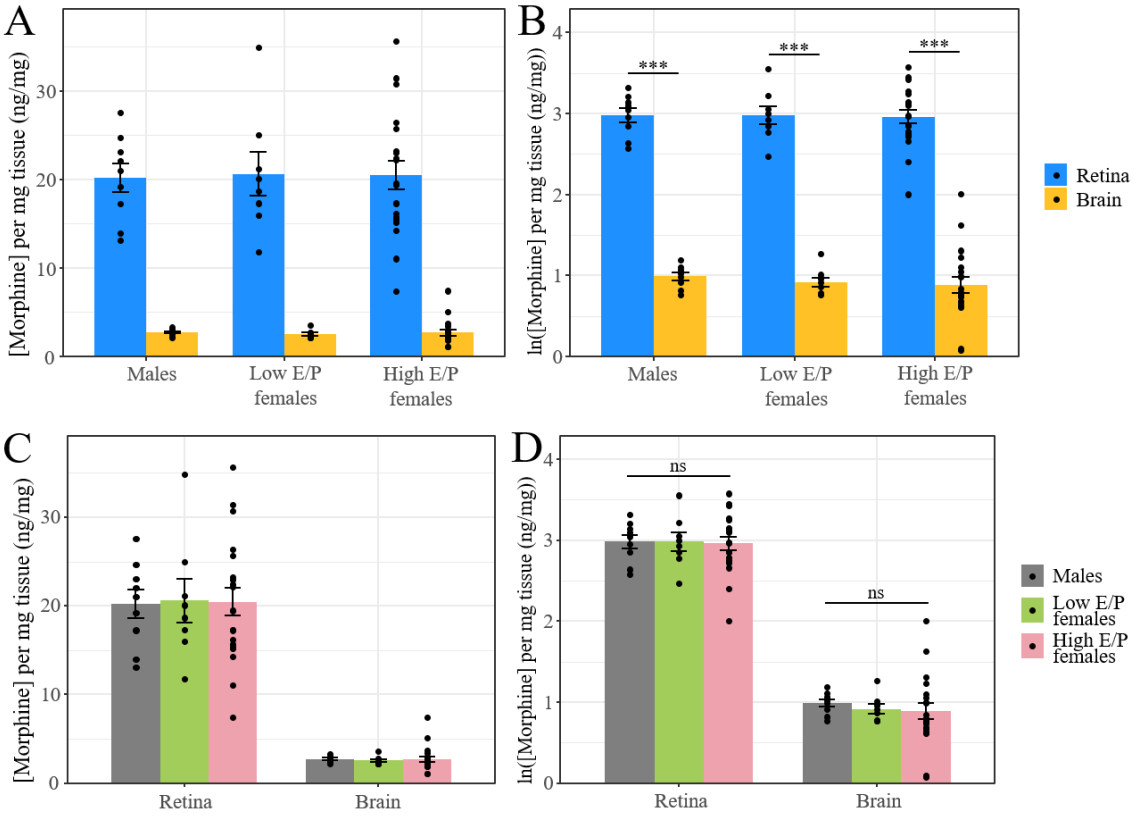


**Figure 3-7. Normalized morphine concentrations in the retina and brain are the same across male and female mice.**
(**A**) Morphine concentrations normalized to the weight of the tissue and (**B**) natural logarithmic (ln) transformed normalized morphine concentrations collected from mice sacrificed 1 h following a 20 mg/kg i.p. morphine injection at light onset (ZT 0) show retinal morphine levels exceed brain levels. (**C** & **D**) No significant differences exist in normalized morphine concentrations in the retina and brain between male and female mice. Data presented as mean ± SEM. Data were ln transformed to satisfy the assumptions for two-way ANOVA with Tukey post-hoc adjustments. ns=not significant ($p$>0.05), *** = $p$<0.0001

As before, only tissue type was a significant factor (F=1421, $p$<2e-16, ANOVA). Morphine content in the retina was again significantly higher than in the brain in male mice (t(34)=19.657, $p$<0.0001), Low E/P females (t(34)=19.218, $p$<0.0001), and High E/P females (t(34)=30.495, $p$<0.0001) (Figure 3-7). No significant sex differences were found in morphine content in the retina or the brain ($p$>0.05) (Figure 3-7).

*3.4C Chronic morphine treatment does not affect opioid transporter expression at the iBRB*

We previously reported that P-gp expression in the retina and brain was not significantly different between male mice that received chronic morphine or vehicle (saline) (Figure 3-8) (Bergum et al., 2022a), consistent with reports that elevated P-gp expression after morphine exposure can be attributed to a withdrawal response rather than the morphine treatment itself (Chaves et al., 2016; Yousif et al., 2012). Here, we tested whether Bcrp expression is influenced by chronic morphine exposure (20 mg/kg for 6 days, twice daily) (n=7) compared to vehicle (saline, n=9). All animals were sacrificed 1 hour following the last injection. Expression of Bcrp, relative to the reference genes *β-actin* and *Tbp*, was calculated using the saline-treated retinas as the control group. The data were $\log_2$ transformed to meet the assumptions of ANOVA (Figure 3-9). Tissue type, but not treatment, was a significant predictor of Bcrp expression (F=96, $p$=1.18e-7).

Similar to P-gp (Bergum et al., 2022a), Bcrp expression was lower in the retina than brain in both the saline-treated (t(14)= -6.24, $p$<0.0001) and morphine-treated groups (t(14)= -7.58, $p$<0.0001) (Figure 3-9). Moreover, we found no significant differences between morphine- and saline-treated mice in terms of Bcrp expression in the retina (t(24.3)= -0.1, $p$=0.92) and brain

(t(24.3)= -1.8, $p$=0.08) (Figure 3-9). Thus, neither P-gp nor Bcrp expression is expected to be altered by morphine administration.

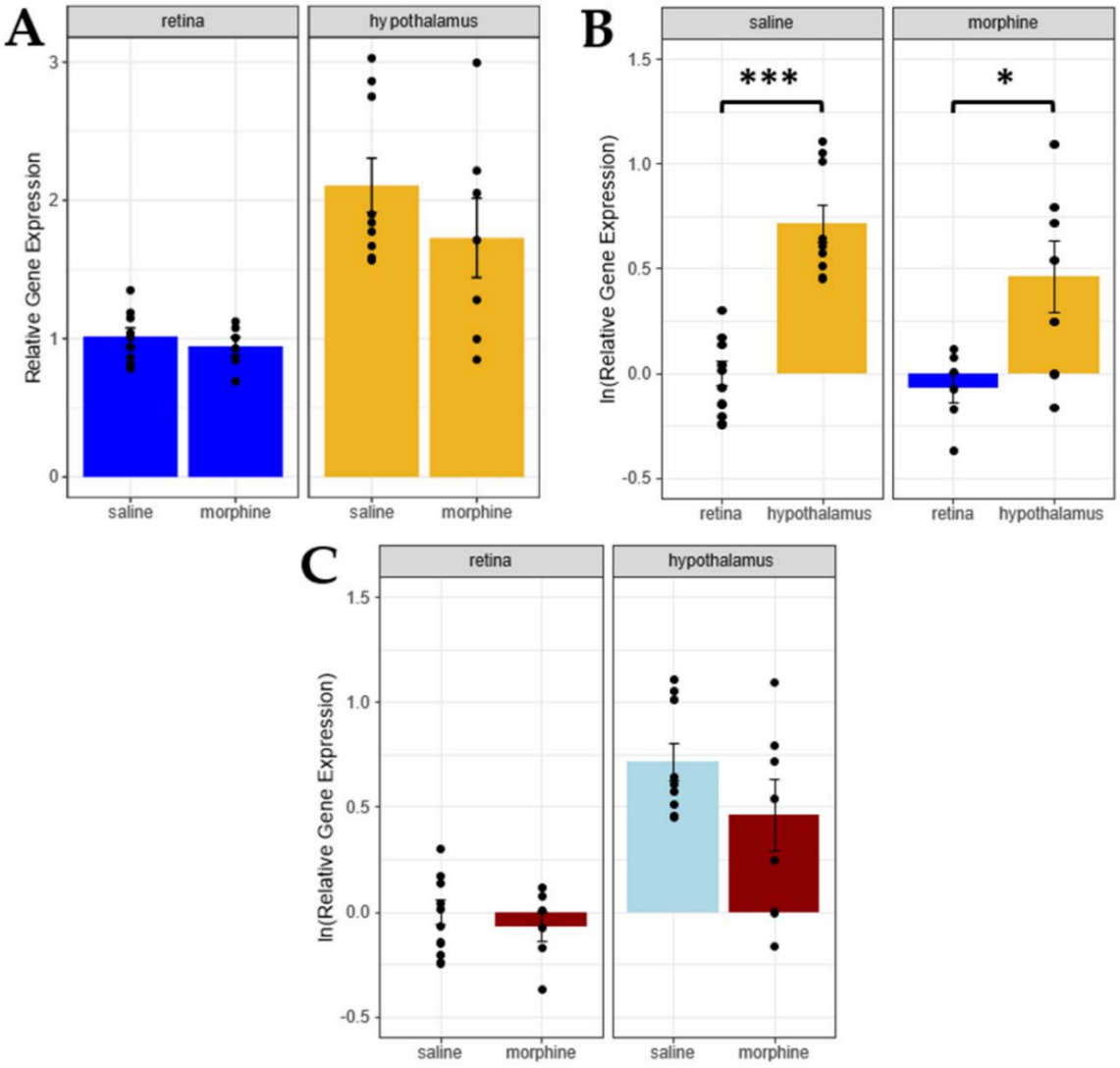


**Figure 3-8. Reduced P-gp expression in the retina may underlie retinal morphine accumulation.**
(**A**) P-gp mRNA expression and (**B**) natural logarithm (ln)-transformed P-gp mRNA expression is lower in the retina than in the hypothalamus at one hour (ZT 1) after an i.p. morphine injection at ZT 0. (**C**) Chronic morphine exposure does not affect P-gp mRNA expression in either tissue at ZT 1. Two-way ANOVA with a Tukey post-hoc adjustment was performed on an ln scale. Data are presented as the mean ± SD. * $p$<0.01, *** $p$<0.0001 [6]

[6] Figure reprinted from Bergum, N., Berezin, C.-T., Dooley, G., & Vigh, J. (2022). Morphine Accumulates in the Retina Following Chronic Systemic Administration. *Pharmaceuticals*, *15*(5) https://doi.org/10.3390/ph15050527 pursuant to the open access Creative Commons CC BY license and the MDPI Open Access Policy (Appendix D).

*3.4D Opioid transporter expression at the iBRB is not dependent on sex/hormonal differences*

We next investigated whether P-gp and Bcrp expression differs between the sexes and/or between female estrous stages in the context of acute morphine treatment (1 h after injection). Expression of P-gp and Bcrp, relative to the reference genes *β-actin* and *Tbp*, in the brains and retinas of acute morphine-treated males (n=8), High E/P females (n=11), and Low E/P females (n=5) was quantified by qRT-PCR using the male retinas as the control group. The relative gene expression (RGE) values were transformed on the $\log_2$ scale to satisfy the assumptions of

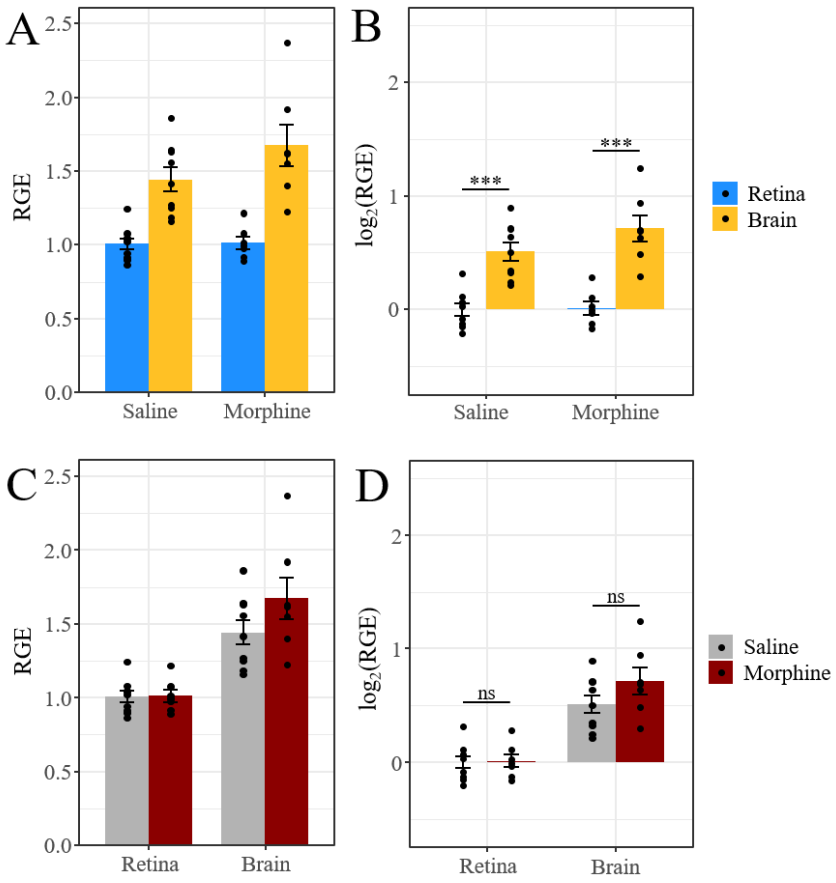


**Figure 3-9. Chronic morphine treatment does not affect Bcrp expression in the retina or brain.** (**A**) Bcrp relative gene expression (RGE) and (**B**) $\log_2$ transformed RGE values are lower in the retina than in the brain 1 h after the last injection of a chronic morphine paradigm (20 mg/kg i.p., twice daily for 6 d). Bcrp mRNA was quantified by qRT-PCR, relative to the reference genes *Tbp* and *β-actin*. (**C** & **D**) Chronic treatment with morphine does not alter Bcrp expression in the retina or brain relative to vehicle (saline) treatment. Data are presented as the mean ± SEM. Data were $\log_2$ transformed to satisfy the assumptions for two-way ANOVA with Tukey post-hoc adjustments. ns=not significant ($p>0.05$), *** = $p<0.0001$

ANOVA. We found that Gene (F=253, $p$<2e-16),Tissue (F=509, $p$<2e-16) and Group (F=4.3, $p$=0.027) were all significant predictors of RGE values, as were the interactions of Gene and Tissue (F=170, $p$<2e-16) and of Tissue and Group (F=4.8, $p$=0.011).

As we showed in chronically treated male mice (Bergum et al., 2022a), P-gp expression was significantly lower in the retina than the brain in all groups: males (t(63)= -14.219,

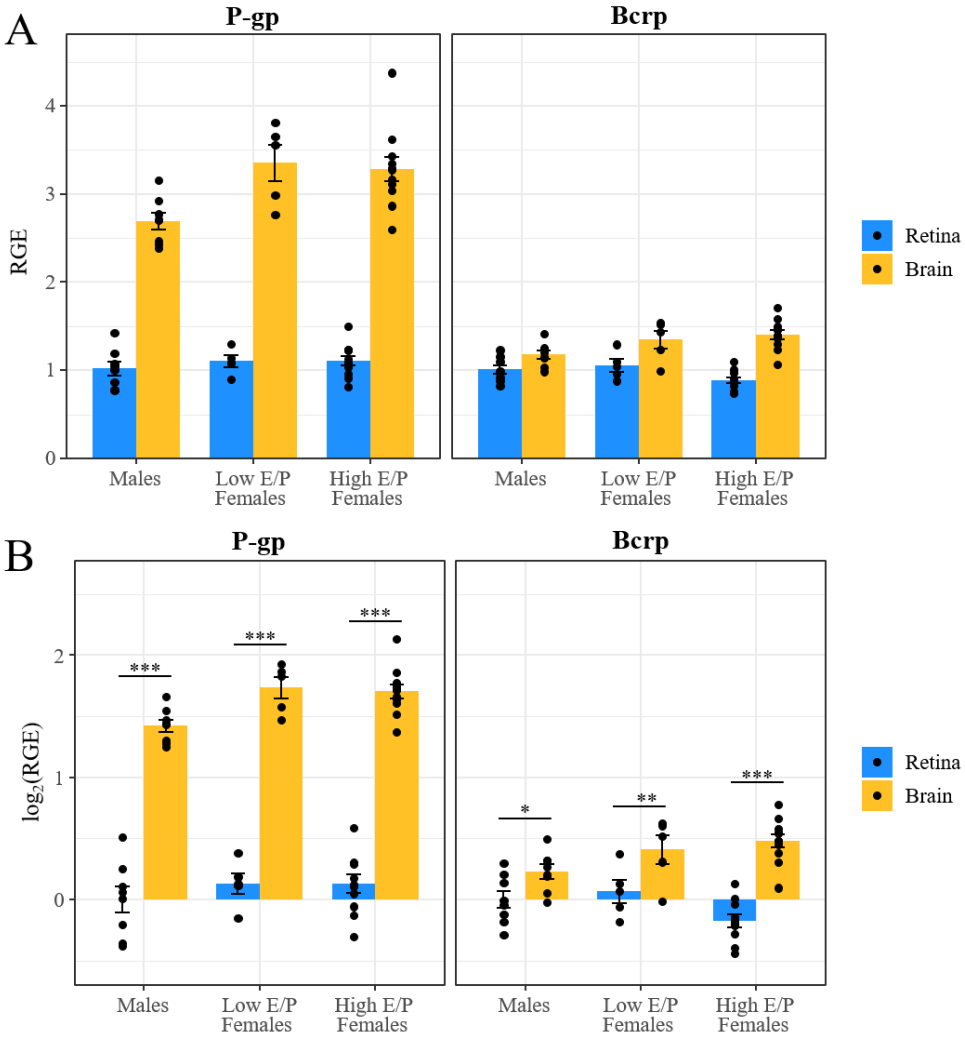


**Figure 3-10. P-gp and Bcrp expression are lower in the retina than brain in male and female mice.**
**(A)** P-gp and Bcrp relative gene expression (RGE) and **(B)** $\log_2$ transformed RGE values are lower in the retina than in the brain 1 h following a morphine injection (20 mg/kg i.p.). P-gp and Bcrp mRNA were quantified by qRT-PCR, relative to the reference genes *Tbp* and *β-actin*. Data are presented as the mean ± SEM. Data were $\log_2$ transformed to satisfy the assumptions for two-way ANOVA with Tukey post-hoc adjustments. * $p$<0.05 ** $p$<0.01 *** $p$<0.0001

$p$<0.0001), Low E/P females (t(63)= -12.66, $p$<0.0001), and High E/P females (t(63)= -18.422, $p$<0.0001) (Figure 3-10). Similarly, Bcrp expression was significantly lower in the retina than the brain in all groups: males (t(63)= -2.287), $p$=0.0255), Low E/P females (t(63)= -2.714, $p$=0.0086), and High E/P females (t(63)= -7.695, $p$<0.0001) (Figure 3-10).

In the brain, P-gp expression was significantly lower in males than both Low E/P females (t(83)=-2.633, $p$=0.027) and High E/P females (t(83)=-2.909, $p$=0.0128) (Figure 3-11). The two female groups were not significantly different from one another (t(83)=0.28, $p$=0.9585) (Figure 3-11). As for Bcrp in the brain, we found that expression in males was significantly lower than High E/P females (t(83)=-2.63, $p$=0.0272), but not significantly different than Low E/P females (t(83) = -1.5, $p$=0.2830) (Figure 3-11). The two female groups were not significantly different from one another (t(83) = -0.65, $p$=0.7926) (Figure 3-11). Together, these results are consistent with female sex hormones influencing opioid transporter expression in some tissues, such as the brain (Tanaka et al., 2005; Suzuki et al., 2006; Bebawy and Chetty, 2009; Shchul'kin et al., 2017; Dalla et al., 2022).

Conversely, there was no effect of sex or estrous stage on retinal P-gp expression, as expression in males was not significantly different than Low E/P females (t(83)= -1.11, $p$=.51) or High E/P females (t(83)= -1.36, $p$=0.37), nor were Low E/P and High E/P females significantly different from one another (t(83)=0.005, $p$=1.0) (Figure 3-11). Furthermore, we found no effect of sex or estrous stage on retinal Bcrp expression; expression in males was not significantly different than Low E/P females (t(83)= -0.56, $p$=0.84) or High E/P females (t(83)=1.82, $p$=0.17), nor were Low E/P and High E/P females significantly different from one another (t(83)=2.155, $p$=0.085) (Figure 3-11). Thus, circulating sex hormones do not appear to significantly impact opioid transporter expression at the iBRB.

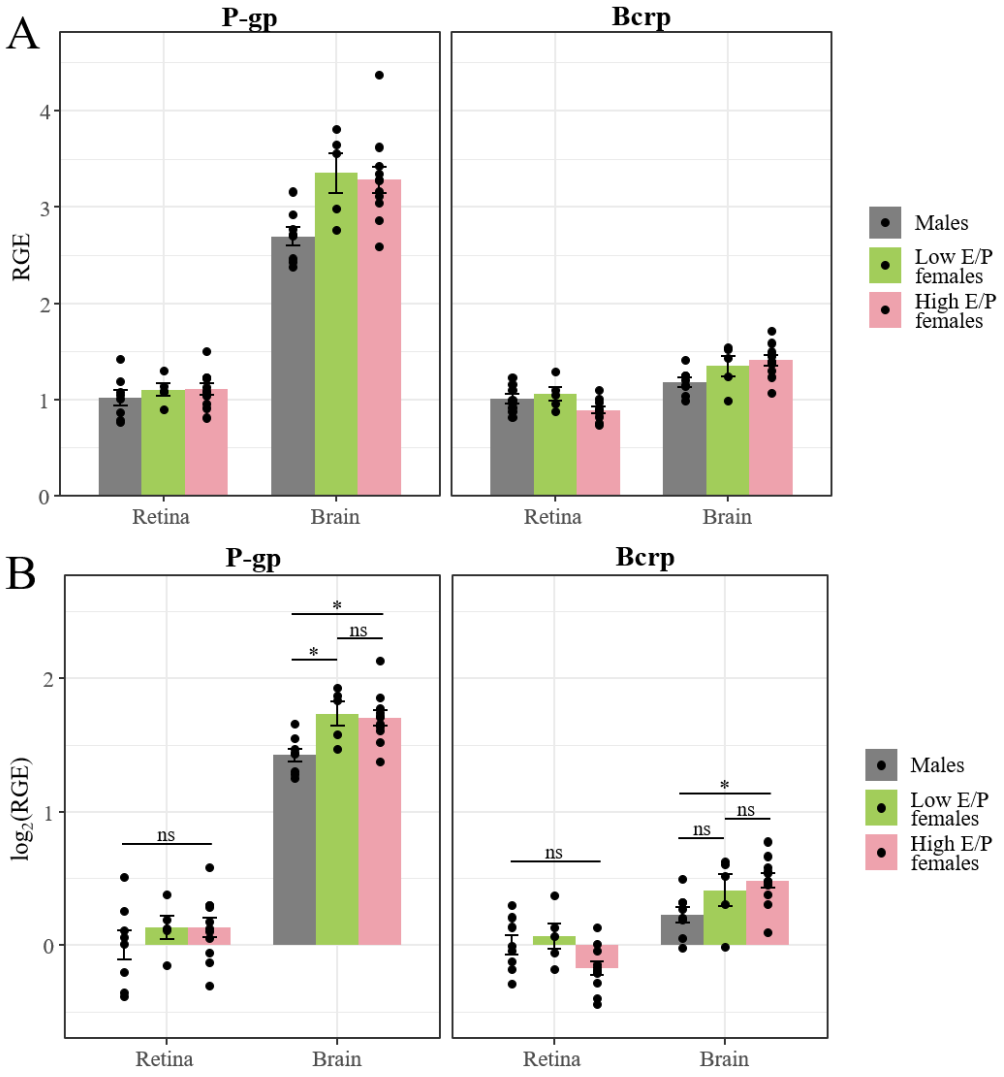


**Figure 3-11. P-gp and Bcrp expression in the retina show no effect of sex or estrous stage.** **(A)** P-gp and Bcrp relative gene expression (RGE) and **(B)** $\log_2$ transformed RGE values show no differences between male and female animals (regardless of estrus stage) 1 h following a morphine injection (20 mg/kg i.p.). Relative Gene Expression (RGE) of P-gp and Bcrp mRNA was quantified by qRT-PCR, relative to the reference genes *Tbp* and *B-actin*. Data are presented as the mean ± SEM. Data were $\log_2$ transformed to satisfy the assumptions for two-way ANOVA with Tukey post-hoc adjustments. ns=not significant ($p>0.05$), * $p<0.05$

*3.4E P-gp is a significant predictor of morphine deposition in the retina*

Our experimental design allowed for a statistical comparison of P-gp and Bcrp expression in the retina and the brain. In the brain, we found a staggering three-fold difference in P-gp expression compared to Bcrp expression in all groups: males ($t(63)=11.9$, $p<0.0001$, ANOVA),

Low E/P females (t(63)=10.46, $p$<0.0001) and High E/P females (t(63)=14.306, $p$<0.0001) (Figure 3-12). Interestingly, in the retina, the expression of the two transporters was more similar. While P-gp expression was greater than Bcrp expression in High E/P females

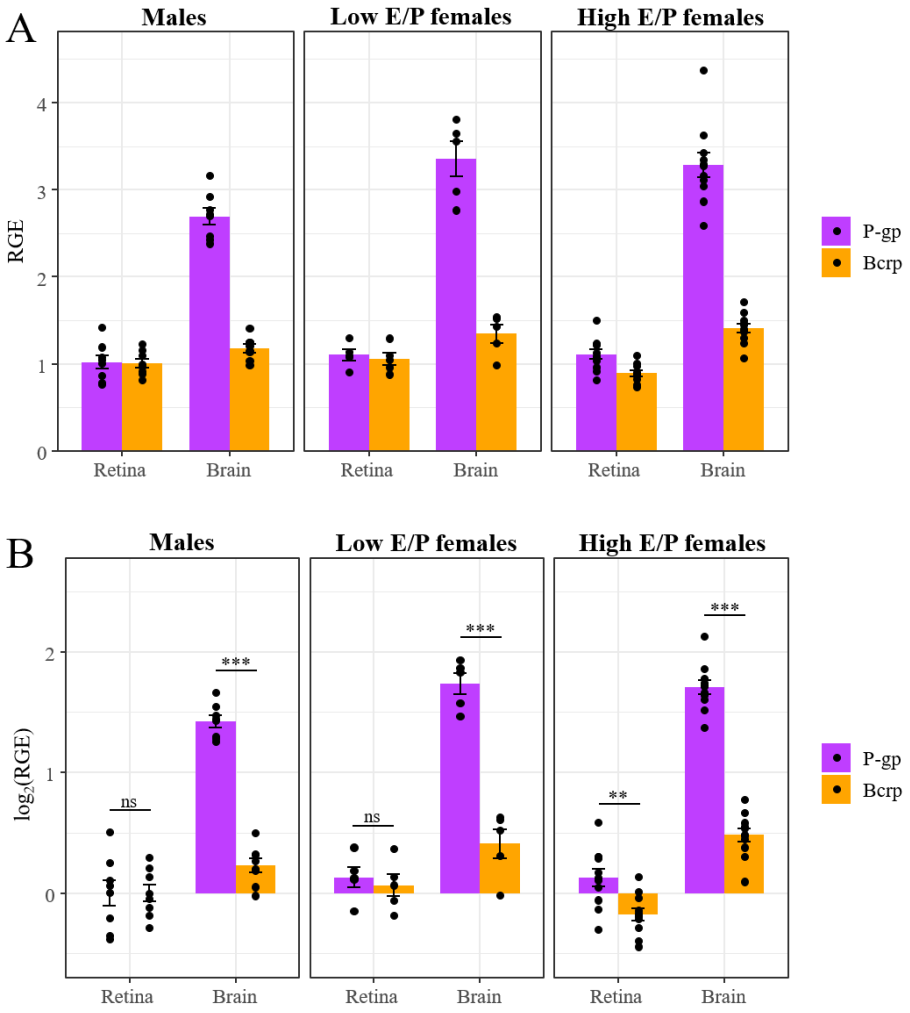


**Figure 3-12. P-gp mRNA expression is higher than Bcrp in the brain, but not the retina, in male and female mice.**
**(A)** P-gp and Bcrp relative gene expression (RGE) and **(B)** $\log_2$ transformed RGE values show increased P-gp expression compared to Bcrp in the brains of male and female mice 1 h following a morphine injection (20 mg/kg i.p.). Contrastingly, there is no difference in P-gp and Bcrp mRNA expression in the retina of male and Low E/P female mice. P-gp and Bcrp mRNA expression was quantified by qRT-PCR, relative to the reference genes *Tbp* and *β-actin*. Data are presented as the mean ± SEM. Data were $\log_2$ transformed to satisfy the assumptions for two-way ANOVA with Tukey post-hoc adjustments. ns=not significant ($p$>0.05), ** $p$<0.001, *** $p$<0.0001

(t(63)=3.58, $p$=0.0007), we found no such significant differences in males (t(63)=0, $p$=1.0) or Low E/P females (t(63)=.516, $p$=0.61) (Figure 3-12).

We then examined the relationship between transporter expression in the retina or brain and the level of morphine deposition in that tissue, combining our male and female groups (n=24) given the lack of sex/estrous effects on either parameter in the retina. Relative gene expression values and normalized morphine content (ng/mg) were left untransformed, and Spearman's non-parametric rank correlation rho (ρ) was calculated for each gene in each tissue. In the brain, we found a weak correlation between transporter expression and morphine deposition. The correlation coefficient, ρ, between P-gp and morphine content was -0.0026 ($p$=0.99), while for Bcrp it was -0.19 ($p$=0.37). Conversely, we found stronger correlations

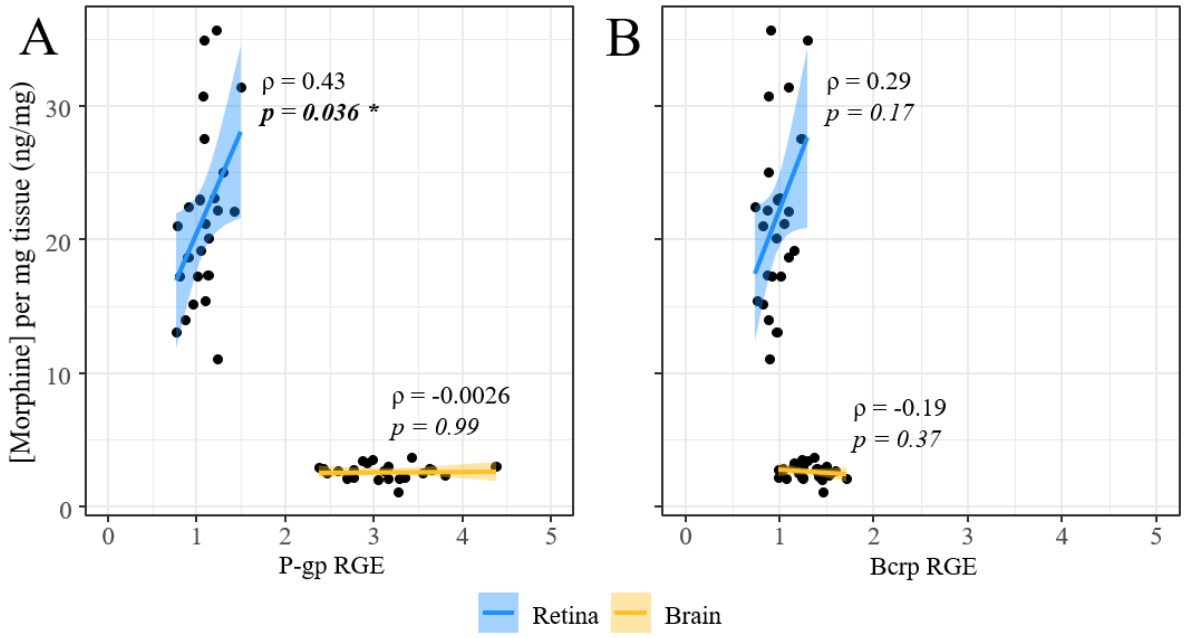


**Figure 3-13. P-gp expression at the iBRB is significantly correlated to morphine deposition in the retina.**
Spearman's rank correlation (rho, ρ) was calculated for the relationship between normalized morphine concentration and relative **(A)** P-gp or **(B)** Bcrp mRNA expression in the retina and brain of male and female mice.

between transporter expression and morphine content in the retina. For Bcrp, ρ was 0.29 ($p$=0.17), while for P-gp we found a statistically significant correlation between expression and morphine deposition (ρ=0.43, $p$=0.036) (Figure 3-13).

*3.4E Chronic morphine treatment does not affect BBB or BRB permeability*

There is some evidence that chronic morphine exposure may impair the integrity of the BBB, which could affect morphine pharmacokinetics in the CNS (Leibrand et al., 2019). If our morphine treatment paradigm affects the integrity of blood-CNS barriers, it may increase the permeability of the barriers to xenobiotics such as morphine. To test this, we used fluorescence imaging of fluorescein isothiocyanate (FITC) extravasation to assess the integrity/permeability of

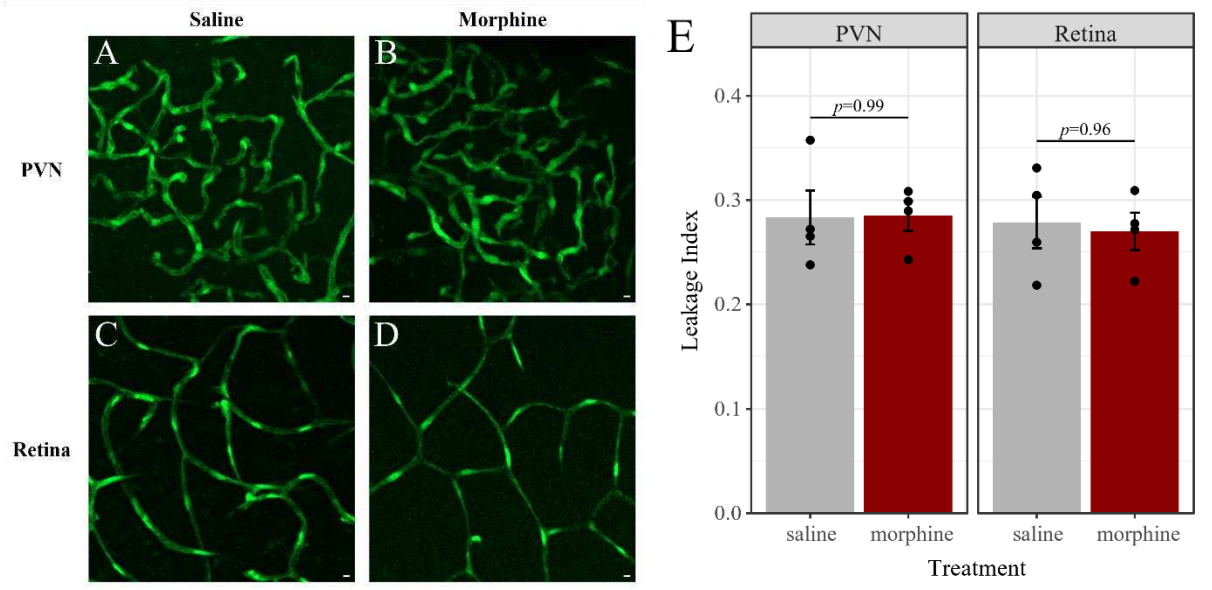


**Figure 3-14. Chronic morphine treatment does not impact BBB or BRB permeability.** Fluorescence imaging of FITC extravasation revealed no differences in barrier leakage between mice that received chronic morphine treatment (20 mg/kg, twice daily, 6 d; n=4; **B**, **D**) and vehicle-treated mice (saline, twice daily, 6 d; n=4; **A**, **C**). Leakage was quantified in the densely vascularized PVN (**A**, **B**) and in retinal capillaries (**C**, **D**) of the same mice. (**E**) Leakage index is defined as the average intensity outside of vessels divided by the average intensity inside vessels. Data are presented as the mean ± SEM. Two-way ANOVA with Tukey post-hoc adjustments found no significant differences ($p$<0.05).

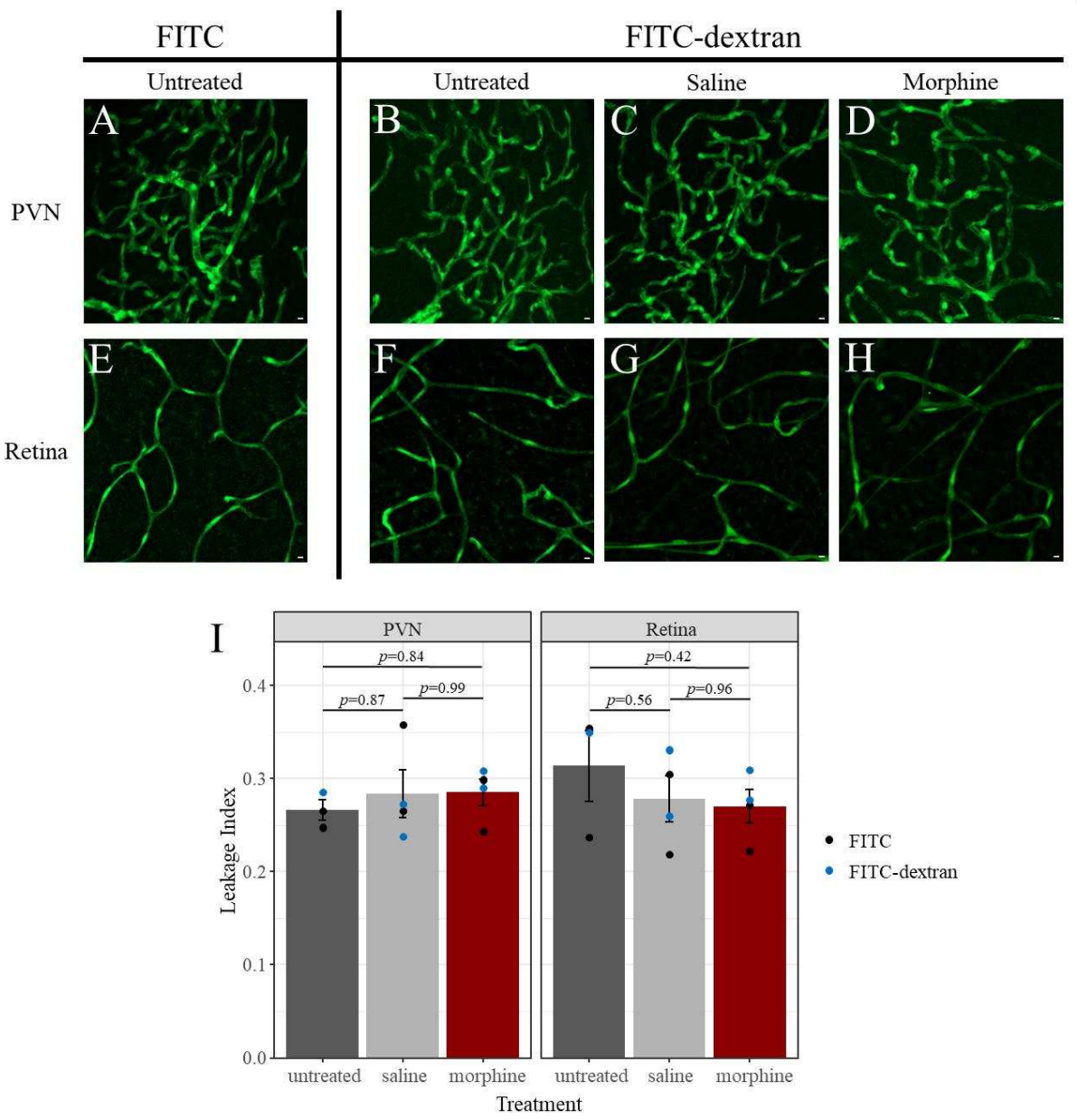


**Figure 3-15. FITC and FITC-dextran extravasation is similar at the BBB and BRB, independent of treatment.**
Fluorescence imaging of FITC (**A**, **E**) and FITC-dextran extravasation (**B-D**, **F-H**) resulted in similar leakage indices in all assessed groups (**I**). Leakage index was calculated in the densely vascularized PVN (**A-D**) and in retinal capillaries (**E-H**), and is defined as the average intensity outside of vessels divided by the average intensity inside vessels. We found no differences in leakage index between mice that received chronic morphine treatment (20 mg/kg, twice daily, 6 d; n=4; **D**, **H**), vehicle-treated mice (saline, twice daily, 6 d; n=4; **C**, **G**) and untreated mice (n=3; **A**-**B**, **E**-**F**). Scale bars = 5 μm. Data are presented as the mean ± SEM. Two-way ANOVA with Tukey post-hoc adjustments found no significant differences ($p<0.05$).

the BBB and BRB (Figure 3-14). Six male mice were perfused with FITC, and an additional five male mice were perfused with FITC conjugated to 10 kDa dextran (FITC-dextran) (Figure 3-15). In each group, mice received either chronic morphine treatment, vehicle (saline) or were left untreated. Treated mice were sacrificed 1 hour after the last injection when morphine concentrations in the brain and retina are at their peak. Barrier leakage was assessed in the retina and the paraventricular nucleus of the hypothalamus (PVN) of each mouse. Notably, the PVN was chosen due to the dense vascularization found in this hypothalamic nucleus (Frahm and Tobet, 2015). Retinal arterioles in the superficial vascular layer, as well as capillaries in the superficial, intermediate, and deep layers of the retinal vasculature were imaged (Kornfield and Newman, 2014). Leakage indices were similar across these layers, thus capillaries in the intermediate layer were chosen as representative images (Figures 3-14, 3-15). Images of FITC extravasation of the retinal arterioles can be found in Figure 3-16.

We obtained similar leakage indices (as defined in the Methods) in mice perfused with FITC and those perfused with FITC-dextran (Figure 3-15). The average leakage index in each tissue and treatment combination was compared by ANOVA. We found that neither tissue ($F(16)=0.24$, $p=0.63$), treatment ($F(16)=0.14$, $p=0.87$), nor the interaction of tissue and treatment ($F(16)=0.95$, $p=0.41$) were significant predictors of the leakage index. Accordingly, there were no significant pairwise differences in the PVN or retina of saline- and morphine-treated mice (Figure 3-14), nor were these different from untreated mice (Figure 3-15). There were also no significant differences between leakage indices in the PVN and retina of mice in the saline-treated group ($t(8)=0.16$, $p=0.88$), the morphine-treated group ($t(8)=0.47$, $p=0.65$), nor in the untreated group ($t(8)=-1.3$, $p=0.22$). Thus, neither chronic morphine nor vehicle treatment significantly altered the permeability of the BBB or BRB.

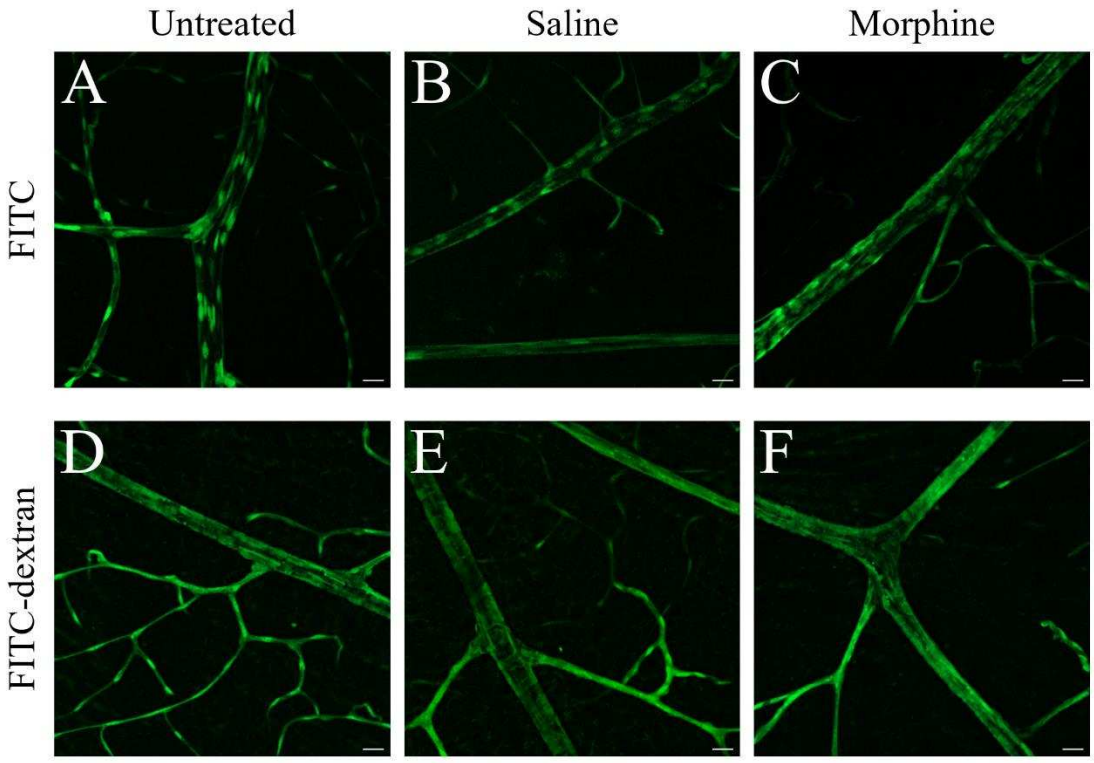


**Figure 3-16. Fluorescence extravasation in retinal arterioles is unchanged by morphine treatment.** Fluorescence imaging of FITC (**A**-**C**) and FITC-dextran extravasation (**D**-**F**) in first-order retinal arterioles in the superficial vascular layer in untreated (**A**, **D**), saline/vehicle-treated (**B**, **E**), and morphine-treated mice (**C**, **F**). Scale bars = 20 μm.

### 3.5 Discussion

Previous work from our group showed that, in male mice, morphine deposition in the retina is higher than in the brain, and furthermore, that morphine persists in the retina while it is cleared from both the systemic circulation and the brain (Bergum et al., 2022a). Thus, in this study we aimed to develop a mechanistic understanding of increased morphine penetrance and persistence in the retina compared to the brain, as well as to assess the role of sex/sex hormones in retinal morphine pharmacokinetics.

Here, we evaluated three ABC transporters (P-gp, Bcrp and Mrp2) as putative opioid transporters at the iBRB. We first validated the presence of these transporters within the retinal vasculature of the iBRB by immunohistochemistry. We found extensive P-gp and Bcrp labeling

at the iBRB of both male and female mice, which is consistent with previous findings in male mice (Tagami et al., 2009; Chapy et al., 2016). Our analyses revealed that P-gp was exclusively expressed within occludin-labeled blood vessels. Interestingly, P-gp labeling was more robust in cryosectioned retinas than in whole-mount preparations (Figures 3-2, 3-3), however, we found true colocalization using Costes' methods in all cases. This phenomenon may represent a decreased ability of the antibody to penetrate and bind P-gp in the whole-mount retina and/or a biologically significant clustering of P-gp at particular regions of iBRB vasculature that is more obvious in a whole-mount preparation. Bcrp immunolabeling was also primarily found in retinal blood vessels, however, some other retinal structures were labeled, which has not been previously reported (Tagami et al., 2009; Chapy et al., 2016). The robust expression of P-gp and Bcrp at the iBRB suggests that these transporters could contribute to morphine transport across the BRB in both males and females, as we did not uncover any differences between sexes in the immunolabeling for either transporter (Figure 3-4). Conversely, we found that Mrp2 is not robustly expressed within blood vessels at the iBRB, which is consistent with previous reports that assessed other Mrp transporters (Tagami et al., 2009; Chapy et al., 2016). Its expression was more prevalent in cells near blood vessels, which may be neurons or cells that support the iBRB (e.g. pericytes, Müller glia). Although future studies could interrogate the identities of Mrp2-expressing cells in the retina, our results suggest that Mrp2 is not a prominent opioid transporter at the iBRB; it may instead play a supporting role in the regulation of drug transport between the systemic circulation and the retina. Furthermore, occludin expression is specific to the tight junctions between the endothelial cells of mammalian retinal vessels, but it is present in all the blood vessels of both the iBRB and outer BRB (Morcos et al., 2001). Thus, colocalization studies of P-gp and Bcrp using markers that are specific to the iBRB in adult mice (i.e. claudin-

5) (Kojima et al., 2002; Greene et al., 2019) and/or that label, not just tight junctions, but the entirety of blood vessels (i.e. collagen IV) (Ramos et al., 2013) may provide additional insight into the expression and function of these transporters at the BRB.

After establishing that Bcrp and P-gp are robustly expressed at the iBRB, we wanted to determine the relative contribution of each protein to retinal morphine transport. Previous studies from our lab showed that P-gp expression is inversely correlated with morphine deposition when comparing the brain and retina (Bergum et al., 2022a); however, these studies were only performed in male mice. To establish a connection between morphine transporters at the iBRB and the potential role of sex/sex hormones in morphine pharmacokinetics, we performed experiments in male and female mice. Importantly, littermate female mice were divided into two different groups based on their estrus stage on the day of sacrifice. The first group of females was either in diestrus or metestrus (Low Estrogen/Progesterone ratio), with hormone profiles more similar to male mice. The second group of females was sacrificed during estrogen-dominant stages (High E/P), proestrus or estrus (Broestl et al., 2018). High E/P female mice have been shown to have lower sensitivity to tactile abdominal stimulation than low E/P females and male mice (Gonzalez and Carrasquillo, 2019; Tramullas et al., 2021). While assaying females in all four estrus stages would be ideal, these groupings were sufficient to elucidate the main effects of sex hormones. Furthermore, this would necessitate the use of at least twice as many female animals to reach the same end. Indeed, the lack of differences found in our study suggests further separation may not have provided more information. This work represents, to our knowledge, the first characterization of P-gp and Bcrp mRNA and protein expression in the male and female retina in the context of morphine treatment. Importantly, there is evidence of circadian oscillations in P-gp-mediated transport (Kervezee et al., 2014; Zhang et al., 2021), which may

alter morphine pharmacokinetics over the course of the day. Since this study examined morphine pharmacokinetics and transporter expression at ZT 1, future experiments are needed to assess how circadian oscillations in transporter expression/function might alter morphine uptake and clearance from the CNS. Furthermore, future studies should also assess how circadian oscillations in opioid receptor expression (Naber et al., 1981; Mitchell et al., 1998; Jabourian et al., 2005; Yoshida et al., 2005; Takada et al., 2013) contribute to the behavioral effects of morphine and its deposition in the brain and retina.

We recapitulated findings that sex hormones influence P-gp and Bcrp expression in the brain, with expression being higher in High E/P females than in males. This is consistent with previous reports of testosterone inhibiting P-gp expression and efflux activity in tissues like the liver, kidney, and cornea (Dey et al., 2004; Suzuki et al., 2006; Shchul'kin et al., 2017), as well as reports that Bcrp is more highly expressed in the female rat brain than in males (Tanaka et al., 2005). Conversely, we did not find an effect of sex or estrus stage on the expression of either P-gp or Bcrp mRNA in the retina (Figure 3-11), consistent with the P-gp and Bcrp immunohistochemical labeling (Figure 3-4). While we anticipated that circulating levels of sex hormones could influence opioid transporter expression, our work is consistent with their effect varying by tissue type and species (Dalla et al., 2022). Furthermore, we found no significant differences in morphine deposition in the brain or retina of males and females. This finding is consistent with past literature that examined morphine pharmacokinetics in the brain (Cicero et al., 1997) and plasma (Sarton et al., 2000), as well as a previous report that the effect of P-gp on morphine content in the brain is not different between female and male mice (Dagenais et al., 2001). In addition, these findings imply that the metabolism of the intraperitoneal morphine injections are not significantly impacted by sex hormones. While we cannot exclude the

possibility that the pharmacokinetics of morphine shows sex-dependent differences at later time-points, our overall results suggest morphine would also accumulate in female retinas upon chronic administration, as previously shown for males (Bergum et al., 2022a). Intraperitoneal injections undergo rapid first-pass metabolism in the liver before reaching the systemic circulation (Handal et al., 2002; Turner et al., 2011), thus future studies using intravenous drug infusions might provide a clearer picture of the role that steroid hormones play in the regulation of opioid transport at the BBB and BRB.

After performing an extensive analysis of the expression patterns of P-gp and Bcrp in the CNS (brain/retina) of male and female mice, we wanted to weigh the relative contribution of each transporter to morphine deposition in the retina relative to the brain. We found that P-gp mRNA expression in the brain was nearly three-fold higher than Bcrp mRNA expression, which aligns with a report of higher expression of P-gp than Bcrp at the BBB measured by mass spectrometry (Kamiie et al., 2008). These data support the existing notion that P-gp is the primary opioid transporter at the BBB (Yang et al., 2018). Contrastingly, P-gp and Bcrp in the retina were similarly expressed in both males and females, with Bcrp expression being only slightly higher than P-gp in High E/P females. Despite their similar expression levels in the retina, two pieces of data suggest that P-gp is a more significant opioid transporter at the iBRB than Bcrp. First is P-gp's exclusive presence in the iBRB compared to the expression of Bcrp by some other retinal structures. Second, only P-gp expression significantly correlated with morphine deposition in the retina, whereas the relationship between retinal Bcrp and morphine content was not statistically significant. Interestingly, the expression levels of both transporters appeared to be relatively poor predictors of brain morphine deposition, suggesting that neither P-gp nor Bcrp expression directly affect morphine concentration in the brain. Although our data

indicates that P-gp is the main transporter involved in regulating morphine deposition in the retina, there is evidence that suggests P-gp and Bcrp work cooperatively to efflux common substrates at the BBB (Agarwal and Elmquist, 2012; Yang et al., 2018). At the iBRB, it has been shown that P-gp transport of verapamil is greater than that by Bcrp (Chapy et al., 2016), however, transporter function is known to be substrate dependent (Yang et al., 2018). Thus, functional studies of opioid (e.g. morphine) transport by P-gp and Bcrp at the iBRB are needed to elucidate the contributions and potential cooperative effect of these transporters. Such investigations should include studies that test the role of these ABC transporters in the retinal deposition of morphine, as well as other commonly administered opioids that are known P-gp substrates, such as methadone, buprenorphine, and fentanyl (Yang et al., 2018).

At first glance, the finding that P-gp expression in the retina, but not the brain, correlates positively with CNS morphine concentrations appears to be at odds with previous findings that P-gp negatively correlates with morphine deposition (Hamabe et al., 2007). Indeed our previous paper reported an inverse relationship between P-gp expression and morphine deposition when comparing the brain and retina (Bergum et al., 2022a). However, we do not believe that these findings are necessarily inconsistent with previous studies examining P-gp's role in morphine transport across blood-CNS barriers. The positive relationship between P-gp expression at the iBRB and morphine deposition in the retina may be due to the relatively low abundance of this transporter at this barrier. In other words, P-gp expression in the brain is much more robust; therefore, small reductions in P-gp expression will not significantly alter the morphine transport across the BBB. On the other hand, with relatively low P-gp expression in the retina, every P-gp transporter at the iBRB has a larger effect on the overall morphine transport. The interpretation of this data is particularly difficult when we consider that P-gp could be expressed at both the

basal and laminar sides of the endothelial cells that make up the iBRB and BBB (Yang et al., 2018). While ABC transporters are typically believed to be located on the luminal membrane of capillary endothelial cells to facilitate morphine efflux (Viscusi and Viscusi, 2020), localization to the sublaminar/basolateral membrane could also facilitate morphine transport into the CNS (Yang et al., 2018). High resolution imaging along with functional transport studies may provide a more detailed understanding of the role of P-gp in the influx/efflux of drugs like morphine across blood-CNS barriers.

Opioid pharmacokinetics in the CNS may not only depend on the activity of transporter proteins but on the integrity of blood-CNS barriers. Fluorescence imaging of FITC or FITC-dextran extravasation is a common assay for measuring BBB or BRB permeability (Li et al., 2011; Miyata and Morita, 2011; Liang et al., 2012; Frahm and Tobet, 2015; Natarajan et al., 2017; Xu et al., 2019). There have been reports of morphine exposure impairing barrier integrity *in vitro* through a reduction of tight junction protein ZO-1 (Wen et al., 2011) as well as reports that chronic morphine exposure (via time-released pelleted implants) increases BBB permeability to fluorescently-labeled dextrans in mice (Leibrand et al., 2019). However, it has also been suggested that, rather than chronic morphine exposure itself affecting BBB permeability, withdrawal from the drug increases BBB permeability (Sharma and Ali, 2006). This is similar to the previous uncertainty regarding whether chronic morphine exposure caused an upregulation of P-gp expression, which is now thought to be a withdrawal effect (Yousif et al., 2008, 2012; Bergum et al., 2022a). Given that morphine clears from the brain within just 3 hours post-injection (Bergum et al., 2022a), it is critical to harvest brain tissue soon after the drug administration to differentiate the effects of morphine exposure from withdrawal effects. As such, we performed these assays approximately 1 hour after the injection to ensure peak

concentrations of morphine were present in the brain and retina. We found no effect of chronic morphine treatment on barrier permeability, suggesting that BRB integrity does not contribute to the selective accumulation of morphine in the retina. Although there is evidence that sex hormones (as well as age and disease) can influence blood-CNS barrier integrity (Bake and Sohrabji, 2004; Wilson et al., 2008; Cipolla et al., 2009; Atallah et al., 2017; Dion-Albert et al., 2022), the permeability of the BBB was reported to be similar in male and female healthy adult mice (Schaffenrath et al., 2021). In conjunction with the lack of sex differences in morphine pharmacokinetics and transporter expression in the retina presented here, these data suggest that barrier integrity does not influence morphine pharmacokinetics and is therefore not a likely source of the sex-dependent differences in morphine efficacy.

The current study establishes the role of ABC transporters in morphine's selective persistence and accumulation in the eye: a phenomenon that has been shown not just in mice (Bergum et al., 2022a) but in humans as well (Wyman and Bultman, 2004; Bévalot et al., 2016). We found that morphine deposition in the CNS (retina/brain) is not dependent on sex/sex hormones. While this is consistent with previous reports, questions remain as to the molecular origins of sex differences in the efficacy of and outcomes associated with opioid drugs. The role of sex on opioid-mediated antinociception is complex, ranging from the physiological (i.e. sex hormones, neuroanatomical differences) to the psychosocial (Nasser and Afify, 2019). As with opioid-mediated antinociception, the relationship between opioids, sleep/wake disturbances and sex is still being unraveled (Tripathi et al., 2020; Huhn and Finan, 2021). Some evidence suggests women are more likely to experience opioid-induced sleep disturbances (OISD) (Finan et al., 2020; Ellis et al., 2022). Importantly, OISD are emerging as a promising therapeutic target for opioid use disorder (Huhn and Finan, 2021). While the mechanisms underlying OISD are still

not known, our recent work suggests that opioids modulate sleep/wake behavior through the μ-opioid receptors (MORs) expressed by intrinsically photosensitive retinal ganglion cells (ipRGCs) (Tripathi et al., 2020; Huhn and Finan, 2021; Bergum et al., 2022c). Indeed, endogenous opioid peptides activate the MORs expressed by ipRGCs to modulate healthy sleep/wake (Berezin et al., 2022). Furthermore, the MORs expressed by ipRGCs mediate morphine-induced sleep/wake changes (i.e. behavioral sensitization) (Bergum et al., 2022b). Thus, the persistence of morphine in the retina may allow for prolonged activation of the MORs expressed by ipRGCs, which could disrupt endogenous opioid signaling and lead to OISD (Berezin et al., 2022; Bergum et al., 2022b, 2022c). The results presented here position P-glycoprotein expression as an important determinant of retinal morphine pharmacokinetics in the inner retina. Continued characterization of opioid pharmacokinetics in the brain and retina will facilitate the development of potential therapeutics for OISD and opioid use disorder.

# CHAPTER 4: Discussion

## 4.1 Overview

The central hypothesis investigated in the current work is that the bioavailability of opioids (i.e. endogenous opioid peptides and/or opioids drugs) in the retina modulates sleep/wake behavior. In Chapter 2, we presented evidence that endogenous opioid peptides contribute to healthy sleep/wake behavior through the MORs expressed by ipRGCs. As will be discussed below, concurrent work showed that chronic morphine treatment interferes with sleep/wake behavior in mice via this endogenous opioid system in the retina. In conjunction with our recent work showing that morphine accumulates in the mouse retina upon chronic treatment, these data present a novel pathway by which opioid-induced sleep disturbances (OISD) may develop. Thus, in Chapter 3, we assessed the molecular machinery that may regulate opioid transport in the retina and found that low expression of the transporter P-glycoprotein (P-gp) may allow morphine to persist in the retina. In this Chapter, the potential for P-gp to be leveraged into a molecular target for modulating opioid bioavailability in the eye and alleviating OISD is discussed.

## 4.2 Modulation of sleep/wake behavior by retinal opioids

Our lab recently developed a mouse line with a cell-specific knockout of MORs from ipRGCs (McKO) by crossing *Opn4*-Cre mice with μflx mice, which have exons 2 and 3 of the *Oprm1* (MOR) gene flanked by loxP sites (Berezin et al., 2022; Cleymaet et al., 2021). Cre-dependent MOR knockout mice have been used to dissect the neuronal populations that mediate the effects of opioids (Boulos et al., 2020; Severino et al., 2020; Weibel et al., 2013). Like those groups before us, we primarily relied on mRNA quantification to validate our McKO line

(Chapter 2.4C, Appendix A), as there are no commercially available antibodies that can accurately differentiate the full-length and truncated MOR sequences (Table A-1). Nevertheless, we found a robust decrease in MOR mRNA expression by both qRT-PCR and digital droplet PCR (ddPCR), which was specific to the retina and not found in any region of the brain.

By measuring sleep/wake activity via wireless telemetry transmitters, we found that McKO mice had altered sleep/wake behavior compared to control mice (Berezin et al., 2022). Specifically, McKO mice had decreased wakefulness, and accordingly, increased slow-wave sleep, in the dark. This suggests that endogenous activation of the MORs expressed by ipRGCs is needed in the dark phase to promote wakefulness in the nocturnal mouse. Since light-evoked firing by ipRGCs is known to promote sleep in mice (Lupi et al., 2008), ipRGCs must be relatively inactive in the dark to inhibit sleep. However, ipRGCs have been shown to spontaneously spike in the dark and are sensitive to even small amounts of light (Do et al., 2009; Zhao et al., 2014). It has been postulated that the firing of ipRGCs must be inhibited to prevent them from continuously signaling the presence of "light" to the brain (Altimus et al., 2008; Schmidt et al., 2011). Our results suggest that this inhibition of light-evoked and/or spontaneous firing by ipRGCs could be achieved by increased activation of their MORs in the dark. Indeed, photoreceptors maintain circadian rhythms in the SCN, even in the dark (Lee et al., 2003). Our results confirm the notion that without MOR-mediated inhibition of ipRGCs in McKO mice, these cells communicate spontaneous "light" signals to the brain which disrupt normal sleep/wake cycles.

Given the cyclic expression of POMC and the light-dependent expression changes in β-endorphin we showed in Chapter 2, β-endorphin is well-positioned to activate the MORs expressed by ipRGCs in the dark. However, we cannot exclude that other opioid peptides (e.g.

shorter forms of β-endorphin and/or enkephalins) don't contribute (Gomes et al., 2020). The anti-β-endorphin antibody used in Chapter 2 recognizes the entire 31-amino acid sequence of β-endorphin, including the Tyr-Gly-Gly-Phe-Leu/*Met* motif, so it may also label shorter β-endorphin peptides (e.g. γ-endorphin, β-endorphin-26, β-endorphin-27) and enkephalins (esp. Met-enkephalin due to higher sequence similarity). While it was previously thought that shorter β-endorphin peptides were not MOR agonists, but rather antagonists or inactive peptides, it was recently shown that they do exhibit MOR agonist activity (Gomes et al., 2020). Thus, while we may overestimate the importance of full-length β-endorphin, we can conservatively say endogenous opioid peptides activate MORs expressed by ipRGCs to modulate sleep/wake activity, in addition to the pupillary light reflex (Berezin et al., 2022; Cleymaet et al., 2021).

In a concurrent study by our group (Bergum et al., 2022b), we showed that MORs expressed by ipRGCs also contribute to opioid-induced behavioral sensitization, which is the well-documented increase in activity rodents display after morphine exposure (Kalivas and Duffy, 1987). In this study, the activity of control (μflx), McKO and global MOR knockout (MKO) mice were compared over a 10-day, twice-daily chronic morphine paradigm. Control mice quickly developed morphine-induced behavioral sensitization and with continuing treatment, their sleep/wake cycles became more entrained to the daily injections than to the light/dark cycle. On the other hand, the activity of MKO mice was unaffected by morphine exposure, consistent with previous reports (Sora and Li, 2001; Tian et al., 1997; Yoo et al., 2003). In between these extremes were the McKO mice, which showed more behavioral sensitization than MKO mice but less than control mice. These differences suggest that although MORs expressed by other parts of the CNS also play a role, the MORs expressed by ipRGCs are important contributors to opioid-induced behavioral sensitization. Therefore, the action of both

endogenous opioid peptides and opioid drugs on the MORs expressed by ipRGCs plays a previously unrecognized role in (dys)regulating mammalian sleep/wake behavior. This presents an exciting new pathway by which OISD may develop and/or persist, however the ability to leverage this knowledge into a therapeutic requires a better understanding of the pharmacokinetics of opioids in the retina.

### 4.3 Opioid pharmacokinetics and transport in the retina

Systemically applied opioids pass the blood-retina barrier and can be detected in the vitreous humor/retina of both humans and mice (Bergum et al., 2022a; Fernández et al., 2013; Wyman and Bultman, 2004). Interestingly, the concentration of morphine that can be detected in the retina is consistently higher than in the brain, with or without normalizing for differences in the weight of each tissue (Chapter 3; Bergum et al., 2022a). This is especially intriguing given that most research on primary opioid effects (in general and on sleep/wake) has focused on the brain. In addition, morphine persists for at least twelve hours in the retina after an intraperitoneal injection, and continues to accumulate to ever higher levels upon chronic administration (Bergum et al., 2022a). Conversely, the pharmacokinetics of morphine in the blood and brain tissue don't change with repeated exposure (Bergum et al., 2022a). The persistence and accumulation of morphine in the retina suggests that opioids in the eye could constitutively activate the MORs expressed by ipRGCs to dysregulate their activity, leading to sleep disruption.

We hypothesized that the unique pharmacokinetics of morphine in the retina compared to the brain could be related to the expression and/or function of opioid transporter proteins at the blood-retina barrier (BRB) and blood-brain barrier (BBB), respectively. ATP-binding cassette (ABC) transporters, especially P-glycoprotein (P-gp) and to a lesser degree, breast cancer

resistance protein (Bcrp), are considered the premier opioid efflux transporters at the BBB (Liu and Liu, 2019; Yang et al., 2018). It has been shown that the function of both Bcrp and P-gp are lower at the BRB than BBB (Bauer et al., 2017; Chapy et al., 2016; Fujii et al., 2014; Liu and Liu, 2019), however little attention has been paid to the role of ABC transporters at the BRB in opioid transport. Thus, in Chapter 3, we characterized ABC transporters at the BRB and BBB in the context of morphine treatment.

First, we found that P-gp and Bcrp expression is unchanged by chronic morphine treatment (twice daily, 6 d, 20 mg/kg i.p.) in both the retina and brain, consistent with reports that upregulation of P-gp is a response to morphine withdrawal, rather than drug exposure itself (Bergum et al., 2022a; Chaves et al., 2016; Yousif et al., 2012). In the context of acute morphine treatment, we found that P-gp is highly expressed in the brain compared to the retina, similar to a previous proteomics report (Zhang et al., 2017). In addition, P-gp was much more highly expressed than Bcrp in the brain. These data are consistent with P-gp's position as the primary morphine extruder at the BBB. Conversely, although the relative expression of P-gp and Bcrp were similar in the retina, overall transporter expression was lower than in the brain. We found a significant correlation between P-gp expression and morphine deposition in the retina, but no significant correlation between retinal Bcrp expression and morphine content, suggesting P-gp is the more important morphine transporter at the BRB. Low ABC transporter (i.e. P-gp and Bcrp) expression might explain the persistence and accumulation of morphine in the retina, compared to the brain where transporter expression is high and morphine is more quickly cleared from the tissue.

Notably, the experiments in Chapter 3 were performed in male mice, as well as two groups of female mice separated by hormone profile: mice in estrus/proestrus with relatively

high estrogen:progesterone ratios (High E/P females) and mice in diestrus/metestrus with relatively low estrogen:progesterone ratios (Low E/P females). Somewhat surprisingly, we found no sex/estrous effects on transporter expression in the retina. Although transporter expression seems to be sex-dependent in some cases, it is well-known that it is also tissue- and species-dependent (Bebawy and Chetty, 2009; Dalla et al., 2022; Piquette-Miller et al., 1998; Robison et al., 2019; Shchul'kin et al., 2017; Suzuki et al., 2006; Tanaka et al., 2005). In addition, our results show that morphine deposition in the retinas of male and female mice are not significantly different 1 hour after injection. This suggests that morphine would accumulate in female retinas upon chronic administration as we've shown with males (Bergum et al., 2022a). Nonetheless, we cannot exclude that morphine pharmacokinetics in the retina differ between males and females at other time points or in ways that we did not measure. For example, it has been shown that differential morphine metabolism between males and females can underlie sex-specific differences in opioid effect (e.g. analgesia) (Gabel et al., 2021). Specifically, the half-life of morphine in the blood and brain is shorter in female mice than males, and levels of morphine's primary metabolite, morphine-3-glucuronide (M3G), are higher, suggesting differences in the rate of morphine metabolism between the sexes (Gabel et al., 2021). Notably, morphine is metabolized into M3G and morphine-6-glucuronide (M6G) in humans, but mice lack the enzyme needed to produce M6G (Gabel et al., 2021).

In addition, while we focused our efforts on two opioid extruders that were well-characterized at the BBB, the influx and efflux of opioids could be affected by other ABC transporters, such as the multidrug resistance proteins (besides Mrp2, given the results presented in Chapter 3), and/or other classes of transporters, such as organic anion transporting polypeptides (OATPs) or organic cation transporters (OCTs) (Dalla et al., 2022). Furthermore,

the permeability and integrity of blood-CNS barriers seem to be regulated by circulating sex hormones (Dion-Albert et al., 2022). For example, ovariectomy and castration both increase BBB permeability in rodents, which can be reversed by estrogen and testosterone treatment, respectively (Atallah et al., 2017; Bake and Sohrabji, 2004; Cipolla et al., 2009; Dion-Albert et al., 2022; Wilson et al., 2008). However, in older, reproductively senescent rats, estrogen treatment further increases BBB permeability in some regions, suggesting an interaction between sex hormones and age (Bake and Sohrabji, 2004). Despite the potential effects of sex hormones on blood-CNS barrier integrity, we found no differences in morphine deposition or transporter expression in the retina between males and females. Morphine itself has been thought to affect blood-CNS barriers, though our results are consistent with this being a withdrawal effect, at least in male mice (Leibrand et al., 2019; Sharma and Ali, 2006). Future studies should explicitly assess BRB permeability in male and female mice both during and after morphine treatment using fluorescent extravasation studies to visualize barrier "leakage" (Frahm and Tobet, 2015).

### 4.4 P-glycoprotein as a therapeutic target for opioid-induced sleep disturbances (OISD)

The data presented in Chapter 3 positions P-gp as a notable opioid transporter at the BRB and BBB of male and female mice. Given its known role as an opioid extruder, low P-gp expression in the retina (compared to the brain) may be insufficient to clear morphine in a timely manner. This could allow for constitutive aberrant activation of the MORs expressed by ipRGCs, thus leading to OISD. Ongoing work seeks to ameliorate this disparity by upregulating P-gp expression at the BRB. Intraperitoneal injection of the non-steroidal anti-inflammatory drug (NSAID), diclofenac, upregulates P-gp expression and function at the BBB (Sanchez-Covarrubias et al., 2014). When given 3 hours before morphine, morphine uptake into the brain

and morphine-induced analgesia are diminished (Sanchez-Covarrubias et al., 2014). In addition, acetaminophen, another NSAID, also upregulates P-gp expression at the BBB and results in lower morphine deposition and decreased analgesia (Slosky et al., 2013). Our preliminary data suggests systemically applied diclofenac indeed upregulates P-gp function at the BRB. However, the penetrance of systemically administered drugs across the blood-retina barrier may be limited (Gulilat et al., 2020) and this mode of administration will likely affect P-gp expression throughout the body. Thus, focal delivery of diclofenac may be the preferred route. While topical diclofenac eye drops exist (Abbas Khan, 2011; Bai et al., 2022; Iwamoto et al., 2017; Lekhanont et al., 2007; Ylinen et al., 2018), intravitreal injection is more likely to efficiently penetrate to the posterior segment of the eye (i.e. the retina) (Durairaj et al., 2009; Soheilian et al., 2010).

### 4.4 Translational considerations

Although they are nocturnal, mice present a great model for studying sleep/wake behavior because they are genetically tractable, allowing us to produce transgenic knockout mice, and because the molecular processes by which ipRGCs fire and communicate with the brain are thought to be similar in humans (Hastings et al., 2018). Yet there are differences and uncertainties between mice and humans that should be noted. In terms of gross eye anatomy, the volume of vitreous humor in the mouse is much smaller than in humans, not just because of the overall size of the eye, but because the mouse lens takes up a much larger proportion of the eye (Skeie et al., 2011). So although opioids can be detected in the vitreous humor of both species (Bergum et al., 2022a; Fernández et al., 2013; Wyman and Bultman, 2004), the dynamics of opioids in the vitreous humor may differ between mice and humans. In addition, while 6 ipRGC subtypes have been described in mice (M1, M2, ..., M6), humans also have giant M1 (GM1)

ipRGCs and it is yet unknown if humans have M5 and M6 ipRGC subtypes (Mure, 2021). However, these subtypes were only recently discovered in rodents (Quattrochi et al., 2019; Stabio et al., 2018), so in time, this uncertainty should be resolved. Furthermore, we cannot use fluorescent tracers to assess ipRGC projections in humans, but retinal neurons do project to hypothalamic nuclei in primates; it is still unclear whether these are ipRGC projections and whether these include hypothalamic sleep/wake centers, such as the SCN and VLPO (Abizaid et al., 2004; Costa et al., 1999; Mure, 2021). Lastly, it is not clear whether human ipRGCs express MORs, but some transcriptomics studies have detected *Oprm1* expression in human retina samples (Liang et al., 2019; Lukowski et al., 2019; Urrutia-Cabrera and Wong, 2020).

We found no sex differences in terms of ABC transporter expression and morphine deposition in the murine retina. However, some evidence suggests women are more likely to experience OISD than men (Coffey, 2018; Ellis et al., 2022; Finan et al., 2020), though larger studies and those using model organisms are needed (Huhn and Finan, 2021; Tripathi et al., 2020). It would therefore be important to repeat the sleep/wake experiments presented in Chapter 2 as well as the behavioral sensitization experiments discussed above in female mice. This would confirm that the MORs expressed by ipRGCs play a role in the (dys)regulation of sleep/wake behavior, and allow potential sex differences to be detected. Nevertheless, the results presented here suggest that ipRGCs present a novel pathway by which opioids modulate sleep behavior and position the upregulation of P-gp at the BRB as a potential therapeutic target for alleviating OISD through increased morphine clearance from the eye.

# REFERENCES


Abbas Khan, 2011. Drug-drug interaction between ciprofloxacin and diclofenac ophthalmic drops at ocular level. Afr. J. Pharm. Pharmacol. 5. https://doi.org/10.5897/AJPP11.381

Abizaid, A., Horvath, B., Keefe, D.L., Leranth, C., Horvath, T.L., 2004. Direct visual and circadian pathways target neuroendocrine cells in primates. European Journal of Neuroscience 20, 2767–2776. https://doi.org/10.1111/j.1460-9568.2004.03737.x

Abrimian, A., Kraft, T., Pan, Y.-X., 2021. Endogenous Opioid Peptides and Alternatively Spliced Mu Opioid Receptor Seven Transmembrane Carboxyl-Terminal Variants. Int J Mol Sci 22, 3779. https://doi.org/10.3390/ijms22073779

Adachi, H., Tominaga, H., Maruyama, Y., Yoneda, K., Maruyama, K., Yoshii, K., Kinoshita, S., Nakano, M., Tashiro, K., 2015. Stage-specific reference genes significant for quantitative PCR during mouse retinal development. Genes Cells 20, 625–635. https://doi.org/10.1111/gtc.12254

Adams, G., 2020. A beginner's guide to RT-PCR, qPCR and RT-qPCR. The Biochemist 42, 48–53. https://doi.org/10.1042/BIO20200034

Agapito, M.A., Zhang, C., Murugan, S., Sarkar, D.K., 2014. Fetal Alcohol Exposure Disrupts Metabolic Signaling in Hypothalamic Proopiomelanocortin Neurons via a Circadian Mechanism in Male Mice. Endocrinology 155, 2578–2588. https://doi.org/10.1210/en.2013-2030

Agarwal, S., Elmquist, W.F., 2012. Insight into the Cooperation of P-glycoprotein (ABCB1) and Breast Cancer Resistance Protein (ABCG2) at the Blood–Brain Barrier: A Case Study Examining Sorafenib Efflux Clearance. Mol. Pharmaceutics 9, 678–684. https://doi.org/10.1021/mp200465c

Al-Hasani, R., Bruchas, M.R., 2011. Molecular Mechanisms of Opioid Receptor-Dependent Signaling and Behavior. Anesthesiology 115, 1363–1381. https://doi.org/10.1097/ALN.0b013e318238bba6

Altimus, C.M., Guler, A.D., Villa, K.L., McNeill, D.S., LeGates, T.A., Hattar, S., 2008. Rods-cones and melanopsin detect light and dark to modulate sleep independent of image formation. PNAS 105, 19998–20003. https://doi.org/10.1073/pnas.0808312105

Altschuler, R.A., Mosinger, J.L., Hoffman, D.W., Parakkal, M.H., 1982. Immunocytochemical localization of enkephalin-like immunoreactivity in the retina of the guinea pig. PNAS 79, 2398–2400. https://doi.org/10.1073/pnas.79.7.2398

Asaad, T.A., Ghanem, M.H., Abdel Samee, A.M., El–Habiby, M.M., 2011. Sleep Profile in Patients With Chronic Opioid Abuse: A Polysomnographic Evaluation in an Egyptian Sample. Addictive Disorders & Their Treatment 10, 21. https://doi.org/10.1097/ADT.0b013e3181fb2847

Atallah, A., Mhaouty-Kodja, S., Grange-Messent, V., 2017. Chronic depletion of gonadal testosterone leads to blood–brain barrier dysfunction and inflammation in male mice. J Cereb Blood Flow Metab 37, 3161–3175. https://doi.org/10.1177/0271678X16683961

Bai, R., Liu, L., Chen, Z., Ma, Q., 2022. Cyclosporine (0.05%) Combined with Diclofenac Sodium Eye Drops for the Treatment of Dry Eye Disease. Journal of Ophthalmology 2022, e2334077. https://doi.org/10.1155/2022/2334077

Bake, S., Sohrabji, F., 2004. 17β-Estradiol Differentially Regulates Blood-Brain Barrier Permeability in Young and Aging Female Rats. Endocrinology 145, 5471–5475. https://doi.org/10.1210/en.2004-0984
Bartley, E.J., Fillingim, R.B., 2013. Sex differences in pain: a brief review of clinical and experimental findings. BJA: British Journal of Anaesthesia 111, 52–58. https://doi.org/10.1093/bja/aet127
Bates, D., Mächler, M., Bolker, B., Walker, S., 2015. Fitting Linear Mixed-Effects Models Using lme4. Journal of Statistical Software 67, 1–48. https://doi.org/10.18637/jss.v067.i01
Bauer, M., Karch, R., Tournier, N., Cisternino, S., Wadsak, W., Hacker, M., Marhofer, P., Zeitlinger, M., Langer, O., 2017. Assessment of P-Glycoprotein Transport Activity at the Human Blood–Retina Barrier with (R)-11C-Verapamil PET. Journal of Nuclear Medicine 58, 678–681. https://doi.org/10.2967/jnumed.116.182147
Baver, S.B., Pickard, Galen E., Sollars, P.J., Pickard, Gary E., 2008. Two types of melanopsin retinal ganglion cell differentially innervate the hypothalamic suprachiasmatic nucleus and the olivary pretectal nucleus. Eur J Neurosci 27, 1763–1770. https://doi.org/10.1111/j.1460-9568.2008.06149.x
Bebawy, M., Chetty, M., 2009. Gender Differences in P-Glycoprotein Expression and Function: Effects on Drug Disposition and Outcome. CDM 10, 322–328. https://doi.org/10.2174/138920009788498996
Beckman, A.L., Llados-Eckman, C., Stanton, T.L., 1992. Reduction of hibernation bout duration by intraventricular infusion of met-enkephalin. Brain Research 588, 159–163. https://doi.org/10.1016/0006-8993(92)91357-K
Beier, C., Zhang, Z., Yurgel, M., Hattar, S., 2021. Projections of ipRGCs and conventional RGCs to retinorecipient brain nuclei. J Comp Neurol 529, 1863–1875. https://doi.org/10.1002/cne.25061
Benyamin, R., Trescot, A., Datta, S., Buenaventura, R., Adlaka, R., Sehgal, N., Glaser, S., Vallejo, R., 2008. Opioid Complications and Side Effects. Pain physician 11, S105-20. https://doi.org/10.36076/ppj.2008/11/S105
Berezin, C.-T., Bergum, N., Luchini, K.A., Curdts, S., Korkis, C., Vigh, J., 2022. Endogenous opioid signaling in the retina modulates sleep/wake activity in mice. Neurobiology of Sleep and Circadian Rhythms 13, 100078. https://doi.org/10.1016/j.nbscr.2022.100078
Bergum, N., Berezin, C.-T., Dooley, G., Vigh, J., 2022a. Morphine Accumulates in the Retina Following Chronic Systemic Administration. Pharmaceuticals 15, 527. https://doi.org/10.3390/ph15050527
Bergum, N., Berezin, C.-T., King, C.M., Vigh, J., 2022b. μ-Opioid Receptors Expressed by Intrinsically Photosensitive Retinal Ganglion Cells Contribute to Morphine-Induced Behavioral Sensitization. International Journal of Molecular Sciences 23, 15870. https://doi.org/10.3390/ijms232415870
Bergum, N., Berezin, C.-T., Vigh, J., 2022c. A retinal contribution to opioid-induced sleep disorders? Frontiers in Neuroscience 16.
Berson, D.M., 2003. Strange vision: ganglion cells as circadian photoreceptors. Trends Neurosci 26, 314–320. https://doi.org/10.1016/S0166-2236(03)00130-9
Bévalot, F., Cartiser, N., Bottinelli, C., Fanton, L., Guitton, J., 2016. Vitreous humor analysis for the detection of xenobiotics in forensic toxicology: a review. Forensic Toxicol 34, 12–40. https://doi.org/10.1007/s11419-015-0294-5

Bicknell, A.B., 2008. The Tissue-Specific Processing of Pro-Opiomelanocortin. J Neuroendocrinol 20, 692–699. https://doi.org/10.1111/j.1365-2826.2008.01709.x
Bolte, S., Cordelières, F.P., 2006. A guided tour into subcellular colocalization analysis in light microscopy. J Microsc 224, 213–232. https://doi.org/10.1111/j.1365-2818.2006.01706.x
Borbe, H.O., Wollert, U., Müller, W.E., 1982. Stereospecific [3H]naloxone binding associated with opiate receptors in bovine retina. Exp Eye Res 34, 539–544. https://doi.org/10.1016/0014-4835(82)90026-4
Borniger, J.C., Weil, Z.M., Zhang, N., Nelson, R.J., 2013. Dim Light at Night Does Not Disrupt Timing or Quality of Sleep in Mice. Chronobiol Int 30, 1016–1023. https://doi.org/10.3109/07420528.2013.803196
Boulos, L.J., Ben Hamida, S., Bailly, J., Maitra, M., Ehrlich, A.T., Gavériaux-Ruff, C., Darcq, E., Kieffer, B.L., 2020. Mu opioid receptors in the medial habenula contribute to naloxone aversion. Neuropsychopharmacology 45, 247–255. https://doi.org/10.1038/s41386-019-0395-7
Brecha, N.C., 2004. Peptide and Peptide Receptor Expression and Function in the Vertebrate Retina, in: Chalupa, L.M., Werner, J.S. (Eds.), The Visual Neurosciences. MIT Press, pp. 334–354.
Broestl, L., Worden, K., Moreno, A.J., Davis, E.J., Wang, D., Garay, B., Singh, T., Verret, L., Palop, J.J., Dubal, D.B., 2018. Ovarian Cycle Stages Modulate Alzheimer-Related Cognitive and Brain Network Alterations in Female Mice. eNeuro 5. https://doi.org/10.1523/ENEURO.0132-17.2018
Brownstein, M.J., 1993. A brief history of opiates, opioid peptides, and opioid receptors. PNAS 90, 5391–5393. https://doi.org/10.1073/pnas.90.12.5391
Burbach, J.P.H., 2010. Neuropeptides from concept to online database www.neuropeptides.nl. Eur J Pharmacol, Cognition Disturbances in Psychiatry: Neurobiology and Treatment (In memory of David de Wied) 626, 27–48. https://doi.org/10.1016/j.ejphar.2009.10.015
Burke, C.K., Peirce, J.M., Kidorf, M.S., Neubauer, D., Punjabi, N.M., Stoller, K.B., Hursh, S., Brooner, R.K., 2008. Sleep problems reported by patients entering opioid agonist treatment. J Subst Abuse Treat 35, 328–333. https://doi.org/10.1016/j.jsat.2007.10.003.
Candido, J., Lutfy, K., Billings, B., Sierra, V., Duttaroy, A., Inturrisi, C.E., Yoburn, B.C., 1992. Effect of adrenal and sex hormones on opioid analgesia and opioid receptor regulation. Pharmacology Biochemistry and Behavior 42, 685–692. https://doi.org/10.1016/0091-3057(92)90015-8
Cawley, N.X., Li, Z., Loh, Y.P., 2016. 60 YEARS OF POMC: Biosynthesis, trafficking, and secretion of pro-opiomelanocortin-derived peptides. J Clin Mol Endocrinol 56, T77–T97. https://doi.org/10.1530/JME-15-0323
Chapy, H., Saubaméa, B., Tournier, N., Bourasset, F., Behar-Cohen, F., Declèves, X., Scherrmann, J.-M., Cisternino, S., 2016. Blood–brain and retinal barriers show dissimilar ABC transporter impacts and concealed effect of P-glycoprotein on a novel verapamil influx carrier. Br J Pharmacol 173, 497–510. https://doi.org/10.1111/bph.13376
Chaves, C., Gómez-Zepeda, D., Auvity, S., Menet, M.-C., Crété, D., Labat, L., Remião, F., Cisternino, S., Declèves, X., 2016. Effect of Subchronic Intravenous Morphine Infusion and Naloxone-Precipitated Morphine Withdrawal on P-gp and Bcrp at the Rat Blood–Brain Barrier. Journal of Pharmaceutical Sciences 105, 350–358. https://doi.org/10.1002/jps.24697

Chaves, C., Remião, F., Cisternino, S., Declèves, X., 2017. Opioids and the Blood-Brain Barrier: A Dynamic Interaction with Consequences on Drug Disposition in Brain. Curr Neuropharmacol 15, 1156–1173. https://doi.org/10.2174/1570159X15666170504095823

Chen, C.P., Kuhn, P., Advis, J.P., Sarkar, D.K., 2004. Chronic ethanol consumption impairs the circadian rhythm of pro-opiomelanocortin and period genes mRNA expression in the hypothalamus of the male rat: Alcohol effects on hypothalamic clocks. J Neurochem 88, 1547–1554. https://doi.org/10.1046/j.1471-4159.2003.02300.x

Chiang, C.-K., Mehta, N., Patel, A., Zhang, P., Ning, Z., Mayne, J., Sun, W.Y.L., Cheng, H.-Y.M., Figeys, D., 2014. The Proteomic Landscape of the Suprachiasmatic Nucleus Clock Reveals Large-Scale Coordination of Key Biological Processes. PLoS Genet 10, e1004695. https://doi.org/10.1371/journal.pgen.1004695

Chu, L.F., Angst, M.S., Clark, D., 2008. Opioid-induced hyperalgesia in humans: molecular mechanisms and clinical considerations. Clin J Pain 24, 479–496. https://doi.org/10.1097/AJP.0b013e31816b2f43

Chung, S., Weber, F., Zhong, P., Tan, C.L., Nguyen, T.N., Beier, K.T., Hörmann, N., Chang, W.-C., Zhang, Z., Do, J.P., Yao, S., Krashes, M.J., Tasic, B., Cetin, A., Zeng, H., Knight, Z.A., Luo, L., Dan, Y., 2017. Identification of preoptic sleep neurons using retrograde labelling and gene profiling. Nature 545, 477–481. https://doi.org/10.1038/nature22350

Cicero, T.J., Nock, B., Meyer, E.R., 1997. Sex-Related Differences in Morphine's Antinociceptive Activity: Relationship to Serum and Brain Morphine Concentrations. J Pharmacol Exp Ther 282, 939–944.

Cipolla, M.J., Godfrey, J.A., Wiegman, M.J., 2009. The Effect of Ovariectomy and Estrogen on Penetrating Brain Arterioles and Blood-Brain Barrier Permeability. Microcirculation 16, 685–693. https://doi.org/10.3109/10739680903164131

Cleymaet, A.M., Berezin, C.-T., Vigh, J., 2021. Endogenous Opioid Signaling in the Mouse Retina Modulates Pupillary Light Reflex. IJMS 22, 554. https://doi.org/10.3390/ijms22020554

Cleymaet, A.M., Gallagher, S.K., Tooker, R.E., Lipin, M.Y., Renna, J.M., Sodhi, P., Berg, D., Hartwick, A.T.E., Berson, D.M., Vigh, J., 2019. μ-Opioid Receptor Activation Directly Modulates Intrinsically Photosensitive Retinal Ganglion Cells. Neuroscience 408, 400–417. https://doi.org/10.1016/j.neuroscience.2019.04.005

Coffey, A.A., 2018. Sleep and Circadian Disruption as an Aspect of Opioid Addiction in Rats and Humans (Ph.D.). The Pennsylvania State University, United States -- Pennsylvania.

Coffey, A.A., Guan, Z., Grigson, P.S., Fang, J., 2016. Reversal of the sleep–wake cycle by heroin self-administration in rats. Brain Research Bulletin, Addiction: From Mouse to Man 123, 33–46. https://doi.org/10.1016/j.brainresbull.2015.09.008

Corbett, A.D., Paterson, S.J., Kosterlitz, H.W., 1993. Selectivity of Ligands for Opioid Receptors, in: Herz, A., Akil, H., Simon, E.J. (Eds.), Opioids, Handbook of Experimental Pharmacology. Springer, Berlin, Heidelberg, pp. 645–679. https://doi.org/10.1007/978-3-642-77460-7_26

Costa, M.S.M.O., Santee, U.R., Cavalcante, J.S., Moraes, P.R.A., Santos, N.P., Britto, L.R.G., 1999. Retinohypothalamic projections in the common marmoset (Callithrix jacchus): A study using cholera toxin subunit B. Journal of Comparative Neurology 415, 393–403. https://doi.org/10.1002/(SICI)1096-9861(19991220)415:3<393::AID-CNE5>3.0.CO;2-R

Costes, S.V., Daelemans, D., Cho, E.H., Dobbin, Z., Pavlakis, G., Lockett, S., 2004. Automatic and Quantitative Measurement of Protein-Protein Colocalization in Live Cells. Biophys J 86, 3993–4003. https://doi.org/10.1529/biophysj.103.038422

Cox, B.M., 1982. Endogenous opioid peptides: A guide to structures and terminology. Life Sciences 31, 1645–1658. https://doi.org/10.1016/0024-3205(82)90179-5

Cutrufello, N.J., Ianus, V.D., Rowley, J.A., 2020. Opioids and sleep. Curr Opin Pulm Med 26, 634–641. https://doi.org/10.1097/MCP.0000000000000733

Czeisler, C.A., Shanahan, T.L., Klerman, E.B., Martens, H., Brotman, D.J., Emens, J.S., Klein, T., Rizzo, J.F., 1995. Suppression of Melatonin Secretion in Some Blind Patients by Exposure to Bright Light. New England Journal of Medicine 332, 6–11. https://doi.org/10.1056/NEJM199501053320102

Dagenais, C., Zong, J., Ducharme, J., Pollack, G.M., 2001. Effect of mdr1a P-glycoprotein gene disruption, gender, and substrate concentration on brain uptake of selected compounds. Pharmaceutical Research 18, 957–963. https://doi.org/10.1023/A:1010984110732

Dalla, C., Pavlidi, P., Sakelliadou, D.-G., Grammatikopoulou, T., Kokras, N., 2022. Sex Differences in Blood–Brain Barrier Transport of Psychotropic Drugs. Front Behav Neurosci 16, 844916. https://doi.org/10.3389/fnbeh.2022.844916

Dean, M., Dean, M., 2002. The Human ATP-Binding Cassette (ABC) Transporter Superfamily. National Center for Biotechnology Information (US).

Deboer, T., 2018. Sleep homeostasis and the circadian clock: Do the circadian pacemaker and the sleep homeostat influence each other's functioning? Neurobiology of Sleep and Circadian Rhythms 5, 68–77. https://doi.org/10.1016/j.nbscr.2018.02.003

Dey, S., Gunda, S., Mitra, A.K., 2004. Pharmacokinetics of Erythromycin in Rabbit Corneas after Single-Dose Infusion: Role of P-Glycoprotein as a Barrier to in Vivo Ocular Drug Absorption. J Pharmacol Exp Ther 311, 246–255. https://doi.org/10.1124/jpet.104.069583

Dhaliwal, A., Gupta, M., 2022. Physiology, Opioid Receptor, in: StatPearls. StatPearls Publishing, Treasure Island (FL).

Dimsdale, J.E., 2022. The Effect of Opioids on Sleep Architecture. Journal of Clinical Sleep Medicine 3.

Dion-Albert, L., Bandeira Binder, L., Daigle, B., Hong-Minh, A., Lebel, M., Menard, C., 2022. Sex differences in the blood–brain barrier: Implications for mental health. Frontiers in Neuroendocrinology 65, 100989. https://doi.org/10.1016/j.yfrne.2022.100989

Do, M.T.H., Kang, S.H., Xue, T., Zhong, H., Liao, H.-W., Bergles, D.E., Yau, K.-W., 2009. Photon capture and signalling by melanopsin retinal ganglion cells. Nature 457, 281–287. https://doi.org/10.1038/nature07682

Dubocovich, M.L., Weiner, N., 1983. Enkephalins modulate [3H]dopamine release from rabbit retina in vitro. J Pharmacol Exp Ther 224, 634–639.

Durairaj, C., Kim, S.J., Edelhauser, H.F., Shah, J.C., Kompella, U.B., 2009. Influence of Dosage Form on the Intravitreal Pharmacokinetics of Diclofenac. Investigative Ophthalmology & Visual Science 50, 4887–4897. https://doi.org/10.1167/iovs.09-3565

Eacret, D., Manduchi, E., Noreck, J., Tyner, E., Fenik, P., Dunn, A.D., Schug, J., Veasey, S.C., Blendy, J.A., 2023. Mu-opioid receptor-expressing neurons in the paraventricular thalamus modulate chronic morphine-induced wake alterations. Transl Psychiatry 13, 1–10. https://doi.org/10.1038/s41398-023-02382-w

Eacret, D., Veasey, S.C., Blendy, J.A., 2020. Bidirectional Relationship between Opioids and Disrupted Sleep: Putative Mechanisms. Mol Pharmacol 98, 445–453. https://doi.org/10.1124/mol.119.119107

Ecker, J.L., Dumitrescu, O.N., Wong, K.Y., Alam, N.M., Chen, S.-K., LeGates, T., Renna, J.M., Prusky, G.T., Berson, D.M., Hattar, S., 2010. Melanopsin-Expressing Retinal Ganglion-Cell Photoreceptors: Cellular Diversity and Role in Pattern Vision. Neuron 67, 49–60. https://doi.org/10.1016/j.neuron.2010.05.023

Ellis, J.D., Mayo, J.L., Gamaldo, C.E., Finan, P.H., Huhn, A.S., 2022. Worsening sleep quality across the lifespan and persistent sleep disturbances in persons with opioid use disorder. Journal of Clinical Sleep Medicine 18, 587–595. https://doi.org/10.5664/jcsm.9676

Fernandez, D.C., Chang, Y.-T., Hattar, S., Chen, S.-K., 2016. Architecture of retinal projections to the central circadian pacemaker. PNAS 113, 6047–6052. https://doi.org/10.1073/pnas.1523629113

Fernández, P., Seoane, S., Vázquez, C., Tabernero, M.J., Carro, A.M., Lorenzo, R.A., 2013. Chromatographic determination of drugs of abuse in vitreous humor using solid-phase extraction: Chromatographic determination of drugs of abuse in vitreous humor. J Appl Toxicol 33, 740–745. https://doi.org/10.1002/jat.2722

Fields, H.L., 2011. The Doctor's Dilemma: opiate analgesics and chronic pain. Neuron 69, 591–594. https://doi.org/10.1016/j.neuron.2011.02.001

Finan, P.H., Mun, C.J., Epstein, D.H., Kowalczyk, W.J., Phillips, K.A., Agage, D., Smith, M.T., Preston, K.L., 2020. Multimodal assessment of sleep in men and women during treatment for opioid use disorder. Drug and Alcohol Dependence 207, 107698. https://doi.org/10.1016/j.drugalcdep.2019.107698

Fisher, S.P., Godinho, S.I.H., Pothecary, C.A., Hankins, M.W., Foster, R.G., Peirson, S.N., 2012. Rapid assessment of sleep/wake behaviour in mice. J Biol Rhythms 27, 48–58. https://doi.org/10.1177/0748730411431550

Flyktman, A., Jernfors, T., Manttari, S., Nissila, J., Timonen, M., Saarela, S., 2017. Transcranial Light Alters Melanopsin and Monoamine Production in Mouse ( Mus musculus ) Brain. Journal of Neurology Research 7, 39–45. https://doi.org/10.14740/jnr.v7i3.427

Frahm, K.A., Tobet, S.A., 2015. Development of the blood–brain barrier within the paraventricular nucleus of the hypothalamus: influence of fetal glucocorticoid excess. Brain Struct Funct 220, 2225–2234. https://doi.org/10.1007/s00429-014-0787-8

Fratta, W., Collu, M., Martellotta, M.C., Pichiri, M., Muntoni, F., Gessa, G.L., 1987. Stress-induced insomnia: opioid-dopamine interactions. Eur J Pharmacol 142, 437–440. https://doi.org/10.1016/0014-2999(87)90084-7

Freedman, M.S., Lucas, R.J., Soni, B., von Schantz, M., Muñoz, M., David-Gray, Z., Foster, R., 1999. Regulation of Mammalian Circadian Behavior by Non-rod, Non-cone, Ocular Photoreceptors. Science 284, 502–504. https://doi.org/10.1126/science.284.5413.502

Freeman, W.M., Walker, S.J., Vrana, K.E., 1999. Quantitative RT-PCR: Pitfalls and Potential. BioTechniques 26, 112–125. https://doi.org/10.2144/99261rv01

Fujii, S., Setoguchi, C., Kawazu, K., Hosoya, K., 2014. Impact of P-Glycoprotein on Blood–Retinal Barrier Permeability: Comparison of Blood–Aqueous Humor and Blood–Brain Barrier Using Mdr1a Knockout Rats. Investigative Ophthalmology & Visual Science 55, 4650–4658. https://doi.org/10.1167/iovs.13-13819

Fuller, J.A., Brun-Zinkernagel, A.-M., Clark, A.F., Wordinger, R.J., 2009. Subtilisin-like proprotein convertase expression, localization, and activity in the human retina and optic

nerve head. Invest Ophthalmol Vis Sci 50, 5759–5768. https://doi.org/10.1167/iovs.08-2616
Fuller, P.M., Gooley, J.J., Saper, C.B., 2006. Neurobiology of the Sleep-Wake Cycle: Sleep Architecture, Circadian Regulation, and Regulatory Feedback. J Biol Rhythms 21, 482–493. https://doi.org/10.1177/0748730406294627
Gabel, F., Hovhannisyan, V., Andry, V., Goumon, Y., 2021. Central metabolism as a potential origin of sex differences in morphine antinociception but not induction of antinociceptive tolerance in mice. British Journal of Pharmacology n/a. https://doi.org/10.1111/bph.15792
Gallagher, S.K., Anglen, J.N., Mower, J.M., Vigh, J., 2012. Dopaminergic amacrine cells express opioid receptors in the mouse retina. Vis Neurosci 29, 203–209. https://doi.org/10.1017/S0952523812000156
Gallagher, S.K., Witkovsky, P., Roux, M.J., Low, M.J., Otero-Corchon, V., Hentges, S.T., Vigh, J., 2010. β-Endorphin expression in the mouse retina. J Comp Neurol 518, 3130–3148. https://doi.org/10.1002/cne.22387
Geissmann, Q., Rodriguez, L.G., Beckwith, E.J., Gilestro, G.F., 2019. Rethomics: An R framework to analyse high-throughput behavioural data. PLOS ONE 14, e0209331. https://doi.org/10.1371/journal.pone.0209331
Gharavi, R., Hedrich, W., Wang, H., Hassan, H.E., 2015. Transporter-Mediated Disposition of Opioids: Implications for Clinical Drug Interactions. Pharm Res. https://doi.org/10.1007/s11095-015-1711-5
Goldstein, A., Tachibana, S., Lowney, L.I., Hunkapiller, M., Hood, L., 1979. Dynorphin-(1-13), an extraordinarily potent opioid peptide. Proc Natl Acad Sci U S A 76, 6666–6670. https://doi.org/10.1073/pnas.76.12.6666
Gomes, I., Sierra, S., Lueptow, L., Gupta, A., Gouty, S., Margolis, E.B., Cox, B.M., Devi, L.A., 2020. Biased signaling by endogenous opioid peptides. PNAS 117, 11820–11828. https://doi.org/10.1073/pnas.2000712117
Gonzalez, S.M., Carrasquillo, Y., 2019. Estrous Cycle and Sex Differences in Referred and Visceral Sensitivity in Rodents. The Journal of Pain 20, S34–S35. https://doi.org/10.1016/j.jpain.2019.01.161
Grace, P.M., Stanford, T., Gentgall, M., Rolan, P.E., 2010. Utility of saccadic eye movement analysis as an objective biomarker to detect the sedative interaction between opioids and sleep deprivation in opioid-naive and opioid-tolerant populations. J Psychopharmacol 24, 1631–1640. https://doi.org/10.1177/0269881109352704
Greco, M.-A., Fuller, P.M., Jhou, T.C., Martin-Schild, S., Zadina, J.E., Hu, Z., Shiromani, P., Lu, J., 2008. Opioidergic projections to sleep-active neurons in the ventrolateral preoptic nucleus. Brain Research 1245, 96–107. https://doi.org/10.1016/j.brainres.2008.09.043
Greenbaum, D., Colangelo, C., Williams, K., Gerstein, M., 2003. Comparing protein abundance and mRNA expression levels on a genomic scale. Genome Biology 4, 117. https://doi.org/10.1186/gb-2003-4-9-117
Guajardo, H.M., Snyder, K., Ho, A., Valentino, R.J., 2017. Sex Differences in μ-Opioid Receptor Regulation of the Rat Locus Coeruleus and Their Cognitive Consequences. Neuropsychopharmacol 42, 1295–1304. https://doi.org/10.1038/npp.2016.252
Güler, A.D., Ecker, J.L., Lall, G.S., Haq, S., Altimus, C.M., Liao, H.-W., Barnard, A.R., Cahill, H., Badea, T.C., Zhao, H., Hankins, M.W., Berson, D.M., Lucas, R.J., Yau, K.-W.,

Hattar, S., 2008. Melanopsin cells are the principal conduits for rod–cone input to non-image-forming vision. Nature 453, 102–105. https://doi.org/10.1038/nature06829
Gulilat, M., Keller, D., Linton, B., Pananos, A.D., Lizotte, D., Dresser, G.K., Alfonsi, J., Tirona, R.G., Kim, R.B., Schwarz, U.I., 2020. Drug interactions and pharmacogenetic factors contribute to variation in apixaban concentration in atrial fibrillation patients in routine care. J Thromb Thrombolysis 49, 294–303. https://doi.org/10.1007/s11239-019-01962-2
Gupta, R., Alexander, T.A., Mitchell, S.M., Belew, A.T., El-Sayed, N.M., Speer, C.M., 2022. Melanopsin-dependent local protein translation in developing retinohypothalamic axons.
Hamabe, W., Maeda, T., Kiguchi, N., Yamamoto, C., Tokuyama, S., Kishioka, S., 2007. Negative Relationship Between Morphine Analgesia and P-Glycoprotein Expression Levels in the Brain. J Pharmacol Sci 105, 353–360. https://doi.org/10.1254/jphs.FP0071287
Hamilton, G.R., Baskett, T.F., 2000. In the arms of morpheus: the development of morphine for postoperative pain relief. Can J Anesth/J Can Anesth 47, 367–374. https://doi.org/10.1007/BF03020955
Harper, D., n.d. Etymology of narcotic [WWW Document]. Online Etymology Dictionary. URL https://www.etymonline.com/word/narcotic (accessed 2.4.23).
Hartwell, E.E., Pfeifer, J.G., McCauley, J.L., Moran-Santa Maria, M., Back, S.E., 2014. Sleep disturbances and pain among individuals with prescription opioid dependence. Addictive Behaviors 39, 1537–1542. https://doi.org/10.1016/j.addbeh.2014.05.025
Hastings, M.H., Maywood, E.S., Brancaccio, M., 2018. Generation of circadian rhythms in the suprachiasmatic nucleus. Nat Rev Neurosci 19, 453–469. https://doi.org/10.1038/s41583-018-0026-z
Hattar, S., Kumar, M., Park, A., Tong, P., Tung, J., Yau, K.-W., Berson, D.M., 2006. Central projections of melanopsin-expressing retinal ganglion cells in the mouse. J Comp Neurol 497, 326–349. https://doi.org/10.1002/cne.20970
Hattar, S., Liao, H.-W., Takao, M., Berson, D.M., Yau, K.-W., 2002. Melanopsin-Containing Retinal Ganglion Cells: Architecture, Projections, and Intrinsic Photosensitivity. Science 295, 1065–1070. https://doi.org/10.1126/science.1069609
Hellemans, J., Mortier, G., De Paepe, A., Speleman, F., Vandesompele, J., 2007. qBase relative quantification framework and software for management and automated analysis of real-time quantitative PCR data. Genome Biol 8, R19. https://doi.org/10.1186/gb-2007-8-2-r19
Hindson, B.J., Ness, K.D., Masquelier, D.A., Belgrader, P., Heredia, N.J., Makarewicz, A.J., Bright, I.J., Lucero, M.Y., Hiddessen, A.L., Legler, T.C., Kitano, T.K., Hodel, M.R., Petersen, J.F., Wyatt, P.W., Steenblock, E.R., Shah, P.H., Bousse, L.J., Troup, C.B., Mellen, J.C., Wittmann, D.K., Erndt, N.G., Cauley, T.H., Koehler, R.T., So, A.P., Dube, S., Rose, K.A., Montesclaros, L., Wang, S., Stumbo, D.P., Hodges, S.P., Romine, S., Milanovich, F.P., White, H.E., Regan, J.F., Karlin-Neumann, G.A., Hindson, C.M., Saxonov, S., Colston, B.W., 2011. High-Throughput Droplet Digital PCR System for Absolute Quantitation of DNA Copy Number. Anal. Chem. 83, 8604–8610. https://doi.org/10.1021/ac202028g
Holden, J.E., Jeong, Y., Forrest, J.M., 2005. The endogenous opioid system and clinical pain management. AACN Clin Issues 16, 291–301. https://doi.org/10.1097/00044067-200507000-00003

Howells, R.D., Groth, J., Hiller, J.M., Simon, E.J., 1980. Opiate binding sites in the retina: properties and distribution. Journal of Pharmacology and Experimental Therapeutics 215, 60–64.
Hughes, J., Smith, T.W., Kosterlitz, H.W., Fothergill, L.A., Morgan, B.A., Morris, H.R., 1975. Identification of two related pentapeptides from the brain with potent opiate agonist activity. Nature 258, 577–579. https://doi.org/10.1038/258577a0
Huhn, A.S., Finan, P.H., 2021. Sleep disturbance as a therapeutic target to improve opioid use disorder treatment. Experimental and Clinical Psychopharmacology. https://doi.org/10.1037/pha0000477
Hutchings, C.J., Koglin, M., Marshall, F.H., 2010. Therapeutic antibodies directed at G protein-coupled receptors. MAbs 2, 594–606. https://doi.org/10.4161/mabs.2.6.13420
Inturrisi, C.E., 2002. Clinical Pharmacology of Opioids for Pain: The Clinical Journal of Pain 18, S3–S13. https://doi.org/10.1097/00002508-200207001-00002
Iwamoto, S., Koga, T., Ohba, M., Okuno, T., Koike, M., Murakami, A., Matsuda, A., Yokomizo, T., 2017. Non-steroidal anti-inflammatory drug delays corneal wound healing by reducing production of 12-hydroxyheptadecatrienoic acid, a ligand for leukotriene B4 receptor 2. Sci Rep 7, 13267. https://doi.org/10.1038/s41598-017-13122-8
Jamali, K.A., Tramu, G., 1999. Control of rat hypothalamic pro-opiomelanocortin neurons by a circadian clock that is entrained by the daily light-off signal. Neuroscience 93, 1051–1061. https://doi.org/10.1016/S0306-4522(99)00208-0
Johnson, D.A., Billings, M.E., Hale, L., 2018. Environmental Determinants of Insufficient Sleep and Sleep Disorders: Implications for Population Health. Curr Epidemiol Rep 5, 61–69. https://doi.org/10.1007/s40471-018-0139-y
Kalivas, P.W., Duffy, P., 1987. Sensitization to repeated morphine injection in the rat: possible involvement of A10 dopamine neurons. | Journal of Pharmacology and Experimental Therapeutics. Journal of Pharmacology and Experimental Therapeutics 241, 204–212.
Kamiie, J., Ohtsuki, S., Iwase, R., Ohmine, K., Katsukura, Y., Yanai, K., Sekine, Y., Uchida, Y., Ito, S., Terasaki, T., 2008. Quantitative Atlas of Membrane Transporter Proteins: Development and Application of a Highly Sensitive Simultaneous LC/MS/MS Method Combined with Novel In-silico Peptide Selection Criteria. Pharm Res 25, 1469–1483. https://doi.org/10.1007/s11095-008-9532-4
Kerdelhue, B., Karteszi, M., Pasqualini, C., Reinberg, A., Mezey, E., Palkovits, M., 1983. Circadian Variations in β-Endorphin Concentrations in Pituitary and in some Brain Nuclei of the Adult Male Rat. Brain Research 261, 243–248. https://doi.org/10.1016/0006-8993(83)90627-3
Kessel, L., Siganos, G., Jørgensen, T., Larsen, M., 2011. Sleep Disturbances Are Related to Decreased Transmission of Blue Light to the Retina Caused by Lens Yellowing. Sleep 34, 1215–1219. https://doi.org/10.5665/SLEEP.1242
Kieffer, B.L., 1995. Recent advances in molecular recognition and signal transduction of active peptides: Receptors for opioid peptides. Cell Mol Neurobiol 15, 615–635. https://doi.org/10.1007/BF02071128
Kim, N.H., Kang, S., Park, G.H., Shim, G., Kang, T.H., Yu, Y.G., 2023. A robust antibody discovery platform for difficult-to-express G protein-coupled receptors. Protein Science 32, e4520. https://doi.org/10.1002/pro.4520

King, C., Masserano, J.M., Codd, E., Byrne, W.L., 1981. Effects of β-Endorphin and Morphine on the Sleep-Wakefulness Behavior of Cats. Sleep 4, 259–262. https://doi.org/10.1093/sleep/4.3.259
Kojima, S., Shingle, D.L., Green, C.B., 2011. Post-transcriptional control of circadian rhythms. J Cell Sci 124, 311–320. https://doi.org/10.1242/jcs.065771
Krishnamurti, C., Rao, S.C., 2016. The isolation of morphine by Serturner. Indian J Anaesth 60, 861–862. https://doi.org/10.4103/0019-5049.193696
Labrecque, G., Vanier, M.-C., 1995. Biological rhythms in pain and in the effects of opioid analgesics. Pharmac. Ther. 68, 129–147. https://doi.org/10.1016/0163-7258(95)02003-9
Larson, M.D., 2008. Mechanism of opioid-induced pupillary effects. Clinical Neurophysiology 119, 1358–1364. https://doi.org/10.1016/j.clinph.2008.01.106
Lee, H.S., Nelms, J.L., Nguyen, M., Silver, R., Lehman, M.N., 2003. The eye is necessary for a circadian rhythm in the suprachiasmatic nucleus. Nat Neurosci 6, 111–112. https://doi.org/10.1038/nn1006
LeGates, T.A., Fernandez, D.C., Hattar, S., 2014. Light as a central modulator of circadian rhythms, sleep and affect. Nat Rev Neurosci 15, 443–454. https://doi.org/10.1038/nrn3743
Leibrand, C.R., Paris, J.J., Jones, A.M., Masuda, Q.N., Halquist, M.S., Kim, W.-K., Knapp, P.E., Kashuba, A.D.M., Hauser, K.F., McRae, M., 2019. HIV-1 Tat and opioids act independently to limit antiretroviral brain concentrations and reduce blood–brain barrier integrity. J. Neurovirol. 25, 560–577. https://doi.org/10.1007/s13365-019-00757-8
Lekhanont, K., Park, C.Y., Smith, J.A., Combs, J.C., Preechawat, P., Suwan-Apichon, O., Rangsin, R., Chuck, R.S., 2007. Effects of Topical Anti-Inflammatory Agents in A Botulinum Toxin B—Induced Mouse Model of Keratoconjunctivitis Sicca. Journal of Ocular Pharmacology and Therapeutics 23, 27–34. https://doi.org/10.1089/jop.2006.0071
Lenth, R.V., 2022. emmeans: Estimated Marginal Means, aka Least-Squares Means.
Lešnik, S., Bertalan, É., Bren, U., Bondar, A.-N., 2021. Opioid Receptors and Protonation-Coupled Binding of Opioid Drugs. International Journal of Molecular Sciences 22, 13353. https://doi.org/10.3390/ijms222413353
Lewis, S.A., Oswald, I., Evans, J.I., Akindele, M.O., Tompsett, S.L., 1970. Heroin and human sleep. Electroencephalography and Clinical Neurophysiology 28, 374–381. https://doi.org/10.1016/0013-4694(70)90230-0
Li, C.H., Lemaire, S., Yamashiro, D., Doneen, B.A., 1976. The synthesis and opiate activity of β-endorphin. Biochemical and Biophysical Research Communications 71, 19–25. https://doi.org/10.1016/0006-291X(76)90243-6
Liang, Q., Dharmat, R., Owen, L., Shakoor, A., Li, Y., Kim, S., Vitale, A., Kim, I., Morgan, D., Liang, S., Wu, N., Chen, K., DeAngelis, M.M., Chen, R., 2019. Single-nuclei RNA-seq on human retinal tissue provides improved transcriptome profiling. Nat Commun 10, 5743. https://doi.org/10.1038/s41467-019-12917-9
Liu, L., Liu, X., 2019. Roles of Drug Transporters in Blood-Retinal Barrier. Drug Transporters in Drug Disposition, Effects and Toxicity 1141, 467–504. https://doi.org/10.1007/978-981-13-7647-4_10
Liu, L., Miao, M., Chen, Y., Wang, Z., Sun, B., Liu, X., 2018. Altered Function and Expression of ABC Transporters at the Blood–Brain Barrier and Increased Brain Distribution of Phenobarbital in Acute Liver Failure Mice. Frontiers in Pharmacology 9.

Liu, Y., Beyer, A., Aebersold, R., 2016. On the Dependency of Cellular Protein Levels on mRNA Abundance. Cell 165, 535–550. https://doi.org/10.1016/j.cell.2016.03.014
Livak, K.J., Schmittgen, T.D., 2001. Analysis of Relative Gene Expression Data Using Real-Time Quantitative PCR and the 2−ΔΔCT Method. Methods 25, 402–408. https://doi.org/10.1006/meth.2001.1262
Locklear, C.E., 2020. Opioids Disrupt Sleep and Wakefulness in C57BL/6J mice (Master's Thesis). University of Tennessee.
Loh, Y.P., Brownstein, M.J., Gainer, H., 1984. Proteolysis in Neuropeptide Processing and Other Neural Functions. Annual Review of Neuroscience 7, 189–222. https://doi.org/10.1146/annurev.ne.07.030184.001201
Loscher, W., Potschka, H., 2005. Blood-brain barrier active efflux transporters: ATP-binding cassette gene family. NeuroRx 2, 13.
Loyd, D.R., Wang, X., Murphy, A.Z., 2008. Sex Differences in μ-Opioid Receptor Expression in the Rat Midbrain Periaqueductal Gray Are Essential for Eliciting Sex Differences in Morphine Analgesia. J. Neurosci. 28, 14007–14017. https://doi.org/10.1523/JNEUROSCI.4123-08.2008
Lu, X.-Y., Shieh, K.-R., Kabbaj, M., Barsh, G.S., Akil, H., Watson, S.J., 2002. Diurnal Rhythm of Agouti-Related Protein and Its Relation to Corticosterone and Food Intake. Endocrinology 143, 3905–3915. https://doi.org/10.1210/en.2002-220150
Lukowski, S.W., Lo, C.Y., Sharov, A.A., Nguyen, Q., Fang, L., Hung, S.S., Zhu, L., Zhang, T., Grünert, U., Nguyen, T., Senabouth, A., Jabbari, J.S., Welby, E., Sowden, J.C., Waugh, H.S., Mackey, A., Pollock, G., Lamb, T.D., Wang, P., Hewitt, A.W., Gillies, M.C., Powell, J.E., Wong, R.C., 2019. A single-cell transcriptome atlas of the adult human retina. EMBO J 38, e100811. https://doi.org/10.15252/embj.2018100811
Luo, Lin, Ambrozkiewicz, M.C., Benseler, F., Chen, C., Dumontier, E., Falkner, S., Furlanis, E., Gomez, A.M., Hoshina, N., Huang, W.-H., Hutchison, M.A., Itoh-Maruoka, Y., Lavery, L.A., Li, W., Maruo, T., Motohashi, J., Pai, E.L.-L., Pelkey, K.A., Pereira, A., Philips, T., Sinclair, J.L., Stogsdill, J.A., Traunmüller, L., Wang, J., Wortel, J., You, W., Abumaria, N., Beier, K.T., Brose, N., Burgess, H.A., Cepko, C.L., Cloutier, J.-F., Eroglu, C., Goebbels, S., Kaeser, P.S., Kay, J.N., Lu, W., Luo, Liqun, Mandai, K., McBain, C.J., Nave, K.-A., Prado, M.A.M., Prado, V.F., Rothstein, J., Rubenstein, J.L.R., Saher, G., Sakimura, K., Sanes, J.R., Scheiffele, P., Takai, Y., Umemori, H., Verhage, M., Yuzaki, M., Zoghbi, H.Y., Kawabe, H., Craig, A.M., 2020. Optimizing Nervous System-Specific Gene Targeting with Cre Driver Lines: Prevalence of Germline Recombination and Influencing Factors. Neuron 106, 37-65.e5. https://doi.org/10.1016/j.neuron.2020.01.008
Lupi, D., Oster, H., Thompson, S., Foster, R.G., 2008. The acute light-induction of sleep is mediated by OPN4-based photoreception. Nat Neurosci 11, 1068–1073. https://doi.org/10.1038/nn.2179
Lydon-Staley, D.M., Cleveland, H.H., Huhn, A.S., Cleveland, M.J., Harris, J., Stankoski, D., Deneke, E., Meyer, R.E., Bunce, S.C., 2017. Daily sleep quality affects drug craving, partially through indirect associations with positive affect, in patients in treatment for nonmedical use of prescription drugs. Addictive Behaviors 65, 275–282. https://doi.org/10.1016/j.addbeh.2016.08.026
Mahr, S., 2017. Breadseed or Opium Poppy, Papaver somniferum [WWW Document]. Wisconsin Master Gardener. URL

https://mastergardener.extension.wisc.edu/files/2017/06/Papaver_somniferum.pdf (accessed 2.3.23).
Maier, T., Güell, M., Serrano, L., 2009. Correlation of mRNA and protein in complex biological samples. FEBS Letters, Systems Biology - Nobel Symposium 146 583, 3966–3973. https://doi.org/10.1016/j.febslet.2009.10.036
Maloney, R., Quattrochi, L., Yoon, J., Souza, R., Berson, D., 2022. Efficacy and Specificity of Melanopsin Reporters for Retinal Ganglion Cells. https://doi.org/10.1101/2022.04.26.489554
Manders, E.M.M., Verbeek, F.J., Aten, J.A., 1993. Measurement of co-localization of objects in dual-colour confocal images. Journal of Microscopy 169, 375–382. https://doi.org/10.1111/j.1365-2818.1993.tb03313.x
Martin, W.R., 1967. Opioid Antagonists. Pharmacol Rev 19, 463–521.
Matthes, H.W.D., Maldonadot, R., Simonin, F., Valverdet, O., Slowet, S., 1996. Loss of morphine-induced analgesia, reward effect and withdrawal symptoms in mice lacking the μ-opioid-receptor gene. Nature 383, 819–823. https://doi.org/10.1038/383819a0
McDowell, K.A., Shin, D., Roos, K.P., Chesselet, M.-F., 2014. Sleep Dysfunction and EEG Alterations in Mice Overexpressing Alpha-Synuclein. J Parkinsons Dis 4, 531–539. https://doi.org/10.3233/JPD-140374
McLean, A.C., Valenzuela, N., Fai, S., Bennett, S.A.L., 2012. Performing Vaginal Lavage, Crystal Violet Staining, and Vaginal Cytological Evaluation for Mouse Estrous Cycle Staging Identification. J. Vis. Exp. 67, 1–6. https://doi.org/doi:10.3791/4389
Medzihradsky, F., 1976. Stereospecific binding of etorphine in isolated neural cells and in retina determined by a sensitive microassay. Brain Research 108, 212–219. https://doi.org/10.1016/0006-8993(76)90180-3
Moraes, M.N., de Assis, L.V.M., Provencio, I., Castrucci, A.M. de L., 2021. Opsins outside the eye and the skin: a more complex scenario than originally thought for a classical light sensor. Cell Tissue Res 385, 519–538. https://doi.org/10.1007/s00441-021-03500-0
Morcos, Y., Hosie, M., Bauer, H.-C., Chan-Ling, T., 2001. Immunolocalization of occludin and claudin-1 to tight junctions in intact CNS vessels of mammalian retina. Journal of neurocytology 30, 107–23. https://doi.org/10.1023/A:1011982906125
Mure, L.S., 2021. Intrinsically Photosensitive Retinal Ganglion Cells of the Human Retina. Front Neurol 12, 636330. https://doi.org/10.3389/fneur.2021.636330
Murray, R.B., Adler, M.W., Korczyn, A.D., 1983. The pupillary effects of oploids. Life Sciences 33, 495–509. https://doi.org/10.1016/0024-3205(83)90123-6
Myer, E.C., Morris, D.L., Brase, D.A., Dewey, W.L., Zimmerman, A.W., 1990. Naltrexone therapy of apnea in children with elevated cerebrospinal fluid β-endorphin. Ann Neurol 27, 75–80. https://doi.org/10.1002/ana.410270112
Nafziger, A.N., Barkin, R.L., 2018. Opioid Therapy in Acute and Chronic Pain. The Journal of Clinical Pharmacology 58, 1111–1122. https://doi.org/10.1002/jcph.1276
Nakamura, A., Nakashima, M., Sakai, K., Niwa, M., Nozaki, M., Shiomi, H., 1989. Delta-sleep-inducing peptide (DSIP) stimulates the release of immunoreactive Met-enkephalin from rat lower brainstem slices in vitro. Brain Research 481, 165–168. https://doi.org/10.1016/0006-8993(89)90498-8
Nakamura, A., Sakai, K., Takahashi, Y., Shiomi, H., 1991. Characterization of Delta-Sleep-Inducing Peptide-Evoked Release of Met-Enkephalin from Brain Synaptosomes in Rats.

Journal of Neurochemistry 57, 1013–1018. https://doi.org/10.1111/j.1471-4159.1991.tb08251.x
Nasser, S.A., Afify, E.A., 2019. Sex differences in pain and opioid mediated antinociception: Modulatory role of gonadal hormones. Life Sciences 237, 116926. https://doi.org/10.1016/j.lfs.2019.116926
Nencini, P., 2022. Facts and Factoids in the Early History of the Opium Poppy. The Social History of Alcohol and Drugs 36, 45–71. https://doi.org/10.1086/718481
Obermeier, B., Daneman, R., Ransohoff, R.M., 2013. Development, maintenance and disruption of the blood-brain barrier. Nat Med 19, 1584–1596. https://doi.org/10.1038/nm.3407
O'Brien, C.B., Locklear, C.E., Glovak, Z.T., Zebadúa Unzaga, D., Baghdoyan, H.A., Lydic, R., 2021. Opioids cause dissociated states of consciousness in C57BL/6J mice. Journal of Neurophysiology 126, 1265–1275. https://doi.org/10.1152/jn.00266.2021
Ollion, J., Cochennec, J., Loll, F., Escudé, C., Boudier, T., 2013. TANGO: a generic tool for high-throughput 3D image analysis for studying nuclear organization. Bioinformatics 29, 1840–1841. https://doi.org/10.1093/bioinformatics/btt276
Onen, S.H., Onen, F., Courpron, P., Dubray, C., 2005. How Pain and Analgesics Disturb Sleep. The Clinical Journal of Pain 21, 422. https://doi.org/10.1097/01.ajp.0000129757.31856.f7
Ono, D., Honma, K., Honma, S., 2015. Circadian and ultradian rhythms of clock gene expression in the suprachiasmatic nucleus of freely moving mice. Sci Rep 5, 12310. https://doi.org/10.1038/srep12310
Orozco-Solís, R., Matos, R.J.B., Lopes de Souza, S., Grit, I., Kaeffer, B., Manhães de Castro, R., Bolaños-Jiménez, F., 2011. Perinatal nutrient restriction induces long-lasting alterations in the circadian expression pattern of genes regulating food intake and energy metabolism. Int J Obes 35, 990–1000. https://doi.org/10.1038/ijo.2010.223
Pack, A.I., Galante, R.J., Maislin, G., Cater, J., Metaxas, D., Lu, S., Zhang, L., Smith, R.V., Kay, T., Lian, J., Svenson, K., Peters, L.L., 2007. Novel method for high-throughput phenotyping of sleep in mice. Physiol Genomics 28, 232–238. https://doi.org/10.1152/physiolgenomics.00139.2006
Papini, A.M., 2018. From morphine to endogenous opioid peptides, e.g., endorphins: the endless quest for the perfect painkiller. Substantia 2, 81–91. https://doi.org/10.13128/Substantia-63
Pasternak, G.W., Pan, Y.-X., 2013. Mu Opioids and Their Receptors: Evolution of a Concept. Pharmacol Rev 65, 1257–1317. https://doi.org/10.1124/pr.112.007138
Paterson, S.J., Corbett, A.D., Gillan, M.G.C., Kosterlitz, H.W., McKnight, A.T., Robson, L.E., 1984. Radioligands for Probing Opioid Receptors. Journal of Receptor Research 4, 143–154. https://doi.org/10.3109/10799898409042545
Pathan, H., Williams, J., 2012. Basic opioid pharmacology: an update. Br J Pain 6, 11–16. https://doi.org/10.1177/2049463712438493
Pert, C.B., Pasternak, G., Snyder, S.H., 1973. Opiate Agonists and Antagonists Discriminated by Receptor Binding in Brain. Science 182, 1359–1361. https://doi.org/10.1126/science.182.4119.1359
Pickworth, W.B., Sharpe, L.G., 1985. Morphine-induced mydriasis and inhibition of pupillary light reflex and fluctuations in the cat. J Pharmacol Exp Ther 234, 603–606.

Pilozzi, A., Carro, C., Huang, X., 2021. Roles of β-Endorphin in Stress, Behavior, Neuroinflammation, and Brain Energy Metabolism. IJMS 22, 338. https://doi.org/10.3390/ijms22010338

Pineyro, G., Nagi, K., 2021. Signaling diversity of mu- and delta- opioid receptor ligands: Re-evaluating the benefits of β-arrestin/G protein signaling bias. Cellular Signalling 80, 109906. https://doi.org/10.1016/j.cellsig.2020.109906

Piquette-Miller, M., Pak, A., Kim, H., Anari, R., Shahzamani, A., 1998. Decreased Expression and Activity of P-GIycoprotein in Rat Liver During Acute Inflammation. Pharm Res 15, 706–711. https://doi.org/10.1023/A:1011962818051

Provencio, I., Rodriguez, I.R., Jiang, G., Hayes, W.P., Moreira, E.F., Rollag, M.D., 2000. A Novel Human Opsin in the Inner Retina. J. Neurosci. 20, 600–605. https://doi.org/10.1523/JNEUROSCI.20-02-00600.2000

Przewlocka, B., Mogilnicka, E., Lason, W., van Luijtelaar, E.L.J.M., Coenen, A.M.L., 1986. Deprivation of REM sleep in the rat and the opioid peptides β-endorphin and dynorphin. Neurosci Lett 70, 138–142. https://doi.org/10.1016/0304-3940(86)90452-0

Quattrochi, L.E., Stabio, M.E., Kim, I., Ilardi, M.C., Fogerson, P.M., Leyrer, M.L., Berson, D.M., 2019. The M6 cell: A small-field bistratified photosensitive retinal ganglion cell. J Comp Neurol 527, 297–311. https://doi.org/10.1002/cne.24556

R Core Team, 2022. R: A language and environment for statistical computing [WWW Document]. R Foundation for Statistical Computing, Vienna, Austria. URL https://www.r-project.org/

Ramirez, J.-M., Burgraff, N.J., Wei, A.D., Baertsch, N.A., Varga, A.G., Baghdoyan, H.A., Lydic, R., Morris, K.F., Bolser, D.C., Levitt, E.S., 2021. Neuronal mechanisms underlying opioid-induced respiratory depression: our current understanding. Journal of Neurophysiology 125, 1899–1919. https://doi.org/10.1152/jn.00017.2021

Rasmussen, N.A., Farr, L.A., 2003. Effects of Morphine and Time of Day on Pain and β-Endorphin. Biol Res Nurs 5, 105–116. https://doi.org/10.1177/1099800403257166

Raynor, K., Kong, H., Chen, Y., Yasuda, K., Yu, L., Bell, G.I., Resine, T., 1993. Pharmacological Characterization of the Cloned K-, d-, mu-Opioid Receptors. Mol Pharmacol 45, 330–334. https://doi.org/10.1002/047120918X.emb0452

Reddy, A.B., Karp, N.A., Maywood, E.S., Deery, M., O'Neill, J.S., Wong, G.K.Y., Chesham, J., Odell, M., Lilley, K.S., Kyriacou, C.P., Hastings, M.H., 2006. Circadian Orchestration of the Hepatic Proteome. Curr Biol 16, 1107–1115. https://doi.org/10.1016/j.cub.2006.04.026

Richter, C., Woods, I.G., Schier, A.F., 2014. Neuropeptidergic Control of Sleep and Wakefulness. Annu Rev Neurosci 37, 503–531. https://doi.org/10.1146/annurev-neuro-062111-150447

Riou, F., Cespuglio, R., Jouvet, M., 1982. Endogenous Peptides and Sleep in the Rat: II Peptides Without Significant Effect on the Sleep-Waning Cycle. Neuropeptides 2, 255–264. https://doi.org/10.1016/0143-4179(82)90015-4

Robertson, J.A., Purple, R.J., Cole, P., Zaiwalla, Z., Wulff, K., Pattinson, K.T.S., 2016. Sleep disturbance in patients taking opioid medication for chronic back pain. Anaesthesia 71, 1296–1307. https://doi.org/10.1111/anae.13601

Robison, L.S., Gannon, O.J., Salinero, A.E., Zuloaga, K.L., 2019. Contributions of sex to cerebrovascular function and pathology. Brain Res 1710, 43–60. https://doi.org/10.1016/j.brainres.2018.12.030

Roehrs, T., Hyde, M., Blaisdell, B., Greenwald, M., Roth, T., 2006. Sleep loss and REM sleep loss are hyperalgesic. Sleep 29, 145–151. https://doi.org/10.1093/sleep/29.2.145

Roehrs, T., Roth, T., 2005. Sleep and Pain: Interaction of Two Vital Functions. Seminars in neurology 25, 106–16. https://doi.org/10.1055/s-2005-867079

Rosenthal, M., Polly Moore, P., Eric Groves, M.D., Tad Iwan, B.A., Lisa Greenberg Schlosser, M.S., Zofia Dziewanowska, M.D., Negro-Vilar, M.D., 2007. Sleep improves when patients with chronic OA pain are managed with morning dosing of once a day extended-release morphine sulfate (AVINZA®): Findings from a pilot study. Journal of Opioid Management 3, 145–154. https://doi.org/10.5055/jom.2007.0052

RStudio Team, 2022. RStudio: Integrated Development for R [WWW Document]. RStudio, PBC, Boston, MA. URL https://www.posit.co/ (accessed 1.25.23).

Rupp, A.C., Ren, M., Altimus, C.M., Fernandez, D.C., Richardson, M., Turek, F., Hattar, S., Schmidt, T.M., 2019. Distinct ipRGC subpopulations mediate light's acute and circadian effects on body temperature and sleep. eLife 1–16. https://doi.org/10.7554/eLife.44358.001

Russo, A.F., 2017. Overview of neuropeptides: awakening the senses? Headache 57, 37–46. https://doi.org/10.1111/head.13084

Sanchez-Covarrubias, L., Slosky, L.M., Thompson, B.J., Zhang, Y., Laracuente, M.-L., DeMarco, K.M., Ronaldson, P.T., Davis, T.P., 2014. P-glycoprotein Modulates Morphine Uptake into the CNS: A Role for the Non-steroidal Anti-inflammatory Drug Diclofenac. PLOS ONE 9, e88516. https://doi.org/10.1371/journal.pone.0088516

Sanz, E., Bean, J.C., Carey, D.P., Quintana, A., McKnight, G.S., 2019. RiboTag: Ribosomal Tagging Strategy to Analyze Cell-Type-Specific mRNA Expression In Vivo. Curr Protoc Neurosci 88, e77. https://doi.org/10.1002/cpns.77

Saper, C.B., Chou, T.C., Scammell, T.E., 2001. The sleep switch: hypothalamic control of sleep and wakefulness. Trends Neurosci 24, 726–731. https://doi.org/10.1016/S0166-2236(00)02002-6

Sarton, E., Olofsen, E., Romberg, R., den Hartigh, J., Kest, B., Nieuwenhuijs, D., Burm, A., Teppema, L., Dahan, A., 2000. Sex Differences in Morphine Analgesia: An Experimental Study in Healthy Volunteers. Anesthesiology 93, 1245–1254. https://doi.org/10.1097/00000542-200011000-00018

Sauer, B., Henderson, N., 1988. Site-specific DNA recombination in mammalian cells by the Cre recombinase of bacteriophage P1. Proc. Natl. Acad. Sci. U.S.A. 85, 5166–5170. https://doi.org/10.1073/pnas.85.14.5166

Saunders, A., Macosko, E.Z., Wysoker, A., Goldman, M., Krienen, F.M., de Rivera, H., Bien, E., Baum, M., Bortolin, L., Wang, S., Goeva, A., Nemesh, J., Kamitaki, N., Brumbaugh, S., Kulp, D., McCarroll, S.A., 2018. Molecular Diversity and Specializations among the Cells of the Adult Mouse Brain. Cell 174, 1015-1030.e16. https://doi.org/10.1016/j.cell.2018.07.028

Sawant, O.B., Horton, A.M., Zucaro, O.F., Chan, R., Bonilha, V.L., Samuels, I.S., Rao, S., 2017. The Circadian Clock Gene Bmal1 Controls Thyroid Hormone-Mediated Spectral Identity and Cone Photoreceptor Function. Cell Reports 21, 692–706. https://doi.org/10.1016/j.celrep.2017.09.069

Scammell, T.E., Arrigoni, E., Lipton, J.O., 2017. Neural Circuitry of Wakefulness and Sleep. Neuron 93, 747–765. https://doi.org/10.1016/j.neuron.2017.01.014

Schaefer, C.P., Tome, M.E., Davis, T.P., 2017. The opioid epidemic: a central role for the blood brain barrier in opioid analgesia and abuse. Fluids and Barriers of the CNS 14, 32. https://doi.org/10.1186/s12987-017-0080-3
Schindelin, J., Arganda-Carreras, I., Frise, E., Kaynig, V., Longair, M., Pietzsch, T., Preibisch, S., Rueden, C., Saalfeld, S., Schmid, B., Tinevez, J.-Y., White, D.J., Hartenstein, V., Eliceiri, K., Tomancak, P., Cardona, A., 2012. Fiji: an open-source platform for biological-image analysis. Nat Methods 9, 676–682. https://doi.org/10.1038/nmeth.2019
Schmidt, T.M., Chen, S.-K., Hattar, S., 2011. Intrinsically photosensitive retinal ganglion cells: many subtypes, diverse functions. Trends Neurosci 34, 572–580. https://doi.org/10.1016/j.tins.2011.07.001
Seleman, M., Chapy, H., Cisternino, S., Courtin, C., Smirnova, M., Schlatter, J., Chiadmi, F., Scherrmann, J.-M., Noble, F., Marie-Claire, C., 2014. Impact of P-glycoprotein at the blood-brain barrier on the uptake of heroin and its main metabolites: behavioral effects and consequences on the transcriptional responses and reinforcing properties. Psychopharmacology 231, 3139–3149. https://doi.org/10.1007/s00213-014-3490-9
Sertürner, F., 1817. Ueber das Morphium, eine neue salzfähige Grundlage, und die Mekonsäure, als Hauptbestandtheile des Opiums. Annalen der Physik 55, 56–89.
Severino, A.L., Mittal, N., Hakimian, J.K., Velarde, N., Minasyan, A., Albert, R., Torres, C., Romaneschi, N., Johnston, C., Tiwari, S., Lee, A.S., Taylor, A.M., Gavériaux-Ruff, C., Kieffer, B.L., Evans, C.J., Cahill, C.M., Walwyn, W.M., 2020. μ-Opioid Receptors on Distinct Neuronal Populations Mediate Different Aspects of Opioid Reward-Related Behaviors. eNeuro 7, ENEURO.0146-20.2020. https://doi.org/10.1523/ENEURO.0146-20.2020
Sharma, H.S., Ali, S.F., 2006. Alterations in Blood–Brain Barrier Function by Morphine and Methamphetamine. Annals of the New York Academy of Sciences 1074, 198–224. https://doi.org/10.1196/annals.1369.020
Shaw, I.R., Lavigne, G., Mayer, P., Choinière, M., 2005. Acute Intravenous Administration of Morphine Perturbs Sleep Architecture in Healthy Pain-Free Young Adults: a Preliminary Study. Sleep 28, 677–682. https://doi.org/10.1093/sleep/28.6.677
Shchul'kin, A.V., Yakusheva, E.N., Chernykh, I.V., Nikiforov, A.A., 2017. The role of testosterone in the regulation of P-glycoprotein functioning. Biol Bull Russ Acad Sci 44, 524–530. https://doi.org/10.1134/S1062359017050168
Sherin, J.E., Shiromani, P.J., McCarley, R.W., Saper, C.B., 1996. Activation of Ventrolateral Preoptic Neurons During Sleep. Science 271, 216–219.
Simon, E.J., Hiller, J.M., Edelman, I., 1973. Stereospecific Binding of the Potent Narcotic Analgesic [3H]Etorphine to Rat-Brain Homogenate. Proc. Natl. Acad. Sci. U.S.A. 70, 1947–1949. https://doi.org/10.1073/pnas.70.7.1947
Skeie, J.M., Tsang, S.H., Mahajan, V.B., 2011. Evisceration of Mouse Vitreous and Retina for Proteomic Analyses. J Vis Exp 2795. https://doi.org/10.3791/2795
Slaughter, M.M., Mattler, J.A., Gottlieb, D.I., 1985. Opiate binding sites in the chick, rabbit and goldfish retina. Brain Research 339, 39–47. https://doi.org/10.1016/0006-8993(85)90619-5
Slosky, L.M., Thompson, B.J., Sanchez-Covarrubias, L., Zhang, Y., Laracuente, M.-L., Vanderah, T.W., Ronaldson, P.T., Davis, T.P., 2013. Acetaminophen Modulates P-Glycoprotein Functional Expression at the Blood-Brain Barrier by a Constitutive

Androstane Receptor–Dependent Mechanism. Mol Pharmacol 84, 774–786. https://doi.org/10.1124/mol.113.086298
Soheilian, M., Karimi, S., Ramezani, A., Peyman, G.A., 2010. Pilot Study of Intravitreal Injection of Diclofenac for Treatment of Macular Edema of Various Etiologies. RETINA 30, 509–515. https://doi.org/10.1097/IAE.0b013e3181bdfa43
Song, A.J., Palmiter, R.D., 2018. Detecting and Avoiding Problems When Using the Cre/lox System. Trends Genet 34, 333–340. https://doi.org/10.1016/j.tig.2017.12.008
Sora, I., Li, X.-F., 2001. μ Opiate Receptor Gene Dose Effects on Different Morphine Actions: Evidence for Differential in vivo μ Receptor Reserve. Neuropsychopharmacology 25, 41–54. https://doi.org/10.1016/S0893-133X(00)00252-9
Stabio, M.E., Sabbah, S., Quattrochi, L.E., Ilardi, M.C., Fogerson, P.M., Leyrer, M.L., Kim, M.T., Kim, I., Schiel, M., Renna, J.M., Briggman, K.L., Berson, D.M., 2018. The M5 Cell: A Color-Opponent Intrinsically Photosensitive Retinal Ganglion Cell. Neuron 97, 150-163.e4. https://doi.org/10.1016/j.neuron.2017.11.030
Stein, M.D., Herman, D.S., Bishop, S., Lassor, J.A., Weinstock, M., Anthony, J., Anderson, B.J., 2004. Sleep disturbances among methadone maintained patients. J Subst Abuse Treat 26, 175–180. https://doi.org/10.1016/S0740-5472(03)00191-0
Steiner, R.A., Kabigting, E., Lent, K., Clifton, D.K., 1994. Diurnal Rhythm in Proopiomelanocortin mRNA in the Arcuate Nucleus of the Male Rat. J Neuroendocrinol 6, 603–608. https://doi.org/10.1111/j.1365-2826.1994.tb00625.x
Stell, W., Marshak, D., Yamada, T., Brecha, N., Karten, H., 1980. Peptides are in the eye of the beholder. Trends Neurosci 3, 292–295. https://doi.org/10.1016/S0166-2236(80)80174-3
Stütz, A.M., Staszkiewicz, J., Ptitsyn, A., Argyropoulos, G., 2007. Circadian Expression of Genes Regulating Food Intake. Obesity 15, 607–615. https://doi.org/10.1038/oby.2007.564
Suzuki, T., Zhao, Y.L., Nadai, M., Naruhashi, K., Shimizu, A., Takagi, Kenji, Takagi, Kenzo, Hasegawa, T., 2006. Gender-related differences in expression and function of hepatic P-glycoprotein and multidrug resistance-associated protein (Mrp2) in rats. Life Sciences 79, 455–461. https://doi.org/10.1016/j.lfs.2006.01.024
Tagami, M., Kusuhara, S., Honda, S., Tsukahara, Y., Negi, A., 2009. Expression of ATP-binding cassette transporters at the inner blood–retinal barrier in a neonatal mouse model of oxygen-induced retinopathy. Brain Research 1283, 186–193. https://doi.org/10.1016/j.brainres.2009.05.095
Tanaka, Y., Slitt, A.L., Leazer, T.M., Maher, J.M., Klaassen, C.D., 2005. Tissue distribution and hormonal regulation of the breast cancer resistance protein (Bcrp/Abcg2) in rats and mice. Biochemical and Biophysical Research Communications 326, 181–187. https://doi.org/10.1016/j.bbrc.2004.11.012
Taylor, S.C., Laperriere, G., Germain, H., 2017. Droplet Digital PCR versus qPCR for gene expression analysis with low abundant targets: from variable nonsense to publication quality data. Sci Rep 7, 2409. https://doi.org/10.1038/s41598-017-02217-x
Terenius, L., 1973. Stereospecific Interaction Between Narcotic Analgesics and a Synaptic Plasma Membrane Fraction of Rat Cerebral Cortex. Acta Pharmacologica et Toxicologica 32, 317–320. https://doi.org/10.1111/j.1600-0773.1973.tb01477.x
Tian, M., Broxmeyer, H.E., Fan, Y., Lai, Z., Zhang, S., Aronica, S., Cooper, S., Bigsby, R.M., Steinmetz, R., Engle, S.J., Mestek, A., Pollock, J.D., Lehman, M.N., Jansen, H.T., Ying, M., Stambrook, P.J., Tischfield, J.A., Yu, L., 1997. Altered Hematopoiesis, Behavior,

and Sexual Function in μ Opioid Receptor–deficient Mice. Journal of Experimental Medicine 185, 1517–1522. https://doi.org/10.1084/jem.185.8.1517
Tierno, A., Fiore, P., Gannon, R.L., 2002. Delta opioid inhibition of light-induced phase advances in hamster circadian activity rhythms. Brain Research 937, 66–73. https://doi.org/10.1016/S0006-8993(02)02468-X
Tramullas, M., Collins, J.M., Fitzgerald, P., Dinan, T.G., O' Mahony, S.M., Cryan, J.F., 2021. Estrous cycle and ovariectomy-induced changes in visceral pain are microbiota-dependent. iScience 24, 102850. https://doi.org/10.1016/j.isci.2021.102850
Trescot, A.M., Datta, S., Lee, M., Hansen, H., 2008. Opioid pharmacology. Pain Physician 11, S133-153.
Tripathi, R., Rao, R., Dhawan, A., Jain, R., Sinha, S., 2020. Opioids and sleep – a review of literature. Sleep Med 67, 269–275. https://doi.org/10.1016/j.sleep.2019.06.012
Tsien, J.Z., 2016. Cre-Lox Neurogenetics: 20 Years of Versatile Applications in Brain Research and Counting…. Frontiers in Genetics 7.
Turk, D.C., Wilson, H.D., Cahana, A., 2011. Treatment of chronic non-cancer pain. The Lancet 377, 2226–2235. https://doi.org/10.1016/S0140-6736(11)60402-9
Turner, P.L., Van Someren, E.J.W., Mainster, M.A., 2010. The role of environmental light in sleep and health: Effects of ocular aging and cataract surgery. Sleep Medicine Reviews 14, 269–280. https://doi.org/10.1016/j.smrv.2009.11.002
Urrutia-Cabrera, D., Wong, R.C.-B., 2020. Using single cell transcriptomics to study the complexity of human retina. Neural Regeneration Research 15, 2045. https://doi.org/10.4103/1673-5374.282253
Valentino, R.J., Volkow, N.D., 2018. Untangling the complexity of opioid receptor function. Neuropsychopharmacol 43, 2514–2520. https://doi.org/10.1038/s41386-018-0225-3
van der Veen, D.R., Gerkema, M.P., 2017. Unmasking ultradian rhythms in gene expression. FASEB J 31, 743–750. https://doi.org/10.1096/fj.201600872R
Vandesompele, J., De Preter, K., Pattyn, F., Poppe, B., Van Roy, N., De Paepe, A., Speleman, F., 2002. Accurate normalization of real-time quantitative RT-PCR data by geometric averaging of multiple internal control genes. Genome Biol 3, research0034.1-0034.11. https://doi.org/10.1186/gb-2002-3-7-research0034
VanGuilder, H.D., Vrana, K.E., Freeman, W.M., 2008. Twenty-five years of quantitative PCR for gene expression analysis. BioTechniques 44, 619–626. https://doi.org/10.2144/000112776
Viscusi, E.R., Viscusi, A.R., 2020. Blood–brain barrier: mechanisms governing permeability and interaction with peripherally acting μ-opioid receptor antagonists. Reg Anesth Pain Med 45, 688–695. https://doi.org/10.1136/rapm-2020-101403
Voigt, T., 1986. Cholinergic amacrine cells in the rat retina. J Comp Neurol 248, 19–35. https://doi.org/10.1002/cne.902480103
Volkow, N.D., Jones, E.B., Einstein, E.B., Wargo, E.M., 2019. Prevention and Treatment of Opioid Misuse and Addiction: A Review. JAMA Psychiatry 76, 208. https://doi.org/10.1001/jamapsychiatry.2018.3126
Waller, E.A., Bendel, R.E., Kaplan, J., 2008. Sleep Disorders and the Eye. Mayo Clinic Proceedings 83, 1251–1261. https://doi.org/10.4065/83.11.1251
Wamsley, J.K., Palacios, J.M., Kuhar, M.J., 1981. Autoradiographic localization of opioid receptors in the mammalian retina. Neurosci Lett 27, 19–24. https://doi.org/10.1016/0304-3940(81)90199-3

Wang, A.M., Doyle, M.V., Mark, D., F., 1989. Quantitation of mRNA by the polymerase chain reaction. PNAS USA 86, 9717–9721. https://doi.org/10.1073/pnas.86.24.9717
Wang, Q., Yue, X.-F., Qu, W.-M., Tan, R., Zheng, P., Urade, Y., Huang, Z.-L., 2013. Morphine Inhibits Sleep-Promoting Neurons in the Ventrolateral Preoptic Area Via Mu Receptors and Induces Wakefulness in Rats. Neuropsychopharmacol 38, 791–801. https://doi.org/10.1038/npp.2012.244
Webster, L.R., Smith, M.D., Mackin, S., Iverson, M., 2015. Comparative Effects of Morning vs Evening Dosing of Extended-Release Hydromorphone on Sleep Physiology in Patients with Low Back Pain: A Pilot Study. Pain Medicine 16, 460–471. https://doi.org/10.1111/pme.12577
Weibel, R., Reiss, D., Karchewski, L., Gardon, O., Matifas, A., Filliol, D., Becker, J.A.J., Wood, J.N., Kieffer, B.L., Gaveriaux-Ruff, C., 2013. Mu Opioid Receptors on Primary Afferent Nav1.8 Neurons Contribute to Opiate-Induced Analgesia: Insight from Conditional Knockout Mice. PLOS ONE 8, e74706. https://doi.org/10.1371/journal.pone.0074706
Whitney, I.E., Keeley, P.W., Raven, M.A., Reese, B.E., 2008. Spatial patterning of cholinergic amacrine cells in the mouse retina. J Comp Neurol 508, 1–12. https://doi.org/10.1002/cne.21630
Wickham, H., 2016. ggplot2: Elegant Graphics for Data Analysis. Springer-Verlag New York.
Williams, J.T., Ingram, S.L., Henderson, G., Chavkin, C., Zastrow, M. von, Schulz, S., Koch, T., Evans, C.J., Christie, M.J., 2013. Regulation of μ-Opioid Receptors: Desensitization, Phosphorylation, Internalization, and Tolerance. Pharmacol Rev 65, 223–254. https://doi.org/10.1124/pr.112.005942
Wilson, A.C., Clemente, L., Liu, T., Bowen, R.L., Meethal, S.V., Atwood, C.S., 2008. Reproductive hormones regulate the selective permeability of the blood-brain barrier. Biochimica et Biophysica Acta (BBA) - Molecular Basis of Disease 1782, 401–407. https://doi.org/10.1016/j.bbadis.2008.02.011
Winters, B.L., Gregoriou, G.C., Kissiwaa, S.A., Wells, O.A., Medagoda, D.I., Hermes, S.M., Burford, N.T., Alt, A., Aicher, S.A., Bagley, E.E., 2017. Endogenous opioids regulate moment-to-moment neuronal communication and excitability. Nat Commun 8, 14611. https://doi.org/10.1038/ncomms14611
Wu, Z., Autry, A.E., Bergan, J.F., Watabe-Uchida, M., Dulac, C.G., 2014. Galanin neurons in the medial preoptic area govern parental behaviour. Nature 509, 325–330. https://doi.org/10.1038/nature13307
Wyman, J., Bultman, S., 2004. Postmortem Distribution of Heroin Metabolites in Femoral Blood, Liver, Cerebrospinal Fluid, and Vitreous Humor. J Anal Toxicol 28, 260–263. https://doi.org/10.1093/jat/28.4.260
Xie, R., Hammarlund-Udenaes, M., De Boer, A.G., De Lange, E.C.M., 1999. The role of P-glycoprotein in blood-brain barrier transport of morphine: transcortical microdialysis studies in mdr1a (−/−) and mdr1a (+/+) mice. British Journal of Pharmacology 128, 563–568. https://doi.org/10.1038/sj.bjp.0702804
Xu, B., Kalra, P.S., Farmerie, W.G., Kalra, S.P., 1999. Daily Changes in Hypothalamic Gene Expression of Neuropeptide Y, Galanin, Proopiomelanocortin, and Adipocyte Leptin Gene Expression and Secretion: Effects of Food Restriction. Endocrinology 140, 2868–2875. https://doi.org/10.1210/endo.140.6.6789

Yang, J., Reilly, B., Davis, T., Ronaldson, P., 2018. Modulation of Opioid Transport at the Blood-Brain Barrier by Altered ATP-Binding Cassette (ABC) Transporter Expression and Activity. Pharmaceutics 10, 192. https://doi.org/10.3390/pharmaceutics10040192

Ylinen, P., Taipale, C., Lindholm, J.-M., Laine, I., Holmström, E., Tuuminen, R., 2018. Postoperative management in cataract surgery: nepafenac and preservative-free diclofenac compared. Acta Ophthalmologica 96, 853–859. https://doi.org/10.1111/aos.13843

Yoo, J.-H., Yang, E.-M., Lee, S.-Y., Loh, H.H., Ho, I.K., Jang, C.-G., 2003. Differential effects of morphine and cocaine on locomotor activity and sensitization in μ-opioid receptor knockout mice. Neuroscience Letters 344, 37–40. https://doi.org/10.1016/S0304-3940(03)00410-5

Yousif, S., Chaves, C., Potin, S., Margaill, I., Scherrmann, J.-M., Declèves, X., 2012. Induction of P-glycoprotein and Bcrp at the rat blood–brain barrier following a subchronic morphine treatment is mediated through NMDA/COX-2 activation. Journal of Neurochemistry 123, 491–503. https://doi.org/10.1111/j.1471-4159.2012.07890.x

Yousif, S., Saubaméa, B., Cisternino, S., Marie-Claire, C., Dauchy, S., Scherrmann, J.-M., Declèves, X., 2008. Effect of chronic exposure to morphine on the rat blood–brain barrier: focus on the P-glycoprotein. Journal of Neurochemistry 107, 647–657. https://doi.org/10.1111/j.1471-4159.2008.05647.x

Zgierska, A., Brown, R.T., Zuelsdorff, M., Brown, D., Zhang, Z., Fleming, M.F., 2007. Sleep and daytime sleepiness problems among patients with chronic noncancerous pain receiving long-term opioid therapy: A cross-sectional study. J Opioid Manag 3, 317–327. https://doi.org/10.5055/jom.2007.0020

Zhang, J., Yang, Z., Wu, S.M., 2005. Development of cholinergic amacrine cells is visual activity-dependent in the postnatal mouse retina. J Comp Neurol 484, 331–343. https://doi.org/10.1002/cne.20470

Zhang, Z., Beier, C., Weil, T., Hattar, S., 2021. The retinal ipRGC-preoptic circuit mediates the acute effect of light on sleep. Nat Commun 12, 5115. https://doi.org/10.1038/s41467-021-25378-w

Zhang, Z., Uchida, Y., Hirano, S., Ando, D., Kubo, Y., Auriola, S., Akanuma, S., Hosoya, K., Urtti, A., Terasaki, T., Tachikawa, M., 2017. Inner Blood–Retinal Barrier Dominantly Expresses Breast Cancer Resistance Protein: Comparative Quantitative Targeted Absolute Proteomics Study of CNS Barriers in Pig. Mol. Pharmaceutics 14, 3729–3738. https://doi.org/10.1021/acs.molpharmaceut.7b00493

Zhao, Q., Wu, B., 2012. Ice breaking in GPCR structural biology. Acta Pharmacol Sin 33, 324–334. https://doi.org/10.1038/aps.2011.187

Zhao, X., Stafford, B.K., Godin, A.L., King, W.M., Wong, K.Y., 2014. Photoresponse diversity among the five types of intrinsically photosensitive retinal ganglion cells. J Physiol 592, 1619–1636. https://doi.org/10.1113/jphysiol.2013.262782

# APPENDIX A: Validation of a Conditional μ-Opioid Receptor Knockout (McKO) Mouse Line

## A.1 Introduction

Critical to this work was the development and use of a conditional cell-specific knockout of μ-opioid receptors (MORs) from intrinsically photosensitive retinal ganglion cells (ipRGCs). Mouse models with global MOR knockout have been indispensable for showing that MORs are necessary for morphine-induced analgesia and reward effect (Matthes et al., 1996). However, understanding how individual cell types and pathways mediate the effects of opioids requires a more nuanced approach. The development of the Cre-lox system has allowed for cell-specific gene deletion in mouse models, via (1) the expression of a Cre recombinase upstream of a cell type-specific promoter and (2) the insertion of loxP sites flanking the to-be-deleted gene sequence ("floxed" sequence) (Sauer and Henderson, 1988; Tsien, 2016). Generating a mouse with the desired deletion requires breeding a Cre mouse (typically +/-, as homozygous (+/+) Cre expression can have deleterious effects on the gene or cause off-target Cre expression) with a floxed mouse (typically +/+ to ensure complete gene editing when crossed with Cre mice) (Luo et al., 2020; Song and Palmiter, 2018; Tsien, 2016). The Cre recombinase will then excise the floxed sequence, resulting in gene deletion.

The global MOR knockout mouse mentioned above was developed by deleting exons 2 and 3 from the MOR gene sequence, which disrupts the coding sequence for the protein and results in a non-functional receptor (Matthes et al., 1996). The same sequence was later floxed (μflx), allowing for Cre-dependent cell-specific MOR knockout (Weibel et al., 2013). This conditional MOR knockout results in a robust, yet incomplete, decrease in MOR mRNA, regardless of the Cre-associated gene (Boulos et al., 2020; Severino et al., 2020; Weibel et al.,

2013). Validation of specific and efficient MOR knockdown is critical for using these mice to understand the behavioral effects of opioids.

In this work, we developed a cell-specific knockout of MORs from intrinsically photosensitive retinal ganglion cells (ipRGCs), which are identified based on the expression of the melanopsin gene, *Opn4*. Homozygous floxed MOR mice (μflx), described above, were crossed with heterozygous *Opn4*-Cre mice, wherein Cre is expressed upstream of the melanopsin promoter, to produce 50% McKO mice with MOR knockout only in ipRGCs, and 50% μflx littermate controls. This Appendix describes the experiments performed to validate cell-specific MOR knockout in this McKO mouse line.

Ideally, lack of MOR expression in *Opn4*-Cre+ cells would be validated by immunohistochemistry (IHC) using an antibody specific to the MOR protein sequence, producing positive labeling in control (μflx) mice but not McKO mice. Antibodies against G-protein coupled receptors (GPCRs), such as the MOR, are notoriously difficult to produce, primarily due to issues purifying GPCRs in their native folded state outside of a cell membrane. This often prevents access to epitopes aside from the extracellular N-terminus of the protein, or results in decreased specificity due to the incomplete elimination of other cellular components (Hutchings et al., 2010; Kim et al., 2023; Zhao and Wu, 2012). Several commercial antibodies against the MOR were tested (Table A-1). Unfortunately, the one antibody specific to the deleted region (exons 2-3, Bioss), failed to produce specific immunolabeling in control retinas. Furthermore, the one commercial antibody which produced a reliable immunological signal (Alomone) also labeled MORs in McKO mice, likely because it targets the N-terminus of the protein, which may still be translated from the truncated MOR mRNA transcript (Table A-1).

**Table A-1. List of available commercial antibodies against MOR.**

| Commercial MOR Antibody | Immunogen/epitope |
|---|---|
| Bioss #bs-3623R | Proprietary; immunogen range corresponds to amino acid residues 165-270/400 for the human μ-Opioid receptor (UniProt accession #P35372). |
| Alomone #AOR-011 | CSPAPGSWLNLSHVDGN, corresponding to amino acid residues 22-38 of the rat μ-Opioid receptor (UniProt accession #P33535). Extracellular, N-terminus. |
| RayBiotech #114-10101 | NHQLENLEAETAPLP, corresponding to amino acid residues 386-400 of the human μ-Opioid receptor (UniProt accession #P35372). Intracellular, C-terminus. |

As such, previous groups have relied on mRNA quantification to validate their conditional MOR knockout lines (Boulos et al., 2020; Severino et al., 2020; Weibel et al., 2013). In Chapter 2, our qRT-PCR experiments revealed that MOR mRNA expression was significantly (~60%) lower in the retinas of McKO mice compared to control (μflx) mice (Figure 2-5a). In addition, we found that decreased MOR mRNA expression was specific to the retina, as there was no significant decrease in MOR expression in the hypothalamus of McKO mice compared to control (Figure 2-6).

Although qRT-PCR has been the premier method for nucleic acid quantification for over thirty years, it is not without limitations (Adams, 2020; Freeman et al., 1999; VanGuilder et al., 2008; Wang et al., 1989). Foremost, qRT-PCR can only provide relative gene quantification (if the starting copy number is unknown, as is the case with tissue extractions), which is dependent on the stable expression of reference genes in the same sample as well as high PCR efficiency (Hellemans et al., 2007; Livak and Schmittgen, 2001; Taylor et al., 2017; Wang et al., 1989). As such, a standard curve of cDNA dilutions must be included in every run to establish that PCR efficiency is within an acceptable range, and this efficiency is assumed to be the same across all samples in the plate. In addition, qRT-PCR is best at detecting large (>2) fold-changes in expression between groups, and the statistical conclusions drawn from the data are strongest with high abundance (>100 copies) targets (Taylor et al., 2017).

Among the many developments in PCR technology over the past three decades, perhaps the most exciting is the development of digital droplet PCR (ddPCR) (Hindson et al., 2011). In ddPCR, absolute quantification of nucleic acid copy number is possible without a standard curve. This is because fluorescence is quantified at the end-point of the reaction, rather than in the exponential phase of growth as in qRT-PCR, which allows reactions to have different efficiencies without compromising the ability to accurately quantify copy number. Furthermore, PCR reactions are partitioned into individual droplets, which are later read as either positive or negative for the target (based on fluorescence amplitude) and analyzed by Poisson statistics, improving precise quantification, especially with low abundance targets (Hindson et al., 2011; Taylor et al., 2017).

Given the ability of ddPCR to detect smaller fold-changes than qRT-PCR and produce higher quality data with low abundance targets, additional validation experiments are presented in this Appendix. MOR mRNA expression in the retina and several brain regions, including the hypothalamus, of McKO and control mice was quantified by ddPCR. Absolute MOR copy number was determined in each sample; the results confirm that MOR knockout is specific to the retinas of McKO mice. Furthermore, we present data from immunohistochemical experiments assessing Cre protein expression in the retinas and brains of McKO and μflx mice, as a proxy for measuring changes in MOR protein expression.[7] This Appendix ends with a comprehensive discussion regarding the validity of the McKO mouse line.

[7] The portions of this Appendix regarding the Cre IHC experiments are partially reproduced from Bergum, N., Berezin, C.-T., King, C. M., & Vigh, J. (2022). μ-Opioid Receptors Expressed by Intrinsically Photosensitive Retinal Ganglion Cells Contribute to Morphine-Induced Behavioral Sensitization. *Int. Jour. of Mol. Sci.*, *23*(24), https://doi.org/10.3390/ijms232415870, with minor modifications for clarity, pursuant to the open access Creative Commons CC BY license and the MDPI Open Access Policy (Appendix D).

## A.2 Materials and Methods

### *A.2i Animals*

*Oprm1*$^{fl/fl}$ (μflx) breeders (Jackson Labs strain #030074) were generously provided by Dr. Brigitte Kieffer (Douglas Research Center, McGill University). μflx mice have exons two and three of the MOR (*Oprm1*) gene flanked by a loxP site and were maintained on a 50% C57BL/6J-50% 129Sv background for five generations before receipt (Weibel et al., 2013). Mice with Cre recombinase expressed upstream of the melanopsin (*Opn4*) promoter [Tg(*Opn4*-cre) SA9Gsat/Mmucd, #036544-UCD; *Opn4*-cre] were purchased from the Mutant Mouse Resource and Research Center (MMRRC) at the University of California, Davis. These *Opn4*-cre mice were backcrossed into a 100% C57BL/6J background prior to purchase and were maintained as hemizygotes (*Opn4*-cre +/−). MOR-conditional knockout (McKO) mice, in which ipRGCs lack functional MORs, were generated as described previously (Berezin et al., 2022; Cleymaet et al., 2021). In brief, μflx and *Opn4*-cre mice were crossed to obtain McKO mice with the floxed *Oprm1* gene on both alleles and *Opn4*-cre on one allele. Thus, the result of this cross produced 50% μflx/control: 50% McKO littermates. Notably, this μflx/McKO line was maintained on a background containing at least 75% C57BL/6J and 25% 129Sv. In all experiments, μflx littermates of McKO mice were used as controls. Mice lacking functional MORs globally (B6.129S2-Oprm1tm1Kff/J; MKO) were purchased from Jackson Labs (strain #007559) (Matthes et al., 1996). MKO mice were backcrossed to C57BL/6J mice for at least 12 generations prior to purchase.

To assess Cre expression in *Opn4*-cre mice by immunohistochemistry, we crossed McKO mice to *Opn4*-EGFP BAC-carrying mice (Tg(*Opn4*-EGFP)ND100Gsat/Mmucd strain, generated by the GENSAT project) (Cleymaet et al., 2019). For a positive control in the brain, we used

mice that had Cre recombinase under control of the galanin (*GAL*) promoter (B6J.FVB(Cg)-Tg(*Gal*-cre)KI87Gsat/Mmucd; *Gal*-cre). These *Gal*-cre animals were crossed to Ai14 (Jackson Labs strain #007914) mice to express tdTomato following *GAL*-driven Cre-dependent recombination (*Gal*-cre-tdTomato).

Adult male animals (8–26 weeks) were housed under a 12-h light:12-h dark cycle (LD) cycle, with lights on at 7:00 a.m. (ZT 0) and lights off at 7:00 p.m. (ZT 12). They were fed standard chow and water ad libitum. All animals used in these studies were handled in compliance with the Institutional Animal Care and Use Committees of Colorado State University (Protocol 18-8395A, 28 January 2019) and in accordance with the ARVO Statement for the Use of Animals in Ophthalmic and Vision Research.

*A.2ii Digital Droplet PCR (ddPCR)*

**Sample Preparation**

Male μflx (n=5) and McKO (n=5) mice were anesthetized with isoflurane (Fluriso, VetOne) and immediately decapitated. The eyes were enucleated and the retinas microdissected in 0.1 M PBS and stored in RNAlater (Sigma #R0901) at 4°C until all samples were collected. The brains were removed and immediately cut into 300 μm coronal sections on a Leica VT1200S vibratome. Four sections were collected for each target area (caudate putamen [CP], hypothalamus [HT], and thalamus [TH]), and the region was microdissected from each section in 0.1 M PBS (Figure A-1). Microdissected brain tissue for each region was pooled per animal, then immediately homogenized in 300 μL Buffer EPRL (QuantaBio) supplemented with DTT (GoldBio) by passing it through a 20-g needle five times and a 27-g needle five times. Brain lysates were stored at -80°C until all samples were collected.

Total RNA was extracted from each tissue sample using the Extracta Plus kit (Quantabio #95214), according to the manufacturer's instructions. In brief, retinas were transferred to 600 µL Buffer EPRL supplemented with DTT, disrupted using a micropestle then homogenized by passing the sample through a 20-g needle five times. Brain lysates (thawed at 37°C for 2 min) and retina lysates (immediately processed) were centrifuged at max speed (14,000 rpm, ~16,000 g) for 3 min. The supernatants were put through the DNA removal columns, then the samples put on the RNA-binding columns, washed, and finally eluted in 30 µL RNase-free $H_2O$. The

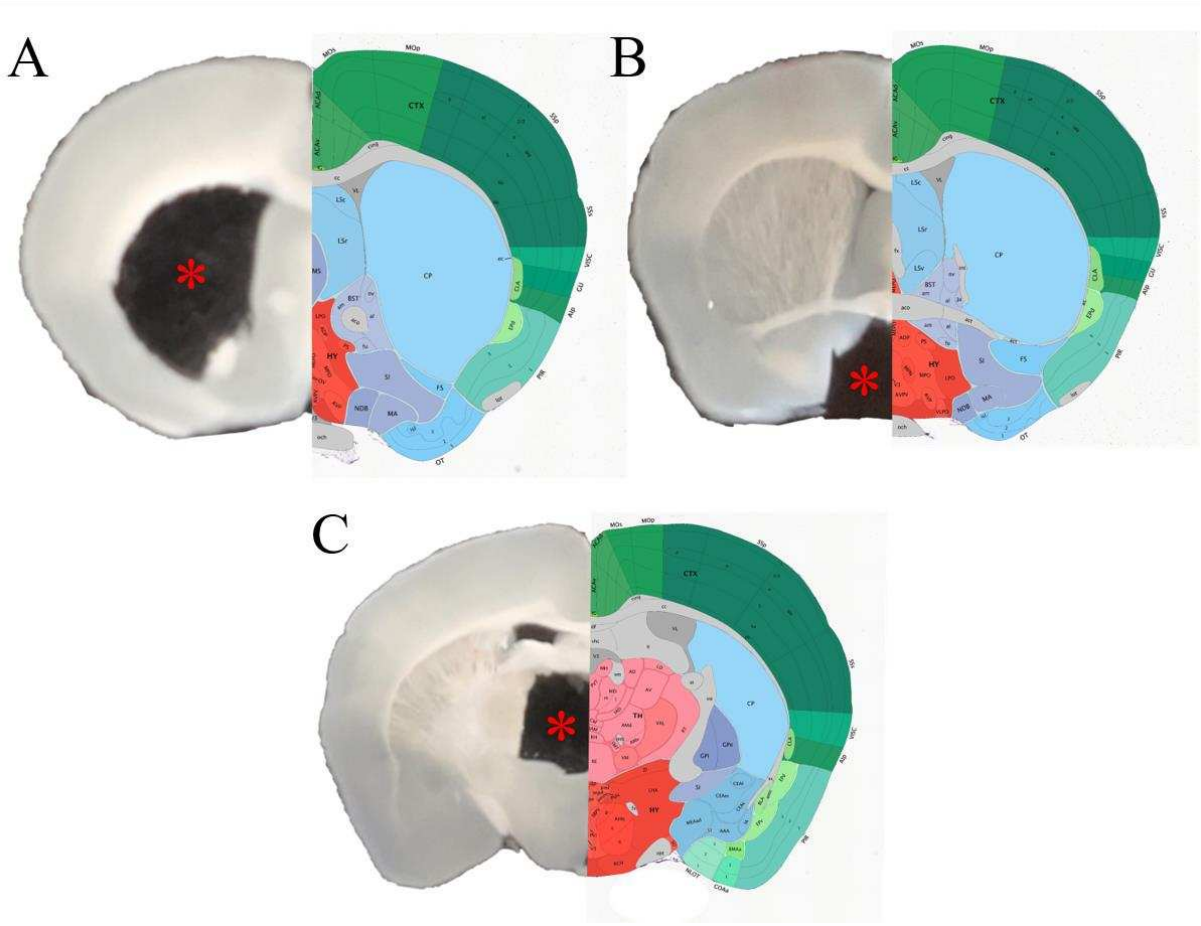


**Figure A-1. Representative images of microdissected regions for ddPCR.**
Mouse brains were sliced into 300 µm coronal sections on a Leica vibratome. Each target area (**A**, caudate putamen; **B**, hypothalamus; **C**, thalamus) was microdissected from four sections (left) using anatomical annotations (right) from the Allen Mouse Brain Atlas as a reference (atlas.brain-map.org). Asterisks indicate the tissue that was removed for each sample. Microdissected tissue was immediately homogenized in lysis buffer for RNA extraction.

concentration and quality of eluted RNA was determined on a ThermoFisher NanoDrop Lite (all $A_{260}/A_{280}$ measurements were above 2.0). RNA was then treated with DNase I, RNase-free (Thermo Scientific #EN0521, lot #00791903): the maximum amount of RNA possible (up to 1000 ng) was used in each 20 µL reaction (70 ng was used for the sample with the lowest concentration). RNA quality was then assessed using a 1% agarose gel; no gDNA contamination or RNA degradation was seen in any sample. DNase-free RNA was stored in RNase-free $H_2O$ at -20°C until all samples were obtained.

RNA was then reverse transcribed into cDNA using qScript XLT cDNA SuperMix (Quantabio #95161), according to the manufacturer's instructions. Briefly, 50, 75, or 100 ng of RNA was reverse transcribed in each 20 µL reaction, depending on the sample concentration. Reactions were prepared on ice, and then incubated at 27°C for 5 min, 42°C for 30 min, 85°C for 5 mins. All cDNA was then diluted to 1 ng/µL in RNase-free water to obtain an equal concentration of cDNA in all samples, as well as to dilute any potential PCR inhibitors. cDNA was stored at -20°C until ddPCR reactions were performed.

**PCR and Droplet Generation**

The design of and sequences for primers (500 nM) and probes (900 nM) against MOR can be found in Chapter 2.3B. Before use in ddPCR, the primers were tested on 10-fold dilutions of cDNA to (1) ensure the primer/probe concentrations resulted in high quality data (Figure A-2) and (2) determine the necessary cDNA input for ddPCR. A lack of amplification was confirmed in negative controls, which were either no-template $H_2O$ controls or no-reverse transcription RNA controls (Figure A-3).

20 µL PCR reactions were prepared using ddPCR Supermix for Probes (No dUTP) (BioRad #1863023, batch #64505749), according to the manufacturer's instructions. All reactions contained 10 µL 2X SuperMix, 2 ng cDNA (2 µL), 1 µL multiplexed primers, 1 µL probe, and 6 µL $H_2O$. The entirety of each 20 µL reaction was pipetted into the sample wells of droplet cartridges (BioRad, #1864008). Then, 70 µL (in excess) of droplet generator oil (BioRad, #1863005) was pipetted into the oil wells of the droplet cartridges. Each droplet cartridge was covered with a gasket (BioRad, #1863009) and droplets were generated with the QX200 Droplet Generator (BioRad, #1864002). The QX200 machine is expected to generate nanoliter-sized droplets. Once droplets were generated, 40 µL of droplets was slowly pipetted into each plate well (Eppendorf, twin.tec semi-skirted 96-well plate #951020362). The PCR plate was kept out of the light while all droplets were generated to protect the fluorescent probes. Distinct separation of emulsion (droplet) and excess oil layers were confirmed in all samples prior to PCR. PCR plates were sealed with foil (BioRad #1814040) using the PX1 PCR Plate Sealer (BioRad, #1814000). Reactions were run on a C1000 Touch thermal cycler (BioRad, #1851197), and the protocol was as follows: enzyme activation at 95°C for 10 min, 40 cycles of denaturation at 94°C for 30 s and annealing/extension at 60°C for 1 min, enzyme deactivation at 98°C for 10 min, then hold at 4°C.

**Droplet Reading and Analysis**

Immediately after PCR completion, droplets were read using the QX200 Droplet Reader (BioRad #1864003). Automatic thresholding across samples was done in QuantaSoft (BioRad, v1.7.4.0917), then manually adjusted to be approximately one-third of the way between negative and positive droplet bands (Figure A-2). Each sample was required to have >10,000 accepted

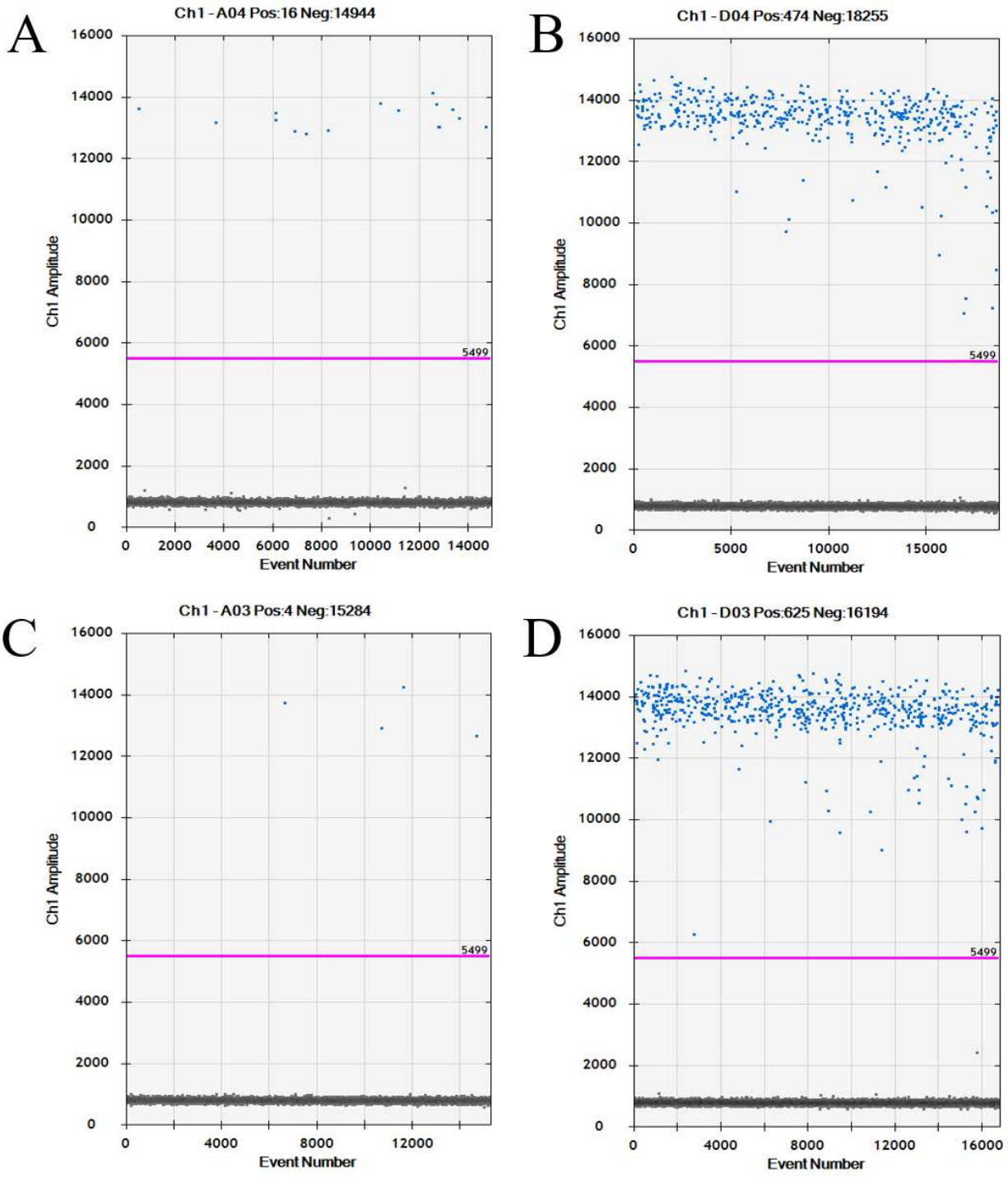


**Figure A-2. Representative 1-D plots of ddPCR reactions.**
MOR expression in the retina (**A, C**) and thalamus (**B, D**) of μflx (**A, B**) and McKO (**C, D**) mice was quantified by probe-based (FAM) ddPCR. Each reaction had at least 10,000 droplets (each droplet is one event on the X-axis), with negative droplets having minimal fluorescence (grey dots) and positive droplets (blue dots) having fluorescence above the threshold (pink line).

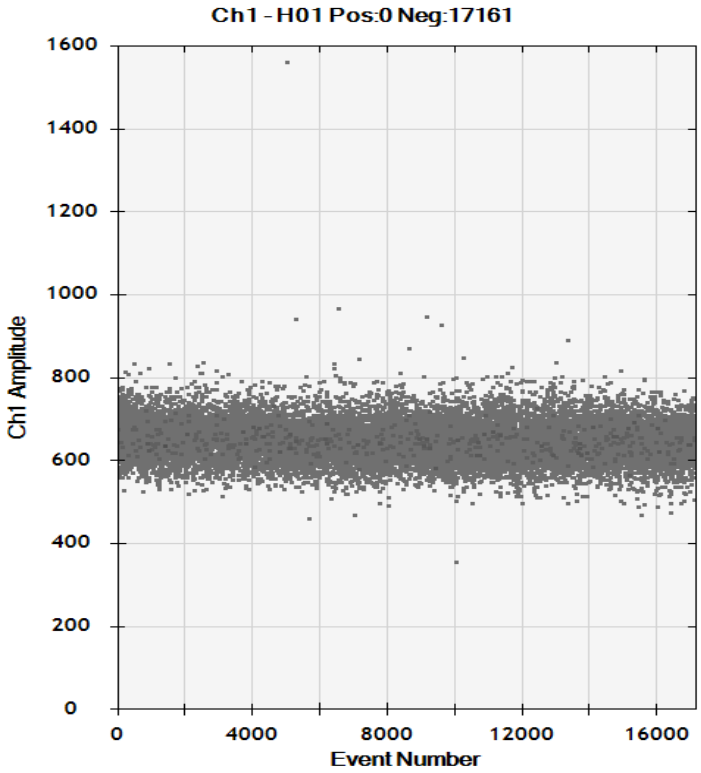


**Figure A-3. Representative 1-D plot of MOR expression in a negative control.**
All negative controls (either no-reverse transcription RNA controls [NRT], or no-template H2O controls [NTC]) had no MOR positive droplets above baseline fluorescence. Shown plot is an NTC from an McKO retina, using more than 2.5x the normal amount of cDNA (5 ng, versus 2 ng).

droplets, else was excluded and rerun; the average number of droplets per sample was 16,365 ± 1,761. Since each sample contained 2 ng input, the copy number per droplet was normalized to copy number per ng RNA. Select samples were re-run on a separate day and showed high inter-experiment reproducibility.

All statistical analysis was performed using R (v4.2.2; R Core Team, 2022) in RStudio (v2022.7.2.576; RStudio Team, 2022). Differences in MOR copy number per ng cDNA between tissue types and/or genotypes was analyzed by a mixed ANOVA, with genotype as a between-subjects factor, tissue as a within-subjects factor, and mouse number as the ID variable. The data were square root-transformed to satisfy the assumptions of ANOVA. No outliers were detected

in the dataset using the *identify_outliers* or *rosnerTest* functions. Normality of the dataset (whole dataset, or within genotype/tissue combinations) was assessed by the *shapiro.test* function and by inspecting Q-Q plots. Homogeneous variance for the within-subjects factor (tissue) was determined with the *levene_test* function. Homogeneity of covariances for the between-subject factor was checked using the *box_m* function. The assumption of sphericity is checked and, if necessary, corrected for within the *aov_car* (ANOVA) function. Indeed, the Greenhouse-Geisser and Huynh-Feldt corrections for departure from sphericity were applied. Pairwise comparisons with Bonferroni corrections were performed using the *emmeans* function (Lenth, 2022).

*A.2ii Immunohistochemistry*

Adult male mice were deeply anesthetized with pentobarbital sodium (Fatal-Plus) and then perfused with 10% sucrose in 0.1 M phosphate-buffered saline (PBS) followed by 4% PFA in PBS. The eyes were enucleated and post-fixed in 4% PFA at RT for 25 min (eyes were puncture-fixed for 20 min before the retinas were dissected out in PBS and returned to the fixative for an additional 5 min). Whole brains were removed and post-fixed in 4% PFA at 4 °C for at least 24 h and then cut into 100 μm sections on a Leica vibratome. Brain slices and whole-mount retinas were washed with PBS then placed in blocking solution (5% serum, 0.5% Triton-X-100 in 0.1 M PBS). Tissues were incubated in the rabbit anti-Cre antibody (1:500 Cell Signaling #15036) for approximately 24 h followed by the appropriate secondary antibody (Goat anti-Rabbit Alexa Fluor 647, ThermoFisher, Waltham, MA, USA). The tissues were stained with DAPI (GeneTex, Irvine, CA, USA) then mounted on Superfrost Plus microscope slides (Fisher Scientific, Hampton, NH, USA) in Vectashield Plus Antifade Mounting Medium (Vector Laboratories, Burlingame, CA, USA).

Tissues were imaged in 1 μm Z-stack increments on a LSM 900 confocal microscope (Carl Zeiss, Oberkochen, Germany) with a 40x oil-immersion objective. For all images, sequential scans at each wavelength were performed, and 4x averaging was performed to improve the signal-to-noise ratio. Automated image analysis was performed using Fiji (v1.53, (Schindelin et al., 2012)). In brief, after initial pre-processing (i.e., adjusting brightness and denoising), a median blur filter was applied to each channel, and the images were thresholded and converted to binary masks. The 3D Objects Counter plugin (Bolte and Cordelières, 2006) was used to count DAPI+, GFP+, and/or Cre+ objects in each mask. The accuracy of GFP+ cell counting was manually verified, and most large (>700 $\mu m^2$) DAPI+ cell clusters were manually watershed segmented using the 3D ROI Manager (Ollion et al., 2013). The "Measure" and "Colocalization" features of the 3D ROI Manager were used to calculate all objects' numbers, volumes, and percent colocalization (Ollion et al., 2013).

## A.3 Results

*A.3i ddPCR shows lower MOR copy number only in McKO retinas compared to μflx*

There was a similar pattern of MOR expression in McKO (n=5) and μflx (n=5) mice across the four tissue types surveyed: the number of MOR copies (per ng RNA) was lowest in the retina (6.38 ± 3.9), followed by the CP (32.87 ± 31.4), the HT (68.36 ± 77.1), and finally, the highest number of MOR copies was found in the TH (176.13 ± 160) (Figure A-4). Accordingly, tissue emerged as a significant factor ($p$=3.317e-5, F(24) =12.84) in our mixed ANOVA (genotype * tissue; between- and within-subjects factors, respectively). After square root-transformation, we found statistically lower MOR copy numbers in every tissue (retina: $p$=0.013,

t(8)=-4.44; CP: $p$=0.036, t(8)=-3.71; and HT: $p$=0.031, t(8)=-3.82; Bonferroni-adjusted) compared to the TH (Figure A-4).

Differences in MOR copy number between McKO and µflx mice within each of the four tissues were then explored (Figure A-5). After square root-transformation, there was no significant difference between µflx and McKO mice in any of the three brain regions: the CP ($p$=0.893, t(8)=0.138), the HT ($p$=0.452, t(8)=0.791), nor the TH ($p$=0.984, t(8)=0.021) (Figure A-5). However, there were significantly more MOR copies (per ng RNA) in µflx retinas (9.06 ± 3.5) compared to McKO retinas (3.7 ± 2.1; $p$=0.021, t(8)=2.854) ) (Figure A-5).

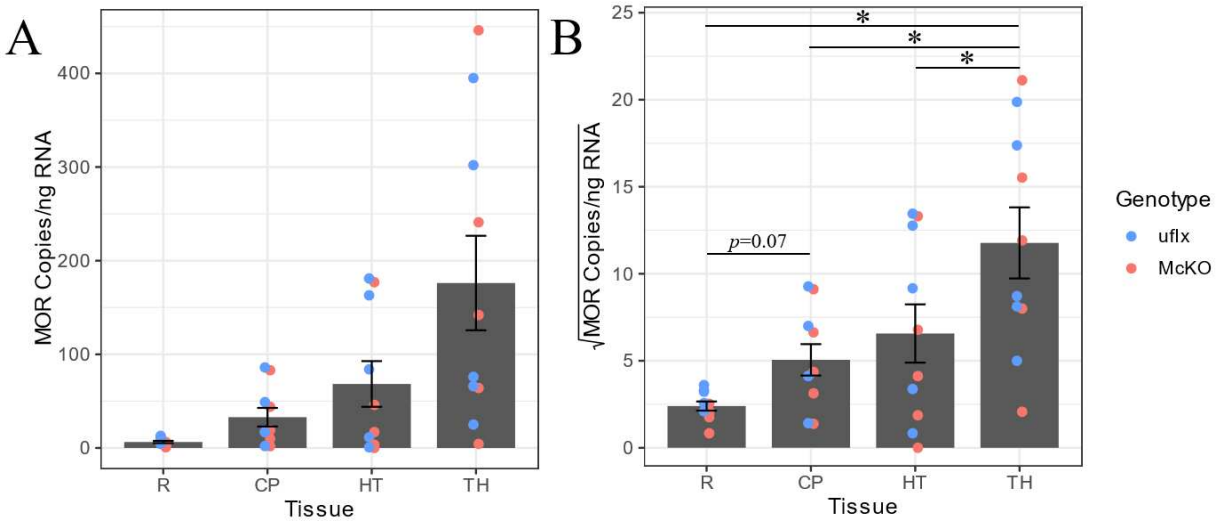


**Figure A-4. MOR expression across the retina and brain is similar in McKO and µflx mice.** (**A**) MOR copy number per ng RNA in the retina (R), caudate putamen (CP), hypothalamus (HT) and thalamus (TH) in McKO (n=5, red) and µflx (n=5, blue) mice was quantified by ddPCR. Expression patterns are similar in the two genotypes, with the lowest expression in the retina and the highest in the TH. (**B**) Data were square root-transformed to meet the assumptions of ANOVA. * $p$>0.05

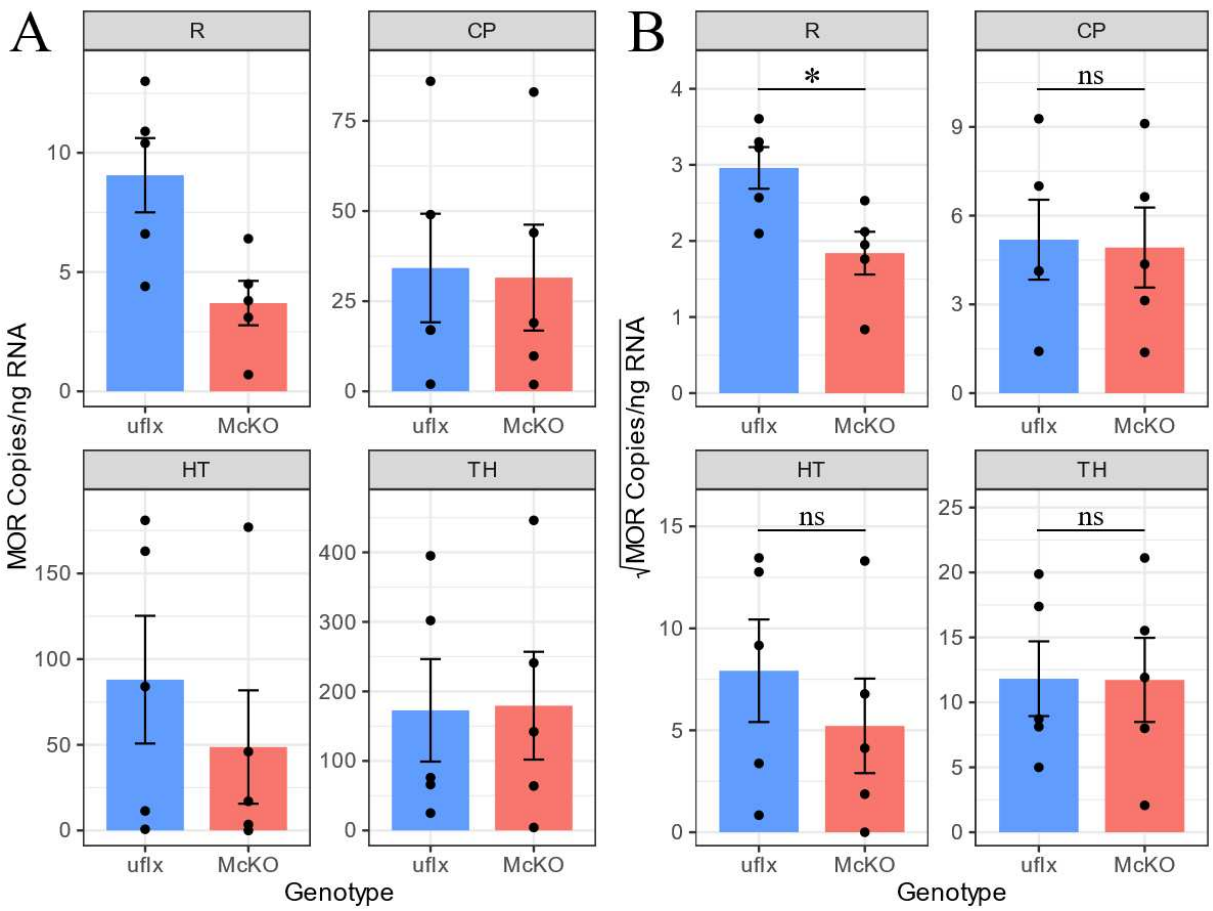


**Figure A-5. MOR copy number is only decreased in the retinas of McKO mice.**
(**A**) MOR copy number per ng RNA in the retina (R), caudate putamen (CP), hypothalamus (HT) and thalamus (TH) in McKO (n=5, red) and µflx (n=5, blue) mice was quantified by ddPCR. (**B**) Data were square root-transformed to meet the assumptions of ANOVA. MOR copy number is only significantly different between McKO and µflx retinas, with no significant differences in any surveyed brain region. Note the different scale in each panel (enlarged to show more detail). * $p$<0.05 ns=non-significant $p$>0.05

*A.3i Robust Cre immunolabeling in the McKO retina*

We aimed to validate that, in McKO mice, *Opn4* drove Cre recombinase (Cre) expression in ipRGCs and not in key ipRGC projections areas within the brain. To accomplish this, we immunolabeled Cre in the hypothalamus (SCN and VLPO), striatum (caudate/putamen [CP]), and the paraventricular nucleus of the thalamus (PVT). We first labeled Cre in the retina of

McKO mice crossed with *Opn4*-EGFP BAC-carrying mice (in which M1-M3 ipRGCs have green somas (Cleymaet et al., 2019)). As shown in Figure A-6 A–C, we found strong somatic immunolabeling of Cre in McKO ipRGCs (26 cells from 2 animals, average cell volume = 213 $\mu m^2$). Notably, we considered a cell a "true positive" if 5% of the cell's volume was Cre+ and found that nearly 70% of ipRGCs were Cre+ (18/26 cells). Within cells that passed our 5% cutoff, the average Cre+ volume percentage in positive ipRGCs was 28.5% (maximum = 87.3%). Due to variable *Opn4* expression between ipRGC subtypes, only M1-M3 ipRGC subtypes can be identified in the *Opn4*-EGFP mouse (Cleymaet et al., 2019). Because we did not quantify Cre+

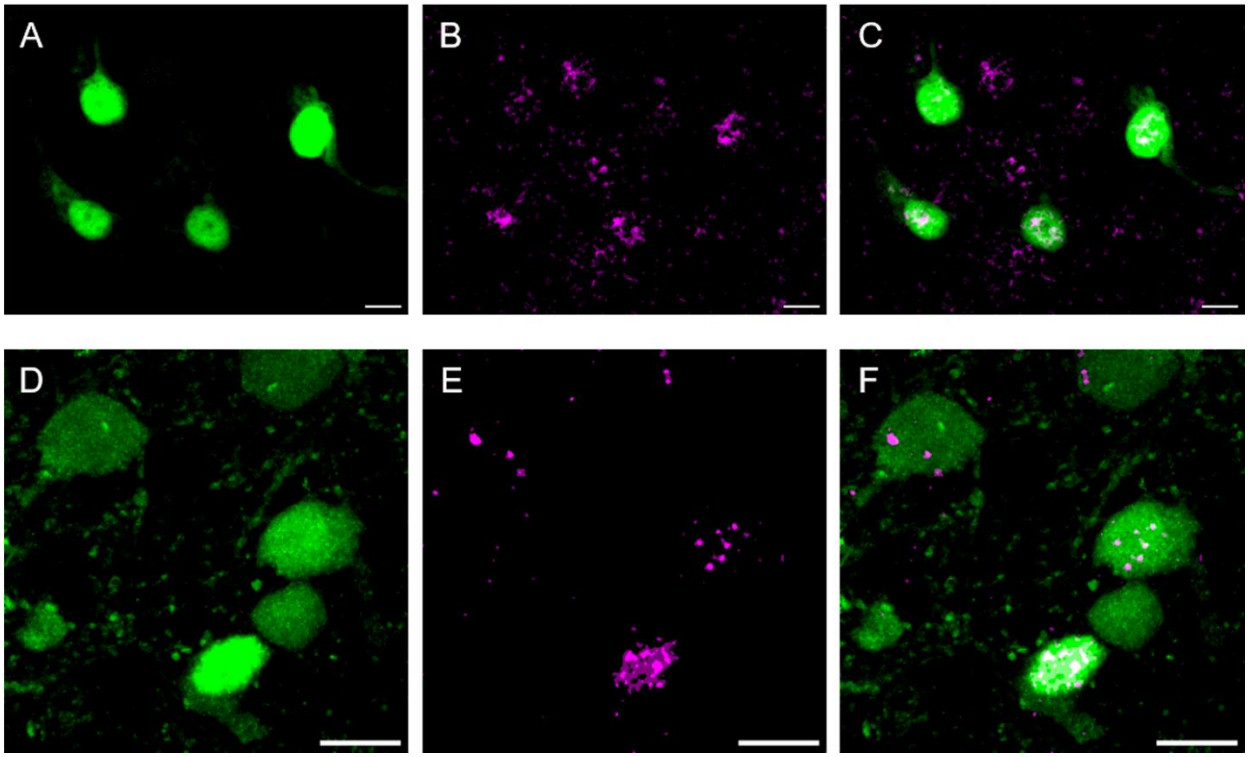


**Figure A-6. Positive controls show somatic Cre immunolabeling.**
**A-C**) Whole-mount retina from a McKO x *Opn4*-EGFP mouse. **A)** Native GFP signal, **B)** Cre antibody labeling (psuedocolored), and **C)** composite image of the maximum projection of all z-stacks containing the cells of interest. **D-F**) *Gal*-cre-tdTomato brain slice containing the preoptic area of the hypothalamus. **D)** Native tdTomato signal (pseudocolored), **E)** Cre antibody labeling (psuedocolored), and **F)** composite image of the maximum projection of all z-stacks containing the cells of interest. Scale bars = 10 μm.

non-ipRGCs (Figure A-6 B,C), we likely underestimated the number of ipRGCs (especially in M4-M6 ipRGC subtypes) that were Cre+ in the McKO retina. To examine Cre expression in the brain, we first had to confirm that the antibody labeled Cre in the brain. To accomplish this, we sectioned the preoptic area of the hypothalamus from mice in which tdTomato was present in Cre-expressing galaninergic neurons (*Gal*-cre-tdTomato). As the preoptic area contains a high number of galanin-expressing cells (Wu et al., 2014), Cre immunolabeling in the *Gal*-cre-tdTomato brain also resulted in somatic labeling, albeit less robust than in the retina (Figure A-6 D–F). This was in strong contrast to the pattern of Cre immunostaining found in the McKO brain (Figure A-7). In single optical sections from all analyzed brain regions, Cre appeared to be primarily localized to the outer surfaces of (i.e., surrounding) DAPI-labeled cells (Figure A-7), suggesting that Cre immunoreactivity in the McKO brain primarily originated from Opn4+ ipRGC processes and not from neurons in the brain themselves. Nevertheless, as in the retina, we considered a cell a true positive if 5% of the cell's volume was Cre+. We found that in the VLPO, 1.4% of cells were Cre+ (12/869; Figure A-7 A–C); in the SCN, 0.89% of cells were Cre+ (4/445); in the CP, 1.7% of cells were Cre+ (15/848 cells; Figure S8D–F); and in the PVT, 3.8% of cells were Cre+ (15/398; Figure A-7 G–I). Although we manually segmented most DAPI cell clusters (resulting in an average cell volume of 361 $\mu m^2$; median = 341 $\mu m^2$), the maximum cell volume (1480 $\mu m^2$) indicates that some cell clusters remain, which may have led to artificially higher percentages of Cre+ cells. Given the low proportion of neurons that express Cre in the brains of McKO animals, their contributions to the behaviors described in this work are likely small if not insignificant.

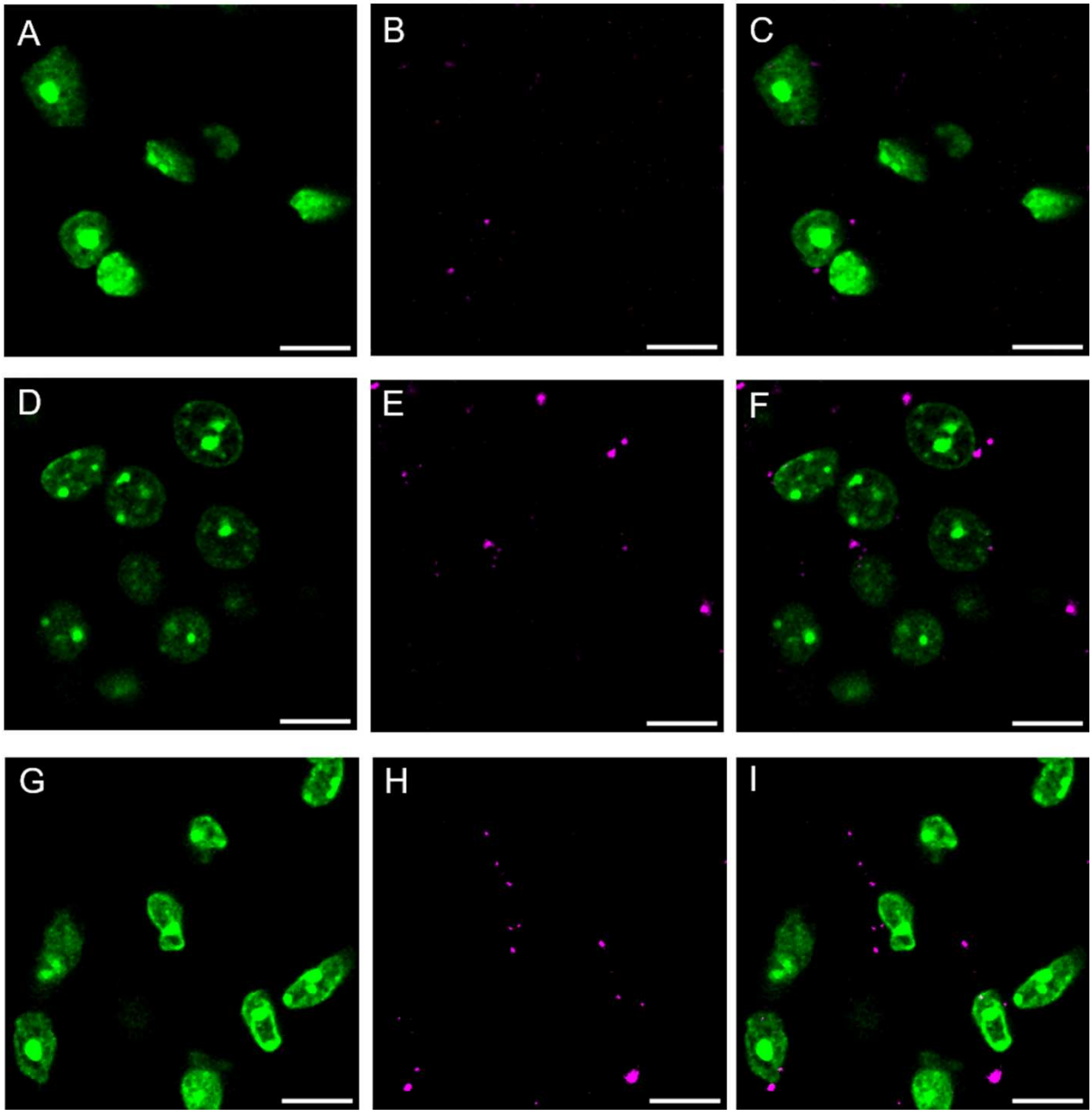


**Figure A-7. Cre immunolabeling in the McKO brain may originate from EGFP+ ipRGCs.** Sections containing the ventrolateral preoptic area of the hypothalamus **(A-C)**, caudate putamen **(D-F)**, and paraventricular nucleus of the thalamus **(G-I)**. Single optical sections showing DAPI nuclear stain (pseudocolored) **(A, D, G)** and Cre antibody labeling **(B, E, H)**. Composite images of single optical sections **(C, F, I)** reveal sporadic Cre immunoreactivity primarily on the surface of (i.e. surrounding) cells, which may not be specific to the neurons in these brain regions. Scale bars = 10 μm.

## A.4 Discussion

In order to draw conclusions about the role of MORs expressed by ipRGCs in modulating sleep/wake behavior, it was critical to validate that McKO mice have decreased MOR expression, specifically in ipRGCs, compared to μflx mice. Unfortunately, there is a lack of commercial anti-MOR antibodies that can accurately distinguish the full-length MOR protein from the truncated MOR protein. Although mRNA and protein levels are not always directly correlated (Greenbaum et al., 2003; Liu et al., 2016; Maier et al., 2009), it appears that all groups using Cre-dependent MOR knockout mouse models rely on mRNA quantification to validate their conditional knockout lines. In a conditional knockout of MORs from voltage-gated sodium channel 1.8 (Nav1.8)-expressing cells, a 60% decrease in MOR mRNA was found by qRT-PCR (Weibel et al., 2013). In dopamine receptor 1 (D1)-expressing cells, conditional MOR knockout results in a 60% decrease in MOR mRNA, while in D2-expressing cells, MOR mRNA is only decreased by 40% (measured by qRT-PCR) (Severino et al., 2020). Lastly, in neurons expressing the B4 nicotinic receptor subunit, conditional MOR knockout results in a 30% reduction in MOR mRNA expression, as measured by qRT-PCR (Boulos et al., 2020). Thus, the ~60% decrease in MOR mRNA we found by qRT-PCR in McKO retinas appears consistent with the results of other Cre-dependent knockout mouse lines.

As discussed above, qRT-PCR is best suited for detecting large fold-changes in expression and the conclusions drawn from the data are strongest in high abundance targets, defined as having over 100 copies (Taylor et al., 2017). In our ddPCR experiments, there were approximately 6 MOR copies in each ng of retinal RNA. Thus in our qRT-PCR experiments, where 10 ng of RNA was used in each reaction, there were fewer than 100 MOR copies in each sample. Therefore, the results from ddPCR experiments are likely more accurate and reliable. In

addition, the samples used for ddPCR were also more precisely gathered, since we microdissected multiple regions out from brain slices, compared to in qRT-PCR where the entire hypothalamus was cut out from the intact brain and other tissues may have been included.

One limitation of both qRT-PCR and ddPCR is that we used the entire retina as our starting material. Although the robust decrease in MOR expression we see in McKO mice suggests ipRGCs are the primary MOR-expressing cells in the retina, there was residual MOR expression, likely from dopaminergic amacrine cells and other ganglion cells (Gallagher et al., 2012). ipRGCs represent a small class of ganglion cells (about 5% of the ~60,000 ganglion cells per mouse retina) (Hattar et al., 2002; LeGates et al., 2014; Provencio et al., 2000; Schmidt et al., 2011). Attempts were made to magnetically separate ganglion cells from dissociated retinal preparations, however these were complicated by low RNA yields and remaining MOR expression. The yield could be improved by pooling retinas from many (>3) mice, however the issue of residual MOR could not be solved as there are no simple methods of isolating ipRGCs from the retina. Nevertheless, we did confirm that MOR knockout in McKO mice is specific to the retina by both qRT-PCR and ddPCR.

The issue of isolating ipRGCs may be avoided by using alternate techniques, such as RNAscope *in situ* hybridization to visualize mRNA expression. While we did find a significant difference in MOR expression in the ipRGCs of McKO and μflx mice (Chapter 2), we were unable to reliably label MOR in conjunction with the ipRGC-specific cell marker, *Opn4*, and a marker for MOR-expressing dopaminergic amacrine cells, tyrosine hydroxylase, in the same retinal section. Such an image would have provided clear evidence that MOR knockout is specific to ipRGCs. Attempts to develop a co-detection method integrating RNAscope with immunohistochemistry were also largely unsuccessful, likely because our standard antigen

retrieval protocol for immunohistochemistry is not compatible with RNAscope. Nevertheless, RNAscope allowed us to probe the distribution of MOR expression in McKO and μflx retinas and the results were consistent with the qRT-PCR and ddPCR data.

Our immunohistochemical results showed that somatic Cre expression was restricted to ipRGCs in *Opn4*-cre mice, consistent with a specific and robust MOR knockout in McKO mice. Although Cre expression is not equivalent to MOR expression, it is a good proxy to verify our McKO mouse line at the protein level. In general, there was a stark difference between Cre expression in the *Opn4*-cre retina compared to the *Opn4*-cre brain, as the retina had robust somatic labeling and a larger proportion of labeled cells. Robust somatic Cre immunostaining was also seen in the brains of *Gal*-cre mice, which acted as a positive control for immunolabeling in the brain. While there was some Cre immunolabeling in the *Opn4*-cre brain, it had a different spatial distribution: Cre expression was primarily seen around and/or on the surface of neurons. While this could represent ectopic Cre expression, it is also plausible that this Cre expression originates from *Opn4*-Cre+ ipRGC projections. Recent work showed that local translation occurs in ipRGC axons: ribosome-associated mRNA transcripts in *Opn4*-Cre+ neurons can be purified from the brain using the RiboTag system (Gupta et al., 2022; Sanz et al., 2019). Interestingly, there is differential gene expression between ipRGC cell bodies in the retina and their axons in the brain: while the retina is enriched in genes with functions like visual and light perception, the axons are enriched for genes relating to, e.g., the regulation of GPCR signaling pathways (Gupta et al., 2022). This work is still in progress, but tentatively suggests that Cre expression in *Opn4*+ ipRGC projections could be detected in the brain.

While all the results discussed here are consistent with the McKO mouse line carrying the expected knockout, there are limitations to the Cre-lox system that should be noted. The Cre-lox

system requires Cre expression to be driven by a cell-type specific promoter: gene editing is incomplete if the marker is not expressed across the entire population, and undesired gene editing occurs if the marker is expressed outside of the population. In the case of *Opn4*-Cre mice, melanopsin (the photopigment produced by *Opn4*) has long been considered an ipRGC-specific marker. However, recent work indicates that all currently available ipRGC reporter mouse lines are plagued by either underrepresentation of ipRGCs (e.g. *Opn4*-EGFP mice) or ectopic labeling (e.g. *Opn4*-cre mice) (Maloney et al., 2022). Specifically, some *Opn4*-Cre mouse lines drive Cre expression in conventional (non-ipRGC) retinal ganglion cells (Ecker et al., 2010; Maloney et al., 2022). However, ipRGCs and conventional retinal ganglion cells, in general, project to different areas; the SCN in particular receives nearly exclusive input from ipRGCs and the few projections from conventional retinal ganglion cells likely do not play a major functional role (Beier et al., 2021). Therefore, the McKO sleep/wake phenotypes seen in this work can most likely be attributed to ipRGCs rather than conventional retinal ganglion cells. In addition, there is evidence that *Opn4* may be expressed in the brain, including in the caudate putamen and hypothalamus (Flyktman et al., 2017; Moraes et al., 2021). However, these *Opn4*-expressing cells may not be the same population as MOR-expressing cells in the same region (Saunders et al., 2018). Thus, although it is possible that *Opn4* expression could drive MOR knockout in the brain, the results presented here suggest that if this does occur, it is at low or undetectable levels such that behavioral phenotypes in the McKO mouse can be primarily attributed to MORs expressed by ipRGCs.

# APPENDIX B: Elsevier License to Reuse Material

ELSEVIER LICENSE
TERMS AND CONDITIONS
Feb 08, 2023

This Agreement between Mrs. Casey-Tyler Berezin ("You") and Elsevier ("Elsevier") consists of your license details and the terms and conditions provided by Elsevier and Copyright Clearance Center.

| | |
|---|---|
| License Number | 5484361186007 |
| License date | Feb 08, 2023 |
| Licensed Content Publisher | Elsevier |
| Licensed Content Publication | Elsevier Books |
| Licensed Content Title | Medical Biochemistry |
| Licensed Content Author | Antonio Blanco,Gustavo Blanco |
| Licensed Content Date | Jan 1, 2017 |
| Licensed Content Pages | 72 |
| Start Page | 573 |
| End Page | 644 |
| Type of Use | reuse in a thesis/dissertation |
| Portion | figures/tables/illustrations |
| Number of figures/tables/illustrations | 1 |
| Format | both print and electronic |
| Are you the author of this Elsevier chapter? | No |
| Will you be translating? | No |
| Title | PhD Thesis |
| Institution name | Colorado State University |
| Expected presentation date | Jun 2023 |
| Portions | Figure 26.3 |
| Requestor Location | Mrs. Casey-Tyler Berezin<br>501 W Prospect Rd<br>FORT COLLINS, CO 80526<br>United States<br>Attn: Mrs. Casey-Tyler Berezin |
| Publisher Tax ID | 98-0397604 |
| Total | 0.00 USD |

Terms and Conditions

## INTRODUCTION

1. The publisher for this copyrighted material is Elsevier. By clicking "accept" in connection with completing this licensing transaction, you agree that the following terms and conditions apply to this transaction (along with the Billing and Payment terms and conditions established by Copyright Clearance Center, Inc. ("CCC"), at the time that you opened your Rightslink account and that are available at any time at http://myaccount.copyright.com).

GENERAL TERMS

2. Elsevier hereby grants you permission to reproduce the aforementioned material subject to the terms and conditions indicated.

3. Acknowledgement: If any part of the material to be used (for example, figures) has appeared in our publication with credit or acknowledgement to another source, permission must also be sought from that source. If such permission is not obtained then that material may not be included in your publication/copies. **Suitable acknowledgement to the source must be made, either as a footnote or in a reference list at the end of your publication, as follows:**

"Reprinted from Publication title, Vol /edition number, Author(s), Title of article / title of chapter, Pages No., Copyright (Year), with permission from Elsevier [OR APPLICABLE SOCIETY COPYRIGHT OWNER]." Also Lancet special credit - "Reprinted from The Lancet, Vol. number, Author(s), Title of article, Pages No., Copyright (Year), with permission from Elsevier."

4. Reproduction of this material is confined to the purpose and/or media for which permission is hereby given.

5. Altering/Modifying Material: Not Permitted. **However figures and illustrations may be altered/adapted minimally to serve your work.** Any other abbreviations, additions, deletions and/or any other alterations shall be made only with prior written authorization of Elsevier Ltd. (Please contact Elsevier's permissions helpdesk here). No modifications can be made to any Lancet figures/tables and they must be reproduced in full.

6. If the permission fee for the requested use of our material is waived in this instance, please be advised that your future requests for Elsevier materials may attract a fee.

7. Reservation of Rights: Publisher reserves all rights not specifically granted in the combination of (i) the license details provided by you and accepted in the course of this licensing transaction, (ii) these terms and conditions and (iii) CCC's Billing and Payment terms and conditions.

8. License Contingent Upon Payment: While you may exercise the rights licensed immediately upon issuance of the license at the end of the licensing process for the transaction, provided that you have disclosed complete and accurate details of your proposed use, no license is finally effective unless and until full payment is received from you (either by publisher or by CCC) as provided in CCC's Billing and Payment terms and conditions. If full payment is not received on a timely basis, then any license preliminarily granted shall be deemed automatically revoked and shall be void as if never granted. Further, in the event that you breach any of these terms and conditions or any of CCC's Billing and Payment terms and conditions, the license is automatically revoked and shall be void as if never granted. Use of materials as described in a revoked license, as well as any use of the materials beyond the scope of an unrevoked license, may constitute copyright infringement and publisher reserves the right to take any and all action to protect its copyright in the materials.

9. Warranties: Publisher makes no representations or warranties with respect to the licensed material.

10. Indemnity: You hereby indemnify and agree to hold harmless publisher and CCC, and their respective officers, directors, employees and agents, from and against any and all claims arising out of your use of the licensed material other than as specifically authorized pursuant to this license.

11. No Transfer of License: This license is personal to you and may not be sublicensed, assigned, or transferred by you to any other person without publisher's written permission.

12. No Amendment Except in Writing: This license may not be amended except in a writing signed by both parties (or, in the case of publisher, by CCC on publisher's behalf).

13. Objection to Contrary Terms: Publisher hereby objects to any terms contained in any purchase order, acknowledgment, check endorsement or other writing prepared by you, which terms are inconsistent with these terms and conditions or CCC's Billing and Payment terms and conditions. These terms and conditions, together with CCC's Billing and Payment terms and conditions (which are incorporated herein), comprise the entire agreement between you and publisher (and CCC) concerning this licensing transaction. In the event of any conflict between your obligations established by these terms and conditions and those established by CCC's Billing and Payment terms and conditions, these terms and conditions shall control.

14. Revocation: Elsevier or Copyright Clearance Center may deny the permissions described in this License at their sole discretion, for any reason or no reason, with a full refund payable to you. Notice of such denial will be made using the contact information provided by you. Failure to receive such notice will not alter or invalidate the denial. In no event will Elsevier or Copyright Clearance Center be responsible or liable for any costs, expenses or damage incurred by you as a result of a denial of your permission request, other than a refund of the amount(s) paid by you to Elsevier and/or Copyright Clearance Center for denied permissions.

LIMITED LICENSE

The following terms and conditions apply only to specific license types:

15. Translation: This permission is granted for non-exclusive world English rights only unless your license was granted for translation rights. If you licensed translation rights you may only translate this content into the languages you requested. A professional translator must perform all translations and reproduce the content word for word preserving the integrity of the article.

16. Posting licensed content on any Website: The following terms and conditions apply as follows: Licensing material from an Elsevier journal: All content posted to the web site must maintain the copyright information line on the bottom of each image; A hyper-text must be included to the Homepage of the journal from which you are licensing at http://www.sciencedirect.com/science/journal/xxxxx or the Elsevier homepage for books at http://www.elsevier.com; Central Storage: This license does not include permission for a scanned version of the material to be stored in a central repository such as that provided by Heron/XanEdu.

Licensing material from an Elsevier book: A hyper-text link must be included to the Elsevier homepage at http://www.elsevier.com . All content posted to the web site must maintain the copyright information line on the bottom of each image.

Posting licensed content on Electronic reserve: In addition to the above the following clauses are applicable: The web site must be password-protected and made available only to bona fide students registered on a relevant course. This permission is granted for 1 year only. You may obtain a new license for future website posting.

17. For journal authors: the following clauses are applicable in addition to the above:

Preprints:

A preprint is an author's own write-up of research results and analysis, it has not been peer-reviewed, nor has it had any other value added to it by a publisher (such as formatting, copyright, technical enhancement etc.).

Authors can share their preprints anywhere at any time. Preprints should not be added to or enhanced in any way in order to appear more like, or to substitute for, the final versions of articles however authors can update their preprints on arXiv or RePEc with their Accepted Author Manuscript (see below).

If accepted for publication, we encourage authors to link from the preprint to their formal publication via its DOI. Millions of researchers have access to the formal publications on ScienceDirect, and so links will help users to find, access, cite and use the best available version. Please note that Cell Press, The Lancet and some society-owned have different preprint policies. Information on these policies is available on the journal homepage.

Accepted Author Manuscripts: An accepted author manuscript is the manuscript of an article that has been accepted for publication and which typically includes author- incorporated changes suggested during submission, peer review and editor-author communications.

Authors can share their accepted author manuscript:

- immediately
    - via their non-commercial person homepage or blog
    - by updating a preprint in arXiv or RePEc with the accepted manuscript
    - via their research institute or institutional repository for internal institutional uses or as part of an invitation-only research collaboration work-group
    - directly by providing copies to their students or to research collaborators for their personal use
    - for private scholarly sharing as part of an invitation-only work group on commercial sites with which Elsevier has an agreement
- After the embargo period
    - via non-commercial hosting platforms such as their institutional repository
    - via commercial sites with which Elsevier has an agreement

In all cases accepted manuscripts should:

- link to the formal publication via its DOI
- bear a CC-BY-NC-ND license - this is easy to do
- if aggregated with other manuscripts, for example in a repository or other site, be shared in alignment with our hosting policy not be added to or enhanced in any way to appear more like, or to substitute for, the published journal article.

Published journal article (JPA): A published journal article (PJA) is the definitive final record of published research that appears or will appear in the journal and embodies all value-adding publishing activities including peer review co-ordination, copy-editing, formatting, (if relevant) pagination and online enrichment.

Policies for sharing publishing journal articles differ for subscription and gold open access articles:

Subscription Articles: If you are an author, please share a link to your article rather than the full-text. Millions of researchers have access to the formal publications on ScienceDirect, and so links will help your users to find, access, cite, and use the best available version.

Theses and dissertations which contain embedded PJAs as part of the formal submission can be posted publicly by the awarding institution with DOI links back to the formal publications on ScienceDirect.

If you are affiliated with a library that subscribes to ScienceDirect you have additional private sharing rights for others' research accessed under that agreement. This includes use for classroom teaching and internal training at the institution (including use in course packs and courseware programs), and inclusion of the article for grant funding purposes.

Gold Open Access Articles: May be shared according to the author-selected end-user license and should contain a CrossMark logo, the end user license, and a DOI link to the formal publication on ScienceDirect.

Please refer to Elsevier's posting policy for further information.

18. For book authors the following clauses are applicable in addition to the above:
Authors are permitted to place a brief summary of their work online only. You are not allowed to download and post the published electronic version of your chapter, nor may you scan the printed edition to create an electronic version. Posting to a repository: Authors are permitted to post a summary of their chapter only in their institution's repository.

19. Thesis/Dissertation: **If your license is for use in a thesis/dissertation your thesis may be submitted to your institution in either print or electronic form.** Should your thesis be published commercially, please reapply for permission. These requirements include permission for the Library and Archives of Canada to supply single copies, on demand, of the complete thesis and include permission for Proquest/UMI to supply single copies, on demand, of the complete thesis. Should your thesis be published commercially, please reapply for permission. Theses and dissertations which contain embedded PJAs as part of the formal submission can be posted publicly by the awarding institution with DOI links back to the formal publications on ScienceDirect.

Elsevier Open Access Terms and Conditions

You can publish open access with Elsevier in hundreds of open access journals or in nearly 2000 established subscription journals that support open access publishing. Permitted third party re-use of these open access articles is defined by the author's choice of Creative Commons user license. See our open access license policy for more information.

Terms & Conditions applicable to all Open Access articles published with Elsevier:

Any reuse of the article must not represent the author as endorsing the adaptation of the article nor should the article be modified in such a way as to damage the author's honour or reputation. If any changes have been made, such changes must be clearly indicated.

The author(s) must be appropriately credited and we ask that you include the end user license and a DOI link to the formal publication on ScienceDirect.

# APPENDIX C: Elsevier Author Rights

Accessed from https://www.elsevier.com/about/policies/copyright#Author-rights on 1/18/23

The below table explains the rights that authors have when they publish with Elsevier, for authors who choose to publish either open access or subscription. These apply to the corresponding author and all co-authors.

| **Author rights in Elsevier's proprietary journals** | **Published open access** | **Published subscription** |
|---|---|---|
| Retain patent and trademark rights | √ | √ |
| Retain the rights to use their research data freely without any restriction | √ | √ |
| Receive proper attribution and credit for their published work | √ | √ |
| Re-use their own material in new works without permission or payment (with full acknowledgement of the original article):<br>1. Extend an article to book length<br>2. Include an article in a subsequent compilation of their own work<br>3. Re-use portions, excerpts, and their own Figures or Tables in other works. | √ | √ |
| Use and share their works for scholarly purposes (with full acknowledgement of the original article):<br>1. In their own classroom teaching. Electronic and physical distribution of copies is permitted<br>2. If an author is speaking at a conference, they can present the article and distribute copies to the attendees<br>3. Distribute the article, including by email, to their students and to research colleagues who they know for their personal use<br>4. Share and publicize the article via Share Links, which offers 50 days' free access for anyone, without signup or registration<br>5. Include in a thesis or dissertation (provided this is not published commercially)<br>6. Share copies of their article privately as part of an invitation-only work group on commercial sites with which the publisher has a hosting agreement | √ | √ |
| Publicly share the preprint on any website or repository at any time. | √ | √ |
| Publicly share the accepted manuscript on non-commercial sites | √ | √ using a CC BY-NC-ND license and usually only after an embargo period (see Sharing Policy for more information) |
| Publicly share the final published article | √ in line with the author's choice of end user license | × |
| Retain copyright | √ | × |

APPENDIX D: MDPI Open Access Policy

Accessed from https://www.mdpi.com/openaccess on 1/18/23

**MDPI Open Access Information and Policy**

All articles published by MDPI are made immediately available worldwide under an open access license. This means:

- everyone has free and unlimited access to the full-text of *all* articles published in MDPI journals;
- everyone is free to re-use the published material if proper accreditation/citation of the original publication is given;
- open access publication is supported by the authors' institutes or research funding agencies by payment of a comparatively low Article Processing Charge (APC) for accepted articles.

**Permissions**

No special permission is required to reuse all or part of article published by MDPI, including figures and tables. For articles published under an open access Creative Common CC BY license, any part of the article may be reused without permission provided that the original article is clearly cited. Reuse of an article does not imply endorsement by the authors or MDPI.